Characterization of outer membrane vesicle production and composition by cationic antimicrobial-adapted *Escherichia coli*

By

Shelby Lynn Reimer

A Thesis Submitted to the Faculty of Graduate Studies of

The University of Manitoba

in Partial Fulfillment of the Requirements of the Degree of

Master of Science

Department of Medical Microbiology and Infectious Diseases

Faculty of Medicine

University of Manitoba

Winnipeg, Manitoba, Canada

Abstract

Antimicrobial resistance (AMR) is a growing global health problem, exacerbated by the widespread use of antimicrobials in healthcare, agriculture, and industrial settings. Cationic antimicrobials (CAs) such as the therapeutic antibiotic colistin (COL) and antiseptics cetrimide (CET) and chlorhexidine (CHX) exert their mechanism of action by disrupting bacterial membranes, leading to cell content leakage and death. Tolerance to CAs is rapidly increasing and of the many known AMR mechanisms, the role of outer membrane vesicle (OMV) formation is least understood. In this thesis, we examined OMV isolation methods in a *tolA* deletion mutant to understand how OMV properties differ when using two common methods (Chapter 3). Using the most robust OMV isolation method, OMV production from a set of CA-tolerant strains were compared to a wild-type (WT) *E. coli* K-12 BW25113 strain (Chapter 4). OMVs from WT and Δ*tolA* strains were isolated from culture supernatants by ultradiafiltration and ultracentrifugation, then analyzed with a light scattering based single particle tracking analysis (NTA) to compare OMV isolation differences. We characterized the morphology of OMVs isolated from each strain by cryo-transmission electron microscopy, compared proteomes using liquid chromatography-mass spectrometry, and evaluated susceptibility changes by antimicrobial susceptibility testing (AST). In Chapter 3, we demonstrated that deletion of the IM protein *tolA* in *E. coli,* an integral part of the membrane integrity Tol-Pal system, resulted in increased vesicle formation and morphological changes to vesicles, including a new kind of vesicle that we coined "G-OMVs". In Chapter 4, we found that the CA-adapted strains all had increased OMV formation as compared to WT, where each strain had distinctive morphological alterations; CET-OMVs were encapsulated and aggregated, CHX-OMVs were multilamellar and COL-OMVs were large and amorphous as compared to WT-OMVs. Proteomic analysis highlighted an increase in proteins associated with stress responses, lipid biosynthesis, and protein folding/transport in CA-adapted strains, and identified cytoplasmic and IM protein carryover into vesicles. AST of WT *E. coli* supplemented with purified CA-adapted OMVs demonstrated that susceptibility could be modulated by the addition of OMVs from CA-adapted strains. Overall, our findings show that CA-adapted *E. coli* have significant ramifications on OMV production, morphology, and susceptibility, highlighting the need for further research in this field.

Acknowledgments

First and foremost, I would like to thank my supervisor, Denice, for your guidance and commitment to this project, for providing me with many oppourtunities to try my hand at techniques I had never encountered before and for pushing me to become a more critical thinker. You saw the potential in me, and had the faith that I would emerge from graduate school a better all-around researcher from the lessons learned in your lab. I have learned so much from you that I will carry with me after long after graduate school. I would also like to thank my committee members, Dr. George Zhanel, Dr. Celine Nadon, and Dr. Amir Ravandi, thank you for your support, you were the driving force that challenged me to work hard and delve deeper into this research than I ever thought I could.

To the past and present members of the Bay lab, Niki Cartwright, Carmine Slipski, Branden Gregorchuk, Kieran Milner, Kari Green, and Ali Doucet, thank you for countless hours of advice, criticism and discussions about research, and for always being there to distract in times when I needed it. You all welcomed me into your midst with open arms (and cold beers), and I will forever be grateful. This last year has taught me the value of having people by your side that support and motivate you, and it has truly been an wonderful experience to work alongside all of you in the Bay Lab. Thank you to Carmine and Branden, for providing me with training and expertise, and for always having the time to answer questions and bounce ideas off of when I was unsure. To Kieran, who was there along with me at all the MSc milestones, and who was always quick with a distraction to ease the burden of experiment failures. Thank you especially to Kari and Ali, I am so grateful to have met you both during the course of this degree. Thank you for keeping me sane during this long journey, for being amazing friends to have in times of quarantine, for all of our adventures together, and for making me love Winnipeg for all it offers.

Lastly, I want to thank my family. To my parents, thank you for teaching me the value of doing what you love. You taught me how important perseverance and commitment are, and inspired me to pursue scientific research. To Taylor, thank you for your constant encouragement and confidence in my abilities. You have all made me the person I am today, and I am so lucky to have your support.

Table of Contents

List of Tables

List of Figures

Abbreviations

ABC	ATP-binding cassette
AMR	Antimicrobial resistance
AST	Antimicrobial susceptibility testing
BCA	Bicinchoninic acid
BSA	Bovine serum albumin
CA	Cationic antimicrobial
CET	Cetrimide bromide
CETR	Cetrimide-adapted *E. coli* K-12 BW25113
CFU	Colony formung units
CHX	Chlorhexidine
CHXR	Chlorhexidine-adapted *E. coli* K-12 BW25113
CLSI	Clinical Laboratory Standards Institute
COL	Colistin
COLR	Colistin-adapted *E. coli* K-12 BW25113
Cryo-TEM	Cryogenic transmission electron microscopy
CY	Cytoplasm
DAVID	Database for annotation, visualization and integrated discovery
DLS	Dynamic light scattering
DMSO	Dimethyl sulfoxide
ECL	Enhanced chemiluminescence
EDTA	Ethylenediaminetetraacetic acid
EUCAST	European Committee on Antimicrobial Susceptibility Testing
EV	Extracellular vesicle
EX	Extracellular
G-OMV	Grouped OMV

GFP	Green fluorescent protein
GO	Gene ontology
HEPES	4-(2-hydroxyethyl)-1-piperazineethanesulfonic acid
HRP	Horseradish peroxidase
IM	Inner membrane
IQR	Interquartile range
kDa	KiloDalton
KEGG	Kyoto Encyclopedia of Genes and Genomes
LB	Lysogeny broth
LPS	Lipopolysaccharide
M-OMV	Multi-layered OMV
MATE	Multi-drug and toxic compounds extrusion transporter
MDR	Multi-drug resistance
MFS	Major facilitator superfamily transporter
MIC	Minimum inhibitory concentration
MV	Membrane vesicle
Nano-LC-MS/MS	Nanoscale liquid chromatography tandem mass spectrometry
NML	National Microbiology Laboratory
NTA	Nanoparticle tracking analysis
O-IMV	Outer-inner membrane vesicle
OD	Optical density
OM	Outer membrane
OMV	Outer membrane vesicle
PACE	Proteobacterial antimicrobial compound efflux
PAGE	Polyacrylamide gel electrophoresis
PES	Polyethersulfone

pEtN	Phosphoethanolamine
PG	Peptidoglycan
PP	Periplasm
QAC	Quaternary ammonium compound
RND	Resistance-nodule division transporter
SD	Standard deviation
SDS	Sodium dodecyl sulfate
SEM	Standard error of the mean
SMR	Small multi-drug resistance transporter
TCE	2,2,2-trichloroethanol
UC	Ultracentrifugation
UF	Ultradiafiltration
UV	Ultraviolet
WT	Wild-type *E. coli* K-12 BW25113

Publication Content Included in this Thesis

Parts of this work have been published in the following manuscript:

Reimer SL, Beniac DR, Hiebert SL, Booth TF, Chong PM, Westmacott GR, Zhanel GG, Bay DC. 2021. Comparative analysis of outer membrane vesicle isolation methods with an *Escherichia coli tolA* mutant reveals a hypervesiculating phenotype with outer-inner membrane vesicle content. Frontiers in Microbiology 12: 628801. doi: 10.3389/fmicb.2021.628801.

Chapter 1. Introduction

This section reviews background information about *Escherichia coli*, the classification of antimicrobials used in this study, their importance and clinical relevance, their mechanisms of antimicrobial action and tolerance, and the implications of antimicrobial cross-resistance. An overview of the enterobacterial cell envelope will be given, outlining each cell compartment and its constituents. The final section will summarize what is currently known about outer membrane vesicles (OMVs), and their reported role in antimicrobial resistance (AMR). Together, these sections highlight the importance of studying OMVs produced by bacteria in order to understand what roles they play against membrane-active antimicrobials, which will be further examined in the subsequent chapters. All writing and figures presented in this chapter were made by Shelby Reimer, with an excerpt reproduced with permission from (1) regarding the Tol-Pal system included in Section 1.4.2. Editing was done by Denice Bay.

1.1 *E. coli* as a model organism

E. coli is a Gram-negative, facultative anaerobic, rod-shaped, coliform bacterium that is commonly found in the lower intestine of warm-blooded organisms, including humans. Most *E. coli* typically exists within its host synergistically, and with mutual benefits as a commensal organism, these strains can cause infections in immunocompromised individuals or when the gastrointestinal barriers are breached by an injury or a disorder such as inflammatory bowel disease (2). Infection with toxigenic and pathogenic serotypes of *E. coli*, such as enterotoxigenic *E. coli*, enteroinvasive *E. coli*, enteroaggregative *E. coli*, adherent invasive *E. coli*, and enteropathogenic *E. coli* can result in a variety of clinical conditions including enteric/diarrhoeal disease and the complication hemolytic uremic syndrome, urinary tract infections, meningitis and sepsis (2, 3). *E. coli* is one of the top three most common blood and urinary tract bacterial pathogens isolated from Canadian hospital laboratories, and has demonstrated a significant trend to increasing multi-drug resistance (MDR) (4, 5). Hence, it is important to understand the mechanisms of tolerance, particularly in species such as *E. coli* that account for a high burden of disease (4, 5).

E. coli has become one of the best studied bacterial organisms for research and is well-known as a model organism because it grows rapidly in rich media (doubling time as short as 20 min), has a high transformation efficiency, and is very easy to maintain and culture in a laboratory setting (6–8). This tractable model organism has been well characterized phenotypically and genetically, with completed genome sequences for 562 reference strains that are publically available from the GenBank database (as of June 21, 2021), including *E. coli* K-12 strain BW25113, which will be studied extensively in the following thesis chapters. This has enabled researchers to perform extensive large-scale genomic studies as well as characterize the effects of specific gene disruptions and responses to stressors like antimicrobials. To aid in this research, one research group has systematically made a set of precisely defined, single-gene deletions of all nonessential genes in *E.coli* K-12 BW25113, producing a library of 3985 mutants (9). These in-frame kanamycin cassette mutants comprise the 'Keio collection', and they provide a valuable resource for high-throughput systematic analyses of unknown gene functions and gene regulatory networks and genome-wide screening/ testing of mutational effects in a common strain background (9). In addition, a complementary library was generated using *E. coli* K-12 W3110 was used to produce a plasmid library of all individually cloned genes in the multicopy plasmid vector pCA24N, called the 'ASKA' clone library (10). This library allows systematic gene complementation and functional genomic analyses using the ASKA and Keio collections (10). In the ASKA library, each open reading frame/ gene product is cloned in pCA24N with a hexahistidine affinity tag at its N-terminal end with or without a green fluorescent protein (GFP)-fused at its C-terminal end (referred to as the "pCA24N+ clones" and the "pCA24N- clones" respectively). pCA24N (+/-) are controlled by a *lac* promoter and are isopropyl β- d-1-thiogalactopyranoside inducible (10). These *E. coli* K-12 libraries are also ideal for studying mechanisms of tolerance due to their genetic tractability. The comprehensive genome and proteomes for *E. coli* K-12 have also been determined, making genetic knockouts and antibiotic challenge studies more informative as they can be compared to this and other *E. coli* reference libraries (11–13).

These research efforts have greatly enhanced our understanding of the *E. coli* genome, however, we still lack systematic understanding and experimental evidence of gene functions for roughly 35% of all known genes (14). Additionally, the membrane biology of *E. coli* in particular is not well understood, as only a few systematic analyses of the *E. coli* outer membrane have been conducted; these studies often do not capture the scope of the processes that occur at the *E. coli* cell's membrane interface with its environment (15, 16). It is therefore important to conduct further studies with *E. coli* to enhance this knowledge. As most antimicrobials must traverse the *E. coli* membrane layers to achieve their mechanisms of action and result in AMR, studies involving *E. coli* are valuable as they can then be generalized to other Enterobacterales and other Gram-negative bacteria. The remainder of this thesis will specifically discuss and focus on antimicrobial systems in *E. coli* and Enterobacterial membranes (unless otherwise specified).

1.2 Antimicrobials

By definition, an antimicrobial is an agent used to minimize the pathogenicity of microorganisms, which can be any infection or disease-causing bacteria, fungi, or virus, in humans and animals. Antimicrobials are ubiquitiously used in a wide variety of household products, industrial settings, and for infection prevention and treatment. Antimicrobials that target bacteria are typically classified by their mechanism of action, and are primarily grouped into three main categories; inhibitors of nucleic/ ribonucleic acid synthesis, inhibitors of protein synthesis, and inhibitors of cell wall synthesis (17). This thesis will focus exclusively on antimicrobials that target and act upon the cell membrane of Gram-negative bacteria, and the following sections will describe in more detail the precise mechanisms of action for these antimicrobials.

1.2.1 Biocides vs. Antibiotics

Biocides are defined as antimicrobial substances (such as antiseptics, algicides, or fungicides) that kill or inhibit the growth of living organisms. Biocides have broad-spectrum antimicrobial properties and are widely used for disinfection, antiseptic, and preservation purposes, whereas antibiotics are used

predominantly for the treatment of bacterial infections in humans and animals (18). Many biocides have been used for centuries and are now an integrated part of the industrialized world. In hospitals, biocides are widely used for disinfection of equipment and surfaces, as well as for hand and wound sanitation for controlling healthcare-associated infections (19). In the food industry, biocides are extensively used in animal husbandries to prevent emergence and dissemination of disease, and in food processing to prevent contamination (19, 20). Biocides are also used for preservative purposes in a range of products to prevent the growth of microorganisms, in cosmetics and household products (21). By comparison, antibiotics are very important for their prophylactic, empiric, and therapeutic use against bacterial infections. These compounds are distinguished from biocides by their parenteral usage (intravenous and oral) and their more stringent and controlled usage (22).

1.2.2 Cationic antimicrobials

Cationic antimicrobials (CAs) are a subcategory of antimicrobials that are membrane-active agents characterized by their positive charge at neutral pH. They function by interacting with the outer membrane of Gram-negative bacteria and disrupting the phospholipid bilayers, causing pore formation or lipid disruption, leading to ion leakage, and eventual cell death (18). The outer membrane of Gram-negative bacteria has a net negative charge due to the combination of molecules such as lipopolysaccharides and the phosphate headgroups of the phospholipids. Under normal circumstances, the negative charges are stabilized by divalent cations such as Mg^{2+} and Ca^{2+} (18, 23). CAs capitalize on these membrane chemical properties by having a strong positive charge along with a hydrophobic region, facilitating the displacement of divalent cations and interaction with the cell membrane (18, 23). CAs integrate into or associate with the membrane, causing loss of membrane fluidity and subsequent cell death (18, 23) (Figure 1.2). The chemical structures and mechanisms of action of the antimicrobials used in this thesis project can be found in Figure 1.1. Three representative classes of CAs will be described in the following sub-sections: polymyxins, quaternary ammonium compounds (QACs), and bisbiguanides.

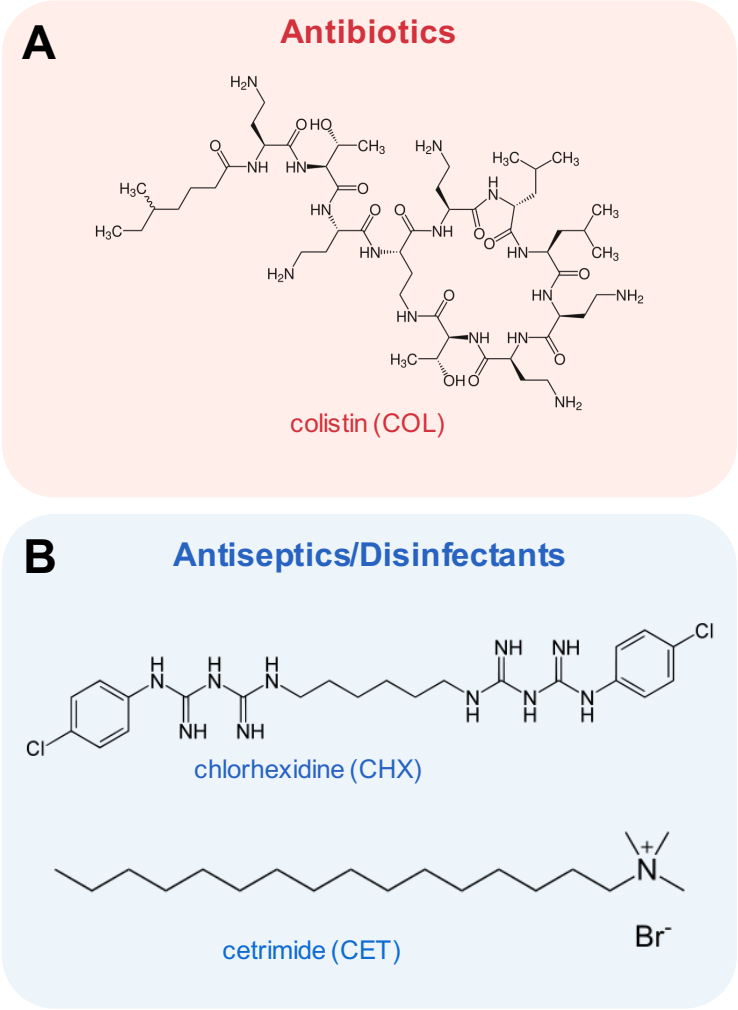

Figure 1.1. Antimicrobials studied in this thesis.**A)** Structure of the polymyxin antibiotic colistin (COL). **B)** Structures of the antiseptic/disinfectant compounds used, including the bisbiguanide chlorhexidine (CHX) and the quaternary ammonium compound cetrimide bromide (CET).

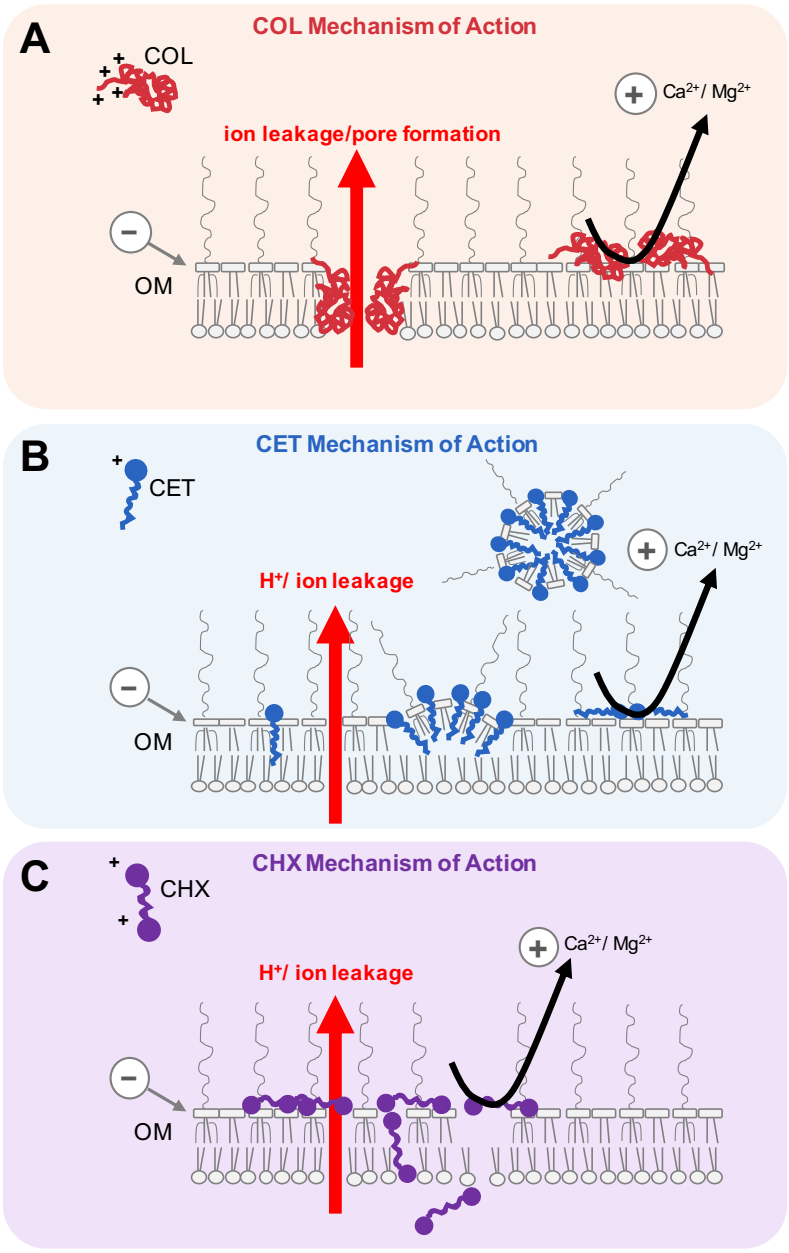

Figure 1.2. Mechanisms of action for the CAs used in this project.The positively charged CA binds to the outer membrane of Gram-negative bacteria, displacing divalent cations (Ca^{2+}/Mg^{2+}). **A)** COL is proposed to cause lipid disruption and pore formation. **B)** CET intercalates into the membrane and causes solubilization of the cell membrane components by forming mixed micellar aggregates. **C)** CHX bridges gaps between phospholipids by binding to headgroups. Each causes H^+ and ion leakage from inside the cell, eventually leading to cell death (18).

1.2.2.1 Polymyxins

Polymyxins (A, B, C, D and E) are a group of polypeptide antibiotics synthesized by *Bacillus polymyxa* that are active against Gram-negative bacteria (24) (Figure 1.1A). Only polymyxin B and E (COL) are used clinically, as the others in this group are highly toxic (24). Colistin (COL) is a cationic multicomponent lipopeptide consisting of a cyclic heptapeptide with a tripeptide side chain acylated at the N terminus by a fatty acid (25). COL has been used for over 50 years and exhibits rapid, concentration-dependent bactericidal activity against Gram-negative bacteria, however, this antibiotic was replaced in clinical treatments with aminoglycoside antibiotics in the 1970's due to studies showing its oto-, nephro-, and neurotoxic side-effects (25). Since the 1990's, the use of COL has been limited to 'last-resort' therapies for infections caused by MDR Gram-negative bacteria, particularly *Pseudomonas aeruginosa, Acinetobacter baumannii,* and *Klebsiella pneuemoniae* (25).

The bactericidal effect of polymyxins is extremely rapid and concentration-dependent, but the exact mechanism(s) by which this antibiotic acts on bacterial cells remains unclear (26) (Figure 1.2A). The currently accepted mechanism is that COL binds to the negatively charged lipopolysaccharide (LPS)-enriched outer layer of the outer membrane of Gram-negative bacteria via electrostatic and hydrophobic interactions, leading to 'self-promoted uptake' (27). COL-LPS interactions displace calcium (Ca^{2+}) and magnesium (Mg^{2+}) cations that normally stabilize the LPS outer layer, disrupting the cell outer membrane (24) (Figure 1.2A). After this point, there are several theories explaining how COL kills bacterial cells. One theory is that COL causes the inner layer of the outer membrane (OM) and the outer layer of the IM (IM) to fuse and come together, resulting in phospholipid exchange and osmotic imbalance (27). Other theories suggest that COL inhibits vital respiratory enzymes (type II NADH-quinone oxidoreductases) at the IM, where COL induces the formation of reactive oxygen species when it crosses the IM, or alternatively, that COL binds to bacterial DNA inhibiting cell replication and transcription (27, 28). Finally, a recent report from Sabnis *et al.* 2021 suggests that COL disrupts the membrane by binding LPS in the IM that is awaiting transport to the OM by Lpt machinery, causing permeabilization of the IM and leakage of intracellular

contents (24). More experimental evidence is needed to clarify how COL acts to disrupt cell membrane integrity that inhibits or kill cells.

1.2.2.2 Quaternary Ammonium Compounds

QACs are amphoteric surfactants containing one quaternary nitrogen associated with at least one major hydrophobic constituent (29) (Figure 1.1B). Members of this class include benzalkonium chloride, cetrimide bromide (CET), cetylpyridinium chloride, alkyl amino alkyl glycines and didecyldimethylammonium chloride (29). QACs are used increasingly for decontamination of environmental surfaces and disinfection of medical equipment, and are also found in a number of industrial, pharmaceutical and consumer products (30). Consumer products containing QACs include eye-wash/artificial tears, nose decongestants, facial cleansers, acne treatment, sun protection creams and lotions, baby lotions, moisturisers, mouthwashes, pain relief poultices or creams, hair conditioners, cosmetics and hand sanitizers (30). Hence, use of these compounds in developed countries is increasing, especially in the last year due to the SARS-CoV-2 global pandemic (31).

QACs mechanism of action against bacterial cells is primarily through the perturbation of the IM, following their adsorption to and diffusion through the OM (32) (Figure 1.2B). The permenant positively charged quaternary nitrogen of QACs associates with the negatively charged head groups of acidic phospholipids on bacterial cell surfaces, and the hydrophobic tail of the QAC integrates into the bacterial hydrophobic membrane bilayer core. This causes a generalized and progressive leakage of cytoplasmic material and loss of osmoregulatory capabilities within the cell, eventually leading to cell death (18). At very high concentrations, this interaction of QACs with the bacterial cell membrane causes solubilization of the cell membrane components by forming mixed micellar aggregates and release of cell contents, which has led many to be cross-identified as detergents (Figure 1.2B). QAC antimicrobial activity is primarily attributed to its membrane-disrupting abilities, however, these compounds have also been reported to cause disruption and denaturation of structural proteins and enzymes, as well as increase reactive oxygen and nitrogen radical formation due to the permanent cationic nitrogen in its structure (33).

1.2.2.3 Bisbiguanides

Bisbiguanides are important antiseptics, disinfectants, pharmaceutical and cosmetic preservatives and antiplaque agents with broad-spectrum antibacterial activity against both Gram-positive and Gram-negative bacteria (18). Bisbiguanides have a structure consisting of two (p-chlorophenyl)guanide units linked by a hexamethylene bridge. This class includes the compounds CHX and alexidine (Figure 1.1B), among the two compunds CHX is one of the most widely used biocides for skin and mucosal disinfection, and it is also used for direct application on domestic animals (34). As it has been shown to decrease microbial flora on the skin and lower infection risks, CHX is often used in hospital/ clinical settings as a skin preparatory agent for surgical procedures, as a surgical hand scrub, or incorporated into intravenous catheters, implanted surgical mesh, and topical dressings for wound sepsis (19). In household settings, CHX is commonly used in mouth rinses, topical antiseptics, disinfectants, and cosmetics, and has been marketed extensively in various dental oral hygiene products as an anti-plaque agent and as a treatment for periodontal disease (19).

The bisbiguanide CHX has a very similar mechanism of action to the QAC biocides, where the cationic biguanides strongly associate with the exposed anionic sites on the cell membrane and cell wall such as the acidic phospholipids and proteins (Figure 1.2C). However, bisbiguanides differ from other cationic biocides because their rigid chemical structure only allows them to interact superficially with the lipid bilayer (18). The structure of CHX alters membrane fluidity through displacement of the cell membrane-associated divalent cations (Mg^{2+} and Ca^{2+}) and headgroup bridging (35) (Figure 1.2C). The hydrophobic region of CHX is six carbons long (rather than the 12-16 carbons of QACs), making this region of CHX rather inflexible and unable to solubilize and integrate in the hydrophobic core of the cell membrane (18). Instead, the molecule extends and bridges gaps between adjacent phospholipids, with each headgroup bound to a biguanide moiety and displacing the associated divalent cations (18). This interaction reduces membrane fluidity at low concentrations and affects the osmoregulatory and metabolic capabilities of the cell membrane and the enzymes within the cell (18). It has been demonstrated that CHX can destabilize the

outer membranes of Gram-negative bacteria, releasing proteins from the periplasm (PP) but not the IM, resulting in detached cytoplasmic membranes from the cell wall at both poles and at cylindrical parts of the bacilliform cells, promoting the leakage of cell content and formation of ghost cells (36). Similar to polymyxins and QACs which show a concentration dependence, at higher in-use concentrations of CHX, the interactions are more severe and cause cell membranes to adopt a liquid crystalline state, where the cell loses its structural integrity and allows precipitation of cellular material (18).

1.3 Antimicrobial resistance (AMR)

Unlike therapeutic antibiotics, antiseptics and disinfectants do not have clinically defined breakpoints that distinguish resistant and susceptible concentrations according to the Clinical Laboratory Standards Institute (CLSI) or European Committee on Antimicrobial Susceptibility Testing (EUCAST) (37). Therefore, for the remainder of this thesis, we will refer to reduced susceptibility phenotypes of QACs and bisbiguanides as "tolerant" and reduced susceptibility phenotypes of polymyxins as "resistant". For clarity, when CETR, CHXR, and COLR are mentioned together, we will refer to these strains as "CA-tolerant strains". The following sections describe the resistance/tolerance mechanisms against polymyxins (Section 1.3.1), QACs and bisbiguanides (Section 1.3.2). While specific mechanisms have been identified for each of these Gram-negative cell membrane-targeting antimicrobials (34, 38–41), there are three common mechanisms employed by most bacteria known to reduce susceptibility to these CAs. These mechanisms are: 1) the up-regulation of expression of efflux pump systems to remove antimicrobials that have entered the cell, 2) down-regulated expression or mutation of porin proteins to prevent antimicrobials from entering the cell, and 3) lipid alterations to reduce the overall anionic charge of the membrane, making it more difficult for positively charged antimicrobials to bind and penetrate (Figure 1.3) (23, 32, 42–44). In the next sections, a discussion of the known AMR mechanisms will be briefly reviewed.

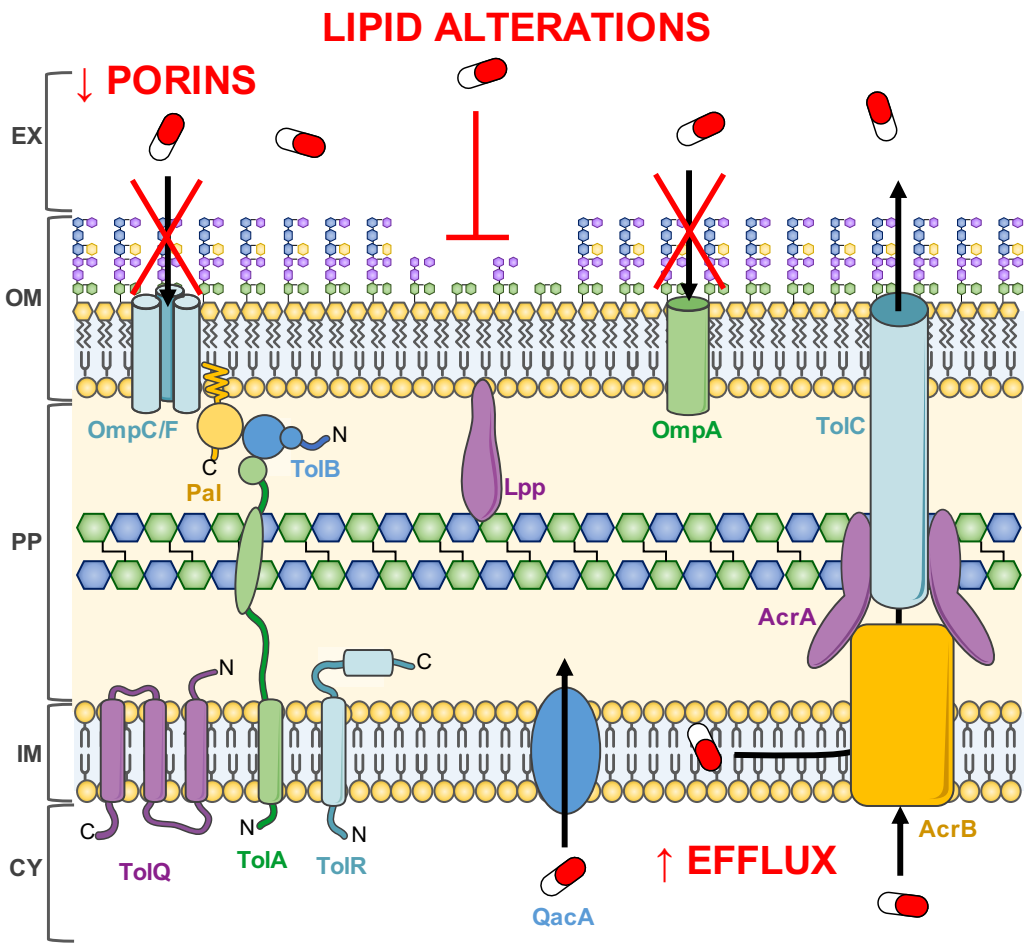

Figure 1.3. Architecture of the Enterobacterial cell envelope highlighting CA tolerance mechanisms and proteins involved in membrane integrity. The cytoplasm (CY) is enveloped by the inner membrane (IM), which contains integral IM proteins and IM lipoproteins. The periplasm (PP) is an aqueous compartment between the IM and the outer membrane (OM); it contains soluble proteins and the peptidoglycan layer. The OM lies on the outside of the cell, containing integral OM proteins and lipoproteins and forming a barrier between the cell and the extracellular (EX) space. The OM is anchored through interactions to the peptidoglycan layer (Lpp) and through protein systems that join to the IM (Tol-Pal proteins). The OM contains LPS in its outer leaflet, which can be altered by the cell to increase tolerance to antimicrobials. Other mechanisms of tolerance include decreased expression of porin proteins (OmpA, OmpC, OmpF), and increased expression of efflux pump systems (AcrAB-TolC, QacA) (45).

1.3.1 Polymyxin resistance

Intrinsic polymyxin resistance in Gram-negative bacteria has primarily been associated with chemical modifications of the LPS molecules on the outer membrane of the bacterial cell (46). LPS modifications are performed enzymatically, where substituents such as 4-amino-4-deoxy-l-arabinose (l-Ara4N), phosphoethanolamine (pEtN) or galactosamine are added onto the lipid A or LPS core (46). These additions change the negative charges of lipid A moeity and/ or alter the fluidity of the LPS in the outer leaflet of the outer membrane. By decreasing the net negative charge of the phosphate residues through modification, these LPS modifications prevent the binding of polymyxin molecules to the bacterial surface and their further penetration into the cell interior (46). Consequently, some COL resistant isolates show a complete loss of LPS from the outer membrane leaflet (47).

Expression of most LPS modifying or biosynthetic pathways is under the control of two specific two-component regulatory systems in *E. coli* species; PhoP-PhoQ (PhoPQ) and PmrA-PmrB (PmrAB) (46). These systems are composed of a transmembrane sensor histidine kinase (e.g. PhoQ, PmrB), that is able to self-phosphorylate under specific stress conditions, and a cytoplasmic response regulator (e.g. PhoP, PmrA), which when phosphorylated by the kinase modulates the expression of target genes (46). Gene mutations and environmental changes that control these two-component systems result in the up-regulation of the LPS modification pathway and subsequently increased polymyxin resistance (46). Additionally, mutations in the *pmrAB* or *phoPQ* operons as well as several other loci (i.e *micA, mgrR, etk*) results in activation of the *eptA* and *arnT* genes (46). The enzymes EptA and ArnT are responsible for the addition of pEtN and l-Ara4N molecules respectively, to LPS phosphate groups, which also increases resistance of *E. coli* to polymyxins. Studies analyzing urine and stool samples from humans and swine attributed polymyxin resistance to the occurrence of mutations in the genes *pmrA*, *pmrB*, and *phoQ* (46, 48, 49). In addition to the mutation mechanisms, acquisition of plasmid-mediated genes (*mcr* genes) have been reported to be a major cause of COL resistance in *E. coli* (46). A major concern with *mcr* genes is their

location on mobile genetic elements and transferable plasmids, as they are becoming more easily disseminated by conjugation among *E. coli* strains and also transmitted to other bacteria (50).

1.3.2 QAC and bisbiguanide tolerance

Tolerance to QACs and bisbiguanides has primarily been attributed to the acquisition or overexpression of MDR efflux pumps, the reduced expression of porins or intrinsic changes to the phospholipid membrane (18, 29, 51). MDR efflux pumps are the primary mechanism of tolerance against QACs in *E. coli*, as they are highly effective at removing antimicrobials from the interior of the cell (52). They are often embedded in the IM of Gram-negative bacteria, allowing bacteria to pump out these compounds after they enter into the CY. MDR efflux pumps proteins can confer tolerance to toxic compounds, antibiotics, and biocides, and function by extruding the offending compounds out of the bacterial cell (52). These MDR efflux pumps can be subdivided into at least five different families, including ATP-binding cassette (ABC) transporters, the small multidrug resistance (SMR) family, the major facilitator superfamily (MFS), the resistance–nodulation–division (RND) family and the multidrug and toxic compounds extrusion (MATE) proteins (30, 52). *E. coli* biocide transporters include the AcrAB efflux pump (RND), the EmrE pump (SMR), the YdhE (MATE) protein, the MdfA (MATE) protein, and the TehA protein (MFS) (30). By inducing or upregulating the function of these pumps, *E. coli* is able to remove any antimicrobials that cross the outer membrane. Up-regulation of the dominant efflux system, AcrAB-TolC efflux pump, can be induced by environmental stimuli such as oxidative stress, organic solvent, or antimicrobial exposure, which activates the Mar-Rob-Sox sytem to upregulate AcrAB expression and confer tolerance (30). Additionally, genes that specifically encode QAC tolerance are encoded on transmissible plasmids, such as the class 1 integron in Enterobacterales carrying *qacE, qacF, qacG,* and *qacH* (30).With respect to chlorhexdine-selective efflux pump genes, the SMR protein family such as *qacA, qacE*, and *qacC* can confer low levels of tolerance to CHX through the upregulation of efflux proteins (34). The proteobacterial antimicrobial compound efflux (PACE) gene *aceI,* MFS efflux pump

gene *smvA,* and CDF family member *cepA* also show specificity for CHX and confer tolerance to CHX (39, 52).

Reduced expression of *ompC* and *ompF* porin genes also reduces the susceptibility of strains to biocides by downregulating the amount of porin proteins present in the outer membrane. Repeated exposure to sub-inhibitory concentrations of QACs has been shown to change the expression of different OMPs in *E. coli* by two-dimensional gel electrophoresis (51). Additionally, a plasmid in *E. coli* (RP1) has been shown to alter the composition of the outer membrane lipopolysaccharides and to reduce the expression level of porin proteins, which also reduces susceptibility to CHX (19). Finally, changes in surface hydrophobicity, outer membrane ultrastructure, and changes in outer membrane fatty acid composition are also associated with increased QAC and bisbiguanide tolerance, although the genetic determinants have not yet been elucidated (23).

1.3.3 Cross-resistance between biocides and antibiotics

The increased use of biocides in recent years has led to concerns over the development of tolerance, both to other biocides (cross-tolerance) as well as to therapeutic antibiotics (cross-resistance) (19). Even though biocides are commonly used at working concentrations well above the minimal inhibitory conecentrations and minimal bactericidal concentration doses, the incorrect or inadequate usage of these compounds can result in sub-inhibitory concentrations of biocides that may select for tolerance (19, 53). However, there is a general lack of consistency between studies that support this claim (19, 20, 30). With the widespread usage and constant exposure to environments or products containing biocide CAs, it is not surprising that concerns have been raised over the potential for tolerance against these compounds in bacteria (20). A recent review concluded that QAC selection of bacteria with decreased susceptibility may contribute to the emergence of microflora with large numbers of bacterial strains that are resistant to clinically important antimicrobial agents (30). Similarly, the overuse of biocides is likely to promote fixation of mobile genetic elements that contribute to the spread of resistance genes (30). More evidence is

arising supporting the claim that exposure to CAs in the environment is a concern because it can confer cross-resistance to clinically relevant antibiotics such as colistin (35, 39, 54, 55).

1.3.4 Cellular mechanisms of CA tolerance

In general, enhanced CA tolerance has been demonstrated when Gram-negative bacteria grow as surface attached sesslie biofilms (35, 56, 57) and when they produce thick extracellular polysaccharide-enriched capsules (58). Recently, antibiotic exposure to beta-lactams has demonstrated that Gram-negative bacteria, including *E. coli,* are more tolerant to these antimicrobials when they produce outer membrane vesicles (OMVs) released from bacterial cells, however it not known if or how OMV formation influences CA tolerance (59). Hence, the role of CA exposure on OMV formation is important to explore given the known CA mechanisms of action. Since all three CA tolerance mechanisms discussed above in section 1.3.0 are also known to increase and overlap with antibiotic resistance, it is important to understand and review Gram-negative bacterial membrane structure and prior to discussing the potential link between CA exposure and OMV formation. The next section will review Enterobacterial cell envelope architecture.

1.4 Enterobacterales cell envelope architecture

The Enterobacterial cell envelope is an important barrier between the cell and its surrounding environment, and performs a variety of functions, including cell communication, gene regulation, cell signalling, transport of essential nutrients and metabolites, and exclusion of harmful antimicrobials (16, 45, 60). As *E. coli* exists primarily as an enteric and environmental bacterium, it must have a cell envelope that is tolerant to harsh environmental changes and antimicrobial challenges (45). There are three layers that make up the Enterobacterial cell envelope; the IM, the peptidoglycan (PG) cell wall, and the OM, between which lies the aqueous PP (Figure 1.3). The following sections will describe in more detail the composition and function of each cellular compartment, and will highlight a few cellular processes that play important roles in AMR and vesicle biogenesis and regulation.

1.4.1 The inner bacterial membrane

The CY of the cell, which houses the majority of the essential cell processess, is protected by the IM, a phospholipid bilayer, which acts as a hydrophobic barrier to polar molecules and regulates the flow of nutrients and metabolic products through the action of protein channels and transporters (45). The IM is incredibly important for energy generation through the action of the electron transport chain, protein secretion, transport of metabolites, lipid biosynthesis, cell signalling, cell attachment and cell division (45). Membrane lipids, including phospholipids and LPS are synthesized on the inner leaflet of the IM, before being flipped to the outer leaflet by MsbA and transported to their final destinations (45). The structural stability of the inner and outer membranes can be attributed primarily to the distribution of specific phospholipids within the membrane. In *E. coli,* the predominant phospolipids are phosphatidylethanolamine (70-80%), phosphatidylglycerol (12-25%), and cardiolipin (5-10%), with small amounts of phosphatidylserine, phosphatidic acid, lysophospholipids, and diacylglycerol (45, 61, 62). Due to it physical properties and zwitterionic nature, phosphatidylethanolamine is able to provide a net neutral charge to support membrane functions, modulate lipid bilayer curvature, and participate in the transport of folded proteins across the membrane (63).

1.4.2 The periplasmic space and the peptidoglycan layer

The PP is an aqueous cellular compartment containing degredative enzymes, periplasmic binding proteins, and chaperones that lies between the outer and IMs of the gram-negative bacterial cell (64). The functions of the PP include protein folding, transport, and oxidation, as well as lipid secretion, sequestration of toxic enzymes, signal transduction and cell division regulation (64). As some of the biomolecules that need to be exported across the PP to the OM or out of the cell are hydrophobic, chaperone proteins and intermembrane transport systems that span the PP are important for transporting substrates, such as the Lpt system for transporting LPS, the Lol system for the transfer of lipoproteins, and the AcrAC-TolC efflux system for removing antimicrobials (65). The PP is also vital for maintaining cell turgor pressure by providing a number of structural systems that join the outer and inner membrae, including lipoproteins,

multidrug efflux systems and the peptidoglycan layer (64). The peptidoglycan layer is made up of alternating *N*-acetylmuramic acid and *N*-acetylglucosamine sugars crosslinked by penta-peptide side chains that provides structural integrity to the cell through covalent attachments with proteins and lipoproteins to the OM, including Braun's lipoprotein (Lpp), OM porin OmpA, and the Tol-Pal system (45).

1.4.3 The outer membrane

The OM of Gram-negative bacteria is distinct due to its asymmetric structure, composed of an inner leaflet of phospholipids and an external leaflet containing the glycolipid LPS (45). This additional membrane provides a secondary, negatively-charged barrier that reduces the entry of toxic compounds, including antimicrobials. LPS is essential to the cell, and is made up of three major components in most Gram-negative species; a hydrophobic domain called lipid A, a nonrepeating core oligosaccharide, and a distal polysaccharide known as O-antigen repeats. The O-antigen moiety is not essential, however, and is missing in the common laboratory strain *E. coli* K-12, but is present in most wild-type and clinical isolates, where it contributes to virulence by protecting bacteria from phagocytosis and complement-mediated killing (66).

The LPS leaflet of the OM is initally constructed at the interface between the CY and the IM, before being flipped across the IM and transported to the OM. Lipid A, which is the membrane anchor of each LPS molecule, is synthesized through the Raetz pathway (67). This pathway involves a series of enzymatic reactions, the first set catalyzed by Lpx machinery (LpxA-D, LpxH, LpxB, LpxK) to form Lipid IV, then the second set catalyzed by WaaA (KdtA), LpxM and LpxL to form Kdo_2-Lipid A (67). The *E. coli* lipid A moiety consists of a glucosamine disaccharide, with 6-7 acyl chains varying between 12, 14, and 16 carbons in length (67, 68). Once lipid A is synthesized, it is subsequently flipped across the IM by MsbA, and this molecule is then combined with the core oligosaccharide and transported to the OM by Lpt machinery (67, 69).

While the pathway for LPS biogenesis is conserved in most Gram-negative bacteria, different species have evolved numerous strategies to alter LPS structure in order to influence lipid packing,

membrane permeability, recognition by immune cells, and resistance to antimicrobials. Variations to the lipid A structure can occur during synthesis of the molecule, or can be modified by enzymes after lipid A has been synthesized and transported to the OM (67, 69). The acyltranferases LpxL and LpxM are particularly prone to altering the acyl chains incorporated into lipid A during its synthesis in response to environmental conditions, while modifications made after lipid A is synthesized typically involve the addition or removal of fatty acids by enzymes in the OM (LpxR, PagL, PagP) (67, 69). The charge of lipid A can be also be altered by removing or masking phosphate groups on the lipid A moiety (EptA, ArnT, FlmK) (67, 69).

Modification of LPS on the cell surface has many implications, affecting OM permeability, resistance to antimicrobials, virulence and recognition by the host immune system, and production of OMVs (69). LPS alterations that remove or modify the phosphate groups of the core oligosaccharide or lipid A, or that alter the acylation of lipid A have all been shown to provide resistance against various antimicrobials (69). In addition, modifying the structure of LPS also impacts the production of OMVs. Specifically, deacylation of LPS by overexpression of PagL in *Salmonella typhimurium* increases the size and amount of OMVs released by the bacterium (70).

1.5 Extracellular vesicles

The production of extracellular vesicles (EVs) is a universally conserved process occurring in all domains of life (71). Characterized by their small size and lipid bilayer-enclosed membranes, these ubiquitous structures remain poorly understood, although studies implicate their importance in many aspects of cellular physiology (71–74). In Eukarya, EV types include microvesicles and exosomes released by normal and diseased cells, oncosomes released by cancer cells and apoptotic bodies released by cells undergoing apoptosis (73). In Bacteria, EV types include membrane vesicles (MVs) from Gram-positive bacteria and mycobacteria, and OMVs from Gram-negative bacteria (75–77). In the following sections only bacterial EV types will be discussed.

1.5.1 Outer membrane vesicles

OMVs are formed by Gram-negative bacteria through the budding of the OM, producing small (20-250 nm) lipid-encapsulated spheres containing both periplasmic cargo as well as integral membrane proteins. Early studies of bacterial OMVs were pioneered by in the laboratory of Terry Beveridge who performed electron microscopy experiments with model organisms such as *Escherichia coli, Neisseria meningitidis, P. aeruginosa, Shigella flexneri, Helicobacter pylori, Legionella pheumophila* and *Shewanella livingstonensis* to identify OMVs (as reviewed by (78–80). The mechanism responsible for OMV biogenesis is still being elucidated; however, current evidence suggests OMV production is controlled by bacterial cells rather than a byproduct of cell lysis (81).

OMVs have many functions both *in vitro* and *in vivo*. They have been reported to act as delivery vehicles for virulence factors and insoluble proteins, promote cell-cell communication via transport of signalling molecules, aid bacteria in nutrient acquisition, contribute to biofilm formation, serve as initial targets for innate and adaptive immune recognition, protect against bacteriophage and antimicrobial challenge, and interact with host cells to aid in pathogenesis during infection (74, 81–84). OMVs are increasingly recognized as important mediators of AMR and studies have proposed that OMV production is important in innate bacterial defence against environmental stressors and antimicrobials that target the cell envelope and OM (82, 85, 86). The current literature regarding these properties of OMVs will be discussed in the following sections, highlighting the gaps in knowledge regarding OMV biogenesis, functions, and composition.

1.5.2 Functional roles of OMVs

1.5.2.1 Transport of insoluble materials

Materials that are both soluble and insoluble can be packaged into OMVs for exportation from the cell. This offers many advantages, as these proteins are protected from proteases in the extracellular environment, they can be delivered at high concentrations at their target site, and can be transported to

targets far away from the cell (80). For example, the highly hydrophobic insoluble quorum signalling molecule PQS in *P. aeruginosa* is secreted by OMVs, which allows the PQS molecule to disperse in aqueous environments (80).

Once the OMV content is delivered to the target, it releases materials through one of two potential mechanisms. In the first mechanism, the OMVs spontaneously lyse, allowing its contents to diffuse into the surrounding environment, however, there is little evidence supporting this mechanism, as OMVs have been found to be stable in extracellular environments (78, 87). The second mechanism involves the OMV attaching to the target and delivering their material through proximal lysis, internalization, or fusion (80). Attachment and fusion of OMV membranes with other Gram-negative bacterial cells can be used to transport content between bacterial cells. Studies conducted by the Beveridge lab used immunogold-labeled LPS to track OMVs from *P. aeruginosa* and *Shigella flexneri* after coincubation with other Gram-negative bacteria, and found that OMV lipids were detected in the OM of target bacteria, demonstrating OMV fusion and delivery of luminal content (78, 88). Transfer of OMV content such as DNA has also been demonstrated (89, 90). DNA-containing vesicles from *E. coli* O157:H7 are transferred to *Salmonella enterica*, resulting in a low frequency of OMV-mediated transformation (frequency of transformation of pGFP by vesicles was 3×10^{-10}) (89).

OMVs from Gram-negative bacteria can also interact with eukaryotic cells, either through the interaction of cell surface proteins or by endocytosis. Post et al. (2005) showed that *N. meningitidis* OMVs secreted with membrane-associated meningococcal endotoxin were able to activate cell surface host proteins (lipid-binding proteins, CD14, MD-2, and TLR4), and that these interactions caused the release of membrane lipids that may facilitate translocation of integral bacterial OM proteins (87). Endocytosis results in the entire OMV entering the eukaryotic cell, which can result in the display of bacterial epitopes to the immune system and the initiation of proinflammatory responses if OMVs are endocytosed into antigen-presenting cells (91).

1.5.2.2 Nutrient acquisition

OMVs can aid in bacterial growth and survival by aiding in acquisition of nutrients. OMVs can carry degradative enzymes that break down macronutrients in the extracellular space and receptors that can bind nutrients to bring to the host cell. One example of this is the PQS molecule of *P. aeruginosa*, which is able to bind to iron in the environment, similar to siderophores. The highly hydrophobic PQS molecule intercalates into the OM and induces OMV formation through influencing membrane curvature, interacting with the T6SS substrate TseF. This PQS-TseF complex facilitates the binding and transport of the iron ions into the lumen of the OMVs, as well as to the cytosol of the bacterial cells (80, 92, 93). A similar process exists in *Mycobacterium tuberculosis*, where OMVs containing the hydrophobic molecule mycobactin are able to bind iron and serve as a donor to support the replication of iron-starved mycobacteria (94).

1.5.2.3 Biofilm formation

An abundance of OMVs are observed in biofilms formed both *in vivo* and *in vitro*, and have been found to be involved in co-aggregation of cells as well as to provide a platform for the interactions between exopolysaccharides, DNA, proteins, and the attachment surface (95). OMVs have been shown to play an important role in biofilm formation of *P. aeruginosa* and *Helicobacter pylori*, with OMVs accounting for the majority (52%) of the LPS in *P. aeruginosa* biofilms and the addition of OMVs stimulating biofilm formation in *H. pylori* (80). As well, *Porphyromonas gingivalis* OMVs contain integral OM proteins called multivalent adhesins that mediate attachment to host tissues and promote coaggregation, leading to the development of dental plaque biofilms (80).

1.5.2.4 Stress Response

When bacteria are challenged with unfavorable conditions (e.g. high salt, oxidative stress) some proteins are denatured within the cells, and OMVs can be used to package the debris and transport it to the outer environment to relieve the cell of the toxic burden (96). Environmental stress, including envelope stress caused by antimicrobial treatment, ethanol exposure, and overexpression of toxic periplasmic

proteins have all been found to result in the overproduction of OMVs (80, 82). Studies have shown that hypervesiculating mutants are better able to survive these harsh conditions, while hypovesiculating mutants are typically more sensitive than wild-type strains (80, 82, 86).

OMVs are also uniquely suited to survive in a stressful host environment during infection, and are able to shield the bacteria causing the infection from the host immune response, activate inflammatory cascades, and facilitate toxin delivery to host cells (80). Vesicles have been shown to be very immunogenic, inducing B-cell activation upon co-incubation with vesicles from *B. burgdorferi*, and eliciting a mucosal and systemic bactericidal antibody response when *N. meningitidis* vesicles are administered intranasally into mice (74). Mice infected with *S. typhimurium* have also been found to generate CD4+ T-cells that recognize antigens in Salmonella OMVs (74). Therefore, even if bacterial OMVs do not carry exotoxins, they can cause damage due to the host inflammatory response.

OMVs are also proposed to be able to protect the host bacterium from antimicrobial exposure. They are able to do this through two proposed mechanisms, by producing OMVs that act as 'decoy' membranes in the environment that the antimicrobial agents bind to rather than the actual target, or by removing membrane-bound antimicrobials that enter the bacteria's OM by inducing OMV production (97). A study conducted by Manning and Kuehn (2011) compared a hyper-vesiculating *E. coli* mutant against a wild-type *E. coli* with exposure to two membrane-active antibiotics, polymyxin B and COL (82). They found that the mutant that produced 10-fold more OMVs survived significantly better than the wild-type, indicating a protective role of OMVs against membrane-active antibiotics (82). In addition, formation of OMVs was found to be significantly induced in the presence of the antimicrobial peptides (82). Similarly, OMVs from *Pseudomonas syringae* was shown to reduce the levels of COL and melittin in solution by sequestering these compounds, and pre-incubation of *Vibrio cholerae* with sublethal amounts of polymyxin B have been found to provide protection against human cathelicidin LL-37 (97). While this OMV-mediated resistance has been shown in several studies, this mechanism is temporary and non-specific as planktonic cells must continuously produce OMVs to maintain a sufficient concentration to provide protection (80).

This high-energy cost, short-term solution gives the bacteria time to develop a more robust and permanent resistance (80).

1.5.3 OMV biogenesis

The current models for the biogenesis and release of OMVs can be summarized by three main mechanisms i) altered OM-IM crosslinking, ii) stress protein build-up in the PP, and iii) accumulation of lipids that enhance membrane curvature (97–100). For mechanism 1) the separation of the OM and the peptidoglycan layer is due to the destruction of envelope crosslinks causes the formation of OMVs. In mechanism 2, the accumulation of misfolded proteins activates stress pathways and induces OMV formation. Lastly, in mechanism 3 the accumulation of particular lipid species and disruption of lipid symmetry in the membrane leads to increased membrane curvature and OMV formation (97, 101, 102). A summary of these models is shown in Figure 1.4. The above models for OMV biogenesis are important to highlight as they are intricately involved with gene pathways in the OM. This is significant because CA tolerance mechanisms are also greatly associated with membrane alterations, specifically with lipid alterations. This overlap suggests that CA adaptation, resulting in genetic alterations to important OM systems, will also likely influence OMV biogenesis. This association will be further discussed in Section 1.6.

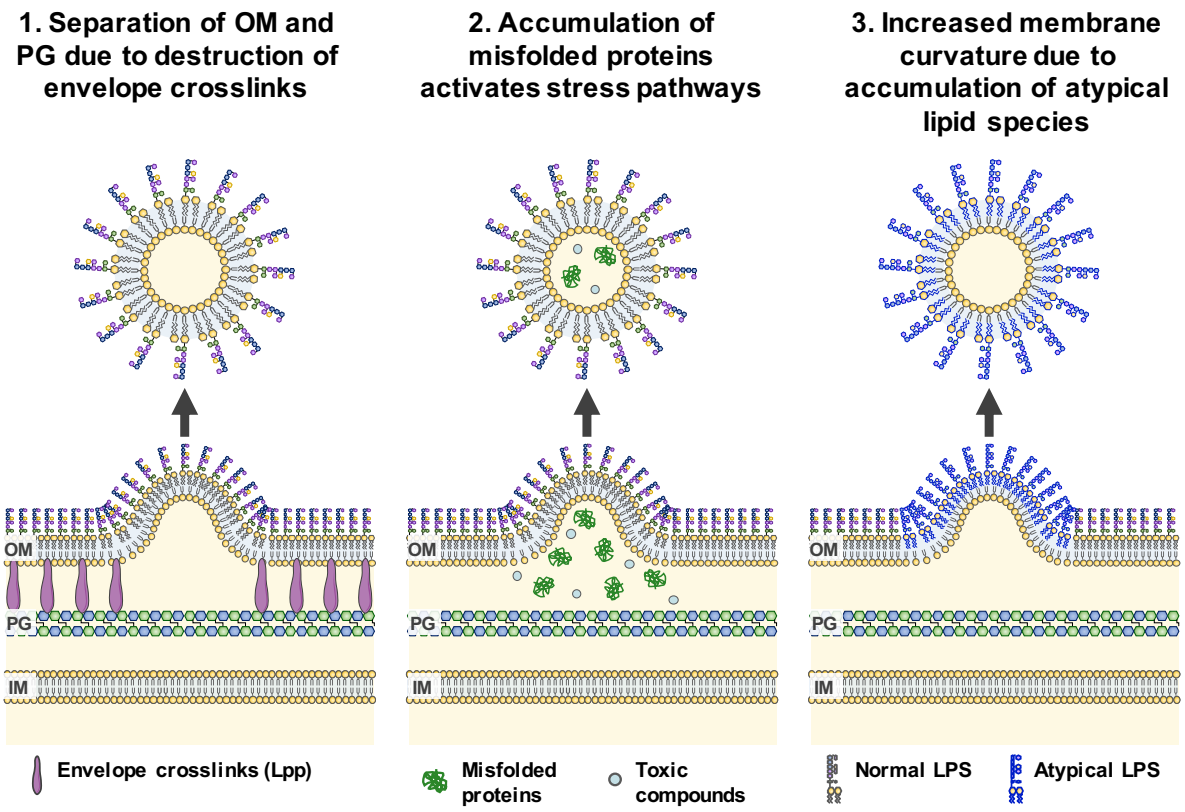

Figure 1.4. A summary of the three proposed intrinsic mechanisms of OMV biogenesis.The first model (1) shows the OM and PG become separated due to the destruction of envelope crosslinks, including Lpp. The second model (2) shows the accumulation of misfolded proteins and activation of stress pathways that induces OMV formation. For the third model (3), certain areas of the OM have atypical lipid species build-up or disrupted lipid symmetry, leading to increased membrane curvature and OMV release (97).

Table 1.1. A summary of identified Gram-negative bacterial mutants associated with altered OMV formation.

Biogenesis mechanism identified	Gene deletion mutations studied	Species	Reference
1. Envelope stability and cross-linking between OM and PG	Δ*lpp* reduces cross-linking between OM and PG	*E. coli* *S. typhimurium*	(84, 103)
	Δ*nlpI* reduces cross-linking between OM and PG	*E. coli*	(104, 105)
	Δ*lpp* and Δ*pal* reduces cross-linking between OM and PG	*E. coli*	(106)
	Deletion of *tolA, tolQ, tolR* disrupts membrane integrity	*E. coli*	(103)
	Deletion of *tolR* disrupts membrane integrity	*E. coli*	(107)
	Deletion of *tolB, pal* disrupts membrane integrity	*H. pylori*	(108)
	Deletion of *tolA, tolB* disrupts membrane integrity	*S. typhimurium*	(84)
	Deletion of *ompA* disrupts membrane integrity	*E. coli* *A. baumannii* *S. typhimurium*	(84, 109, 110)
	Deletion of *oprF, oprI* disrupts membrane integrity	*P. aeruginosa*	(111)
2. Envelope stress and accumulation of misfolded proteins	Deletion of *rseA*, *degP, degS* results in accumulation of misfolded OM proteins	*E. coli*	(104)
	Deletion of *algU* results in accumulation of misfolded OM proteins	*P. aeruginosa*	(98)
	Deletion of *mucD* results in accumulation of misfolded proteins in PP	*P. aeruginosa*	(112)
3. Atypical lipid build-up and membrane curvature	Deletion of *vacJ/yrb* genes leads to accumulation of PLs in the OM	*H. influenzae* and *V. cholera*	(113)
	Deletion of *mla* pathway leads to accumulation of phospholipids in the OM	*C. jejuni*	(114)
	Overexpression of PagL deacylase modifies lipid A and induces curvature	*S. enterica*	(100)

1.5.4 OMV composition

The composition of OMVs has been a highly debated topic, with many researchers postulating that OMVs should consist only of proteins and lipids derived from the OM and PP of the bacterium (80, 115). However, investigation of the chemical components of OMVs has shown that these vesicles can contain proteins and in rare cases nucleic acids that orginate from the IM and CY of the cell (116–121). It is increasingly appreciated that bacteria change their production and relative distribution of OMVs under different physiological conditions, however the implications for this are not yet well understood. Therefore, it is important to understand the consensus profile of OMV contents in order to determine the effect of antimicrobial exposure on OMV composition, and to identify any molecular markers of AMR that are carried over into OMVs. The following sections will discuss the so called 'typical' protein and lipid profiles of OMVs, and the implications of compositional changes on OMV functions.

1.5.4.1 OMV protein profile

OMV protein profiles have been determined using western blotting, mass spectrometry, and functional experiments, and have confirmed that the majority of proteins found in OMVs are typical abundant OM proteins (104, 122) (Figure 1.5). These include major porins or transmembrane channel proteins, lipoproteins, ABC transporters, efflux pumps, and receptors (95, 97, 120, 121). As well, periplasmic proteins including chaperones, proteases, and hydrolases are commonly reported in OMV proteomic studies (86, 120, 121). In total, around 0.2-0.5% of OM and periplasmic proteins from *E. coli* are packaged into OMVs (101). OMVs are also known to transport metabolites, quorum sensing signals and other small molecules (97).

1.5.4.2 OMV lipid profile

Phospholipids and LPS are the major lipid components found in OMV membranes (101). Studies using techniques such as thin layer chromatography and mass spectrometry have identified lipids in high proportions in OMVs that are only detected in the OM in low proportions, indicating that there is a sorting

system that preferentially packages certain lipids into OMVs (95). As an example, the phospholipid composition of the OM is distinct from OMVs from *P. aeruginosa*, with OMVs enriched in phosphatidylglycerol and the OM containing a higher concentration of phosphatidylethanolamine (123). In addition, the relative amount of saturated fatty acyl chains in OMVs was higher as compared with the OM, making the OMVs more rigid (123). This suggests that membrane rigidity is associated with OMV biogenesis and could indicate that bacterial cells shed OMVs as a way to maintain the fluidity of their OM and increase survival under different growth conditions (123).

1.5.4.3 Virulence-associated composition of OMVs

Conditions that exert stress upon bacteria, including growth phase (124), temperature (98), media composition (125), iron availability (126), anoxic conditions (127), and antimicrobial exposure (98, 128) can alter the composition of OMVs (101, 129). In many cases, in addition to OM components, OMV proteomes reveal IM and cytosolic components as well as genetic material like DNA and RNA even after rigorous preparation and purification of samples (97). These bacterial OMVs have virulence-associated activities and are often found to be enriched for active toxins that can be delivered to host cells. In pathogenic strains, virulence factors such as enzymes (proteases, lipases, ureases, and cellulases), molecular chaperones (Hsp 60), toxins (Shiga toxin, heat labile enterotoxin, cholera toxin) and fimbriae can be partitioned into OMVs (101). Proteomic analysis of *Campylobacter jejuni* OMVs identified 151 proteins, including the cytolethal distending toxin that causes the symptomology of gastroenteritis (130). *C. jejuni* OMVs possess cytotoxic activity and induce a host immune response from intestinal epithelial cells after coincubation, demonstrating that these OMVs are able to deliver the toxin to host cells without the involvement of the whole bacterial cell (130). Other toxins associated with OMVs include the heat labile enterotoxin produced by enterotoxigenic *E. coli*, cytolysin A (ClyA) produced by *E. coli*, leukotoxin produced by *Actinobacillus actinomycetemcomitans*, vacuolating toxin (VacA) produced by *H. pylori*, and the Shiga toxin produced by *E. coli* O157:H7 and *Shigella dysenteriae* (74). In some cases, OMVs are found to carry the enzyme β-lactamase, which converts β-lactam antibiotics (penicillins and cephalosporins) into

microbiologically inactive and/or therapeutically inffective compounds (90, 101, 122). This vesicle-transported β-lactamase enzyme has been observed to protect not only the producer organism (*P. aeruginosa*) but also other bacteria known to co-occur in the human respiratory tract (90). Recently it has also been demonstrated that vesicle-associated β-lactamases produced by some members of the Bacteroides spp (e.g., *Salmonella typhimurium*) are able to protect from the third-generation cephalosporin cefotaxime (131).

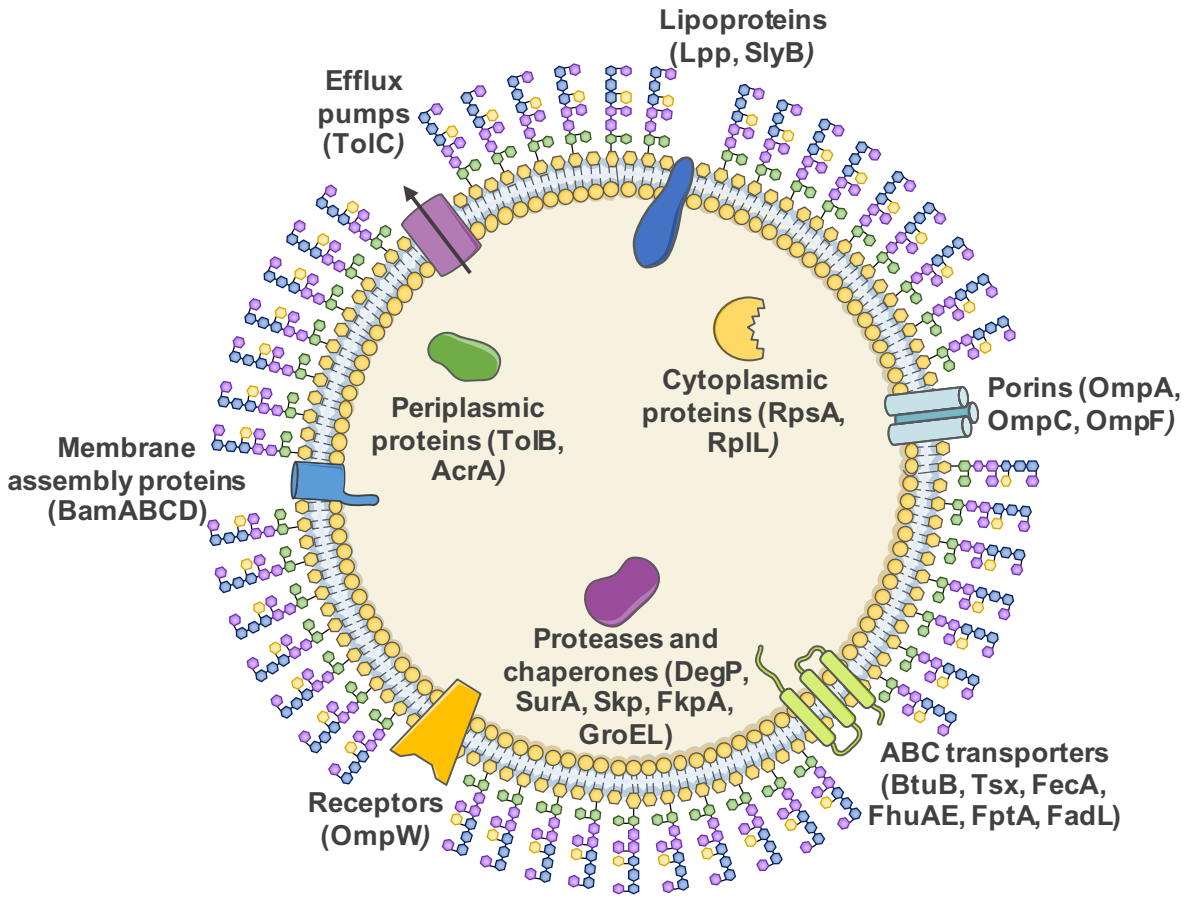

Figure 1.5. Model of an *E. coli* OMV showing representative proteins and functions identified by mass spectrometry studiesOM protein systems, including porins, efflux pumps, ABC transporters, membrane assembly proteins, OM receptors and OM lipoproteins as well as soluble proteins including periplasmic chaperones and proteases are found in high abundance in OMV samples. In addition, mass spectrometry also identified a number of cytoplasmic proteins in OMVs, including ribosomal proteins involved in synthesis (86, 120, 121, 132–134).

1.5.5 OMV isolation and purification methods

Given the many physiological functions of OMVs, it is of great importance to develop methods in order to study OMVs in a replicable way that maintains their integrity. The current challenge in OMV research has been to develop methods to isolate enough OMVs to reproducibly analyze heterogenous populations of various sizes, densities, and cargo contents to answer specific research questions. This is challenging due to their extremely low rate of production in normal cell populations, resulting in low yield from bacterial cultures. The following sections will describe the current methods available to isolate OMVs, as well as ways that OMVs can be induced and purified for study.

1.5.5.1 Isolation of OMVs

In order to obtain sufficent amounts of OMVs to study, large scale methods have traditionally been used to grow bacterial cells and isolate their OMVs. OMVs are typically isolated by differential centrifugation and filtration, to remove whole cells, cell debris, large protein and membrane aggregates, followed by concentration via diafiltration or precipitation (135). Most studies grow cultures of bacteria up in large flasks to stimulate aeration and grow them until they reach late logarithmic or early stationary phase (85, 135, 136). At this point the sample is typically put through one round of low speed centrifugation to remove whole cells and sterile filtration to remove any residual bacteria (85, 135). It is important that the filtration step correlates with the size of the bacteria, as a small filter such as a typical 0.22 μm sterilization filter will capture OMVs at the upper end of the size range (~200-300 nm) and reduce the overall yield of the OMV product (135). This could also potentially skew analysis for the size and contents of OMVs.

Studies typically follow this filtration step either with repeated ultracentrifugation (UC) to pellet the OMVs from the supernatant of the culture, or chemical precipitation to isolate OMVs (135, 137). Ultrafiltration or ultradiafiltration (UF) is also used in some studies to concentrate large volumes of culture supernatent before one final ultracentrifugation step to pellet OMVs (135). UC or UF are generally preferred over precipitation, as they are the least selective for products. For UC, supernatant samples are

generally concentrated by repeated centrifugation at ~40,000 rpm for several hours, followed by consolidation of samples and a final centrifugation run. Precipitation involves the addition of a high concentration of salt into a protein solution, to perturb the hydrogen bonds and cause aggregation of the proteins (80). Ammonium sulphate is ideal for OMV isolation due to its solubility in water and ionic strength (80). To perform a precipitation, solid $(NH_4)_2SO_4$ is added to the bacterial supernatant while stirring at 4˚C, followed by reconstitution by dialysis against a buffer like phosphate buffered saline (80). For UF, the bacterial supernatent is passed through a low molecular weight cutoff membrane (~50-100 kDa) to remove the majority of the supernatant and non-OMV associated proteins and debris (135).

1.5.5.2 Induction of OMVs

As one of the issues with OMV isolation is the low yield, several methods exist to induce OMV formation. OMVs can be induced by addition of detergents such as deoxycholate or sodium dodecyl sulfate (SDS), extracting agents such as ethylenediaminetetraacetic acid (EDTA) sub-lethal concentrations of antibiotics, or by sonicating bacteria to disrupt the membrane (82, 138–140). Additionally, genetic modifications can also be used to stimulate increased OMV production, which is discussed further in Section 1.5.3. Importantly, while these methods do increase OMV formation, they can also affect the resulting OMV's size, stability, and composition, which may affect their function both *in vitro* and *in vivo.*

1.5.5.3 Purification of OMVs

Purification methods are sometimes used in OMV studies in order to separate OMVs from other extracellular materials like flagella, fimbriae, pili, and large protein complexes or aggregates (80). For the purification of OMV samples, density gradient centrifugation or gel filtration are the preferred methods cited in the literature (116, 141). Density-gradient centrifugation involves mixing the crude OMV sample with high density gradient medium such as iodixanol, sucrose, or dextran, and overlaying it with step gradients of lower-density solutions (135). During centrifugation, the OMVs will migrate and equilibrate into a position according to their buoyant density, and after centrifugation individual fractions are collected

and analyzed for their OMV components (135). Gel filtration is another method for purifying OMVs, especially when high purity and high size homogeneity is required as in vaccine preparation (135). Gel filtration chromatography separates macromolecules like proteins on the basis of size, by allowing molecules to move through a column of porous beads composed of dextran polymers (Sephadex), agarose (Sepharose), or polyacrylamide (Sephacryl or BioGel P), diffusing into the beads to greater or lesser degrees (135). The pore sizes of these porous beads can be used to estimate the dimensions of the macromolecules, however, with greater variability in OMV sizes the fractions will be less defined (135).

1.6 Thesis objectives and hypotheses

The ability of Gram-negative bacteria to alter the composition of their OM in response to environmental conditions is essential to their survival (45). As reviewed above, Gram-negative Enterobacteria have developed various tolerance mechanisms to CAs that involve efflux pump, lipid alterations and changes in porin proteins within the membrane that reduce the overall anionic charge of the membrane, making it harder for CAs to bind and perturb the membrane (43). As OMVs are a product of the bacterial OM, and impacted by environment and stressors, including antimicrobials, we propose that OMV production and composition may be altered in CA-tolerant strains of Enterobacterales, but to date no studies have investigated this phenomenon.

To address this gap in knowledge, the aim of this thesis was to determine the effect of CA exposure on OMV production and composition in CA-tolerant and CA-susceptible (wild-type) strains of *E. coli.* We hypothesize that CA-tolerant strains of *E. coli* will have increased OMV production when compared to CA-susceptible strains. We also hypothesize that the CA-tolerant strains will have membrane modifications acquired during CA adaptation that will influence the lipid and proteomic contents of the resulting CA-adapted OMVs. To test this hypothesis, the following questions were examined in Chapters 3 to 4 of this thesis:

1. What OMV isolation method is most effective for obtaining high yield heterogenous OMV populations with minimal impurities? (Addressed in Chapter 3)

2. Does a single-gene deletion mutant affecting cell membrane integrity increase OMV production compared to a wild-type control strain? (Addressed in Chapter 3)
3. Do CA-adapted strains of *E. coli* produce more OMVs compared to a susceptible wild-type control strain? (Addressed in Chapter 4)
4. Are there differences in lipid and protein contents between OMVs isolated from CA-adapted strains and a wild-type control? (Addressed in Chapter 4)
5. Are OMVs isolated from CA-adapted strains able to increase or decrease susceptibility against CAs when they are supplemented into cultures of wild-type or CA-adapted strains of *E. coli*? (Addressed in Chapter 4)

To address these questions, we evaluated two common methods for OMV isolation from bacterial cultures with a single-gene deletion mutant from the Keio collection and a laboratory control strain of *E. coli* (Chapter 3). We compared OMV production and composition of several CA-tolerant strains developed by the Bay lab through a gradual exposure method (Chapter 4). We measured the total protein and phosphorous for each sample to compare OMV production, and quantified particle counts using nanoparticle tracking analysis and dynamic light scattering (Chapter 3/4). We visually asssessed each strain's OMV production and morphology further using electron microscopy. In addition, we performed mass spectrometry on proteins isolated from OMV samples in order to determine whether these contents had changed due to CA-adaptation (Chapter 4). Antimicrobial susceptibility (AST) was assessed by supplementing bacterial cultures with pure OMV samples in 96-well plates and performing growth curves and minimal inhibitory concentration (MIC) assays. Together, my thesis results show that CA exposure does increases the formation of OMVs, and the OMVs produced by each CA-adapted strain are unique, each with distinct morphologies, phenotypic and compositional characteristics that we suggest are the result of genetic differences between the CA-adapted strains that are specific to each CA's mechanism of action.

Chapter 2. Materials and Methods

The methods described in this section were all conducted by Shelby Reimer, with the exception of the dynamic light scattering (DLS), cryogenic transmission electron microscopy (cryo-TEM) and nanoscale liquid chromatography tandem mass spectrometry (nano-LC-MS/MS) procedures. DLS samples were prepared by Shelby Reimer for experimental analysis by Wyatt Technology Corporation. OMV samples for cryo-TEM were prepared by Shelby Reimer, where the preparation of cryo-TEM quantifoil was conducted by Dr. Dan Beniac at the National Microbiology Laboratory (NML) in Dr. Timothy Booth's lab (Director of Viral Diseases Division, NML) with assistance from Shelby Reimer. All cryo-TEM imaging in this chapter was conducted by Shelby Reimer, with technical assistance from Dr. Dan Beniac, and Shannon Hiebert. OMV samples for proteomic analysis were prepared by Shelby Reimer, and protein sample preparation, nano LC-MS/MS and raw data collection and processing were performed by Drs. Patrick Chong and Stuart McCallister (Proteomics Core, NML) in collaboration with Dr. Garrett Westmacott's lab (Chief of Mass Spectrometry and Proteomics, NML). The methodological comparison between ultradiafiltration and ultracetrifugation of *E. coli* BW25113 and JW0729 (Δ*tolA*) in this section was recently published in the manuscript (1) in February 2021 and some method descriptions are directly included from this article in these sections.

2.1 Bacterial strains, chemicals, and antimicrobials

The bacterial strains used in this thesis are detailed in Table 2.1. The wildtype *E. coli* K-12 BW25113 (WT) strain and its corresponding single gene deletion mutants from the Keio collection (9) were obtained from the Coli Genetic Stock Center (Yale University, New Haven, CT). The CA-adapted strains (CETR, CHXR, COLR) were previously generated by Dr. Nicola Cartwright following a gradual adaptation method by Bore *et al* (142–144). For these strains, *E. coli* K-12 BW25113 was repeatedly subcultured with sub-inhibitory concentrations of each CA (CET, CHX, COL) in triplicate, generating three strains CHXR, CETR, and COLR with decreased susceptibility as compared to WT (≥2 -fold increased MIC) (143). All

chemicals and antimicrobials were purchased from Millipore Sigma (Massachusetts, USA), Fisher Scientific (New Hampshire, USA), or TCI America (Oregon, USA).

2.2 Media, Growth

Unless otherwise noted, all *E. coli* strains were grown in lysogeny broth (LB) in accordance with Cold Spring Harbour Protocols (145). To culture *E. coli*, a pipette tip was used to scrape a small amount of frozen cells from a 16% w/v dimethyl sulfoxide (DMSO) stock stored at -80˚C, and the scrapings were suspended in liquid LB broth in test tubes. Aspetically inoculated tubes were incubated at 37°C in a shaking incubator at 170 RPM overnight unless otherwise specified. To maintain antimicrobial selection for the three different CA-adapted strains (CHXR, COLR, and CETR) the following concentrations were added to the growth medium of these strains; CHX (2.4 μg/mL) CET (40 μg/mL), and COL (100 μg/mL).

Table 2.1 *E. coli* strains used in this study.

Name	Strain	Genotype	Antimicrobial MIC (µg/mL)	Source
WT	*E. coli* K-12 BW25113	Wild type parental strain from Keio collection. F-, *Δ(araD-araB)567, ΔlacZ4787(::rrnB-3), λ-, rph-1, Δ(rhaD-rhaB)568, hsdR514*	CET (30) CHX (2.0) COL (1.0)	CGSC
Δ*tolA*	*E. coli* K-12 JW0729-3	F-, *Δ(araD-araB)567, ΔlacZ4787(::rrnB-3), ΔtolA788::kan, λ-, rph-1, Δ(rhaD-rhaB)568, hsdR514*	-	(9)
CETR	*E. coli* CETR R1 G40	*E. coli* K-12 BW25113 adapted to 101 µg/mL CET	CET (240)	(143)
CHXR	*E. coli* CHXR R1 G20	*E. coli* K-12 BW25113 adapted to 2.4 µg/mL CHX	CHX (9.6)	(143)
COLR	*E. coli* COLR R1 G32	*E. coli* K-12 BW25113 adapted to 110.2 µg/mL COL	COL (300)	(143)

Abbreviations: CHX; CHX, CHXR; CHX-tolerant strain, COL; COL, COLR; COL-resistant strain, CET; CET, CETR; CET-tolerant strain, R1; Bioreplicate 1, G20; 20th subcultured generation, G32; 32nd subcultured generation, G40; 40th subcultured generation, MIC; minimum inhibitory concentration.

2.3 Growth rate measurements of various strains in this study

As discussed in Chapter 3, to ensure that OMV production was not associated with impaired growth phenotypes, optical density (OD) growth curves of all strains were performed. Bacterial cells were inoculated into LB broth from frozen cryostocks and grown overnight. The resulting culture was standardized to 1.0 OD_{600nm}, and diluted 1/100 in LB into flat-bottom 96-well polystrene NUNC™ microtitre plates (Thermo Fisher Scientific, USA). Strains were grown for 24 hours (h) in LB media at 37˚C with continuous shaking, where OD_{600nm} was measured every 2 h in a BioTek EL808 microplate reader (BioTek, Vermont, USA). Growth of each strain was measured in triplicate from 6 biological replicates (n=6). In Chapter 3, Mann-Whitney U tests were performed to determine OD_{600nm} values that differed significantly ($p < 0.05$) from WT at all time points, and in Chapter 4, two-way ANOVA with Dunnett's multiple comparisons tests were used to determine significance of CA-adapted strains compared to WT ($p < 0.05$).

2.4 Isolation of OMVs

OMVs from the strains listed in Table 2.1 were isolated for further analysis in Chapters 3 and 4. OMVs were isolated from culture supernatants as described by previous methods with slight modifications summarized below (Figure 2.1) (85, 120, 133). Briefly, *E. coli* cells were inoculated into LB broth from frozen cryostocks and grown overnight (18 h). The resulting culture was standardized to 1.0 OD_{600nm} unit, washed two times with LB to prevent carryover of OMVs, and diluted 1/100 into 1 L of LB broth. This culture was incubated at 37˚C for 18 h with constant shaking (160 RPM). OD_{600nm} measurements were monitored to confirm early stationary growth phase OD_{600nm} values in reference to the growth curves performed in section 2.3. Cells were separated from the culture by centrifugation at 6,000 RPM for 15 min at 4˚C in an JLA9.1000 rotor using an Avanti J-E High Speed centrifuge (VWR Part of Avantor, USA). The collected supernatant was filtered with a 0.45 µm polyethersulfone (PES) vacuum filter (MilliporeSigma, USA) to remove any residual bacteria. Filtered supernatant aliquots from each strain preparation were spread plated onto LB agar and incubated at 37˚C for 24 h to confirm the absence of intact,

viable cells. In results Chapter 3, the resulting supernatant filtrate was divided into two equal parts to be assessed by both ultracentrifugation (UC) and ultradiafiltration (UF) methods. In Chapter 4, only ultradiafiltration was used to isolate OMVs, both methods are summarized below.

2.4.1 Ultracentrifugation (UC) OMV isolation

The designated UC filtered supernatant was centrifuged at 40,000 RPM in polycarbonate tubes for 2 h at 4°C in a Ti70 rotor using a Beckman Coulter® Optima XPN Ultracentrifuge (VWR Part of Avantor, USA). The supernatant was carefully decanted to prevent pellet disruption. After all the filtrate had been centrifuged, the pellets in each tube were resuspended in 200 µL 50 mM 4-(2-hydroxyethyl)-1-piperazineethanesulfonic acid (HEPES) buffer (Fisher Scientific, New Hampshire, USA) then stored at -20°C (146).

2.4.2 Ultradiafiltration (UF) OMV isolation

The designated UF filtered supernatant was concentrated 50-fold in 50 mM HEPES buffer in a 400 mL capacity Amicon® stirred cell (MilliporeSigma, USA) ultradiafiltration system using a 500 kiloDalton (kDa) molecular weight cut off (MWCO) polyethersulfone (PES) ultrafiltration disc (MilliporeSigma, USA). The concentrated retentate was collected and divided into 30 mL capacity polycarbonate centrifuge tubes (Beckman) before ultracentrifugation at 40,000 RPM for 2 h at 4°C. The pellet was resuspended in 200 µL 50 mM HEPES buffer and stored at -20°C until further use (146).

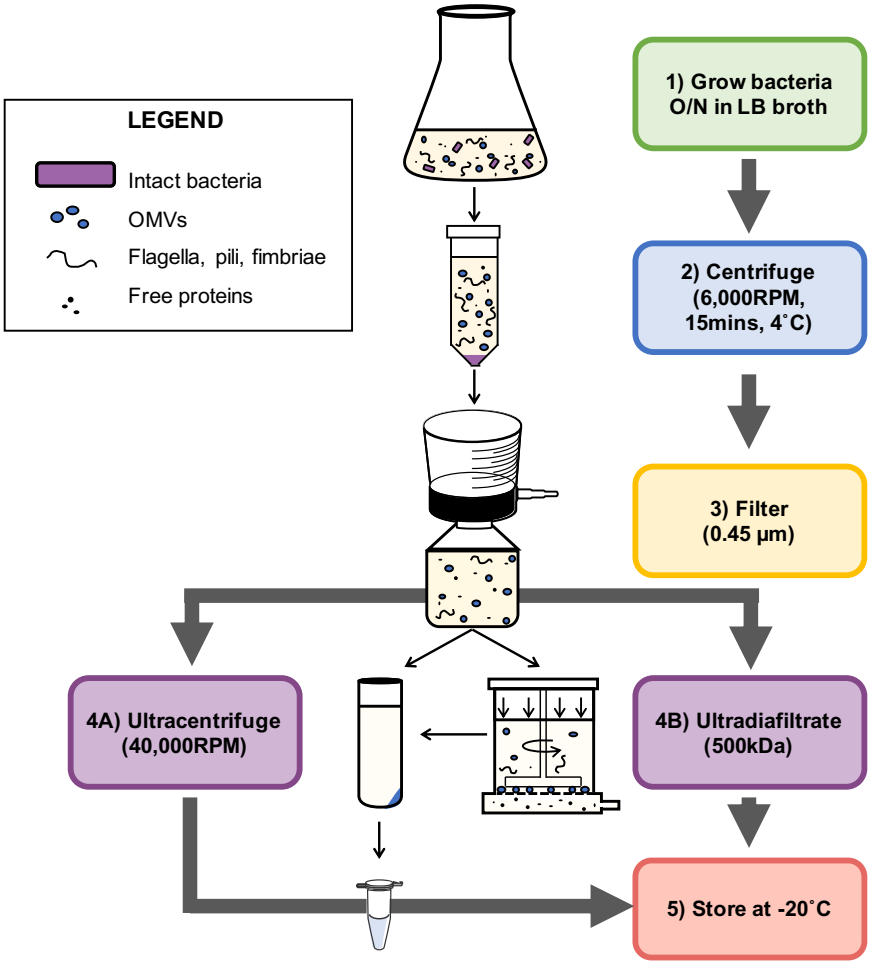

Figure 2.1. Workflow diagram of the isolation of OMVs from *E. coli* used in this project.Vesicle isolation involved the following steps: **1)** cultivation of bacterial isolations to stationary phase (18hr); **2)** removal of intact bacteria by low-speed centrifugation (6,000 RPM); **3)** sterile filtration to remove any residual bacterial cells; **4A)** concentration of supernatant by ultracentrifugation (40,000 RPM) or **4B)** concentration by ultradiafiltration; and **5)** final ultracentrifugation to pellet OMVs and resuspension of the OMV pellet in 50mM HEPES buffer.

2.5 Quantification of OMVs

OMVs produced by *E. coli* cultures examined in Chapters 3 and 4 were indirectly quantified by protein and phosphate detection assays in order to approximate concentration as described in detail below.

2.5.1 OMV protein content determination

Protein concentrations were measured with a bicinchoninic acid (BCA) assay (Thermo Fisher Scientific, USA). This assay detects protein in an alkaline solution by the colourmetric detection of Cu^{1+} by BCA in a two-step reaction. This BCA/copper complex exhibits a linear absorbance with increasing protein concentrations at 562 nm (A_{562nm}) . Due to the high number of samples to measure, OMV protein detection used a microplate procedure, where the sample to working reagent ratio was 1:8. Briefly, samples were diluted 1/5 into a microplate, and combined with the working reagent supplied by the kit. Plates were incubated at 37˚C for 30 min and the A_{562nm} was read using a BioTek EL808 microplate reader (BioTek, Vermont, USA). Samples were measured in triplicate and concentrations were determined from a standard curve plot of serial diluted bovine serum albumin (BSA).

2.5.2 OMV phosphate content detemination

Lipid content was inferred by measuring the OMV total phosphate content using a malachite green phosphate detection assay (Millipore Sigma, USA). This assay quantifies the amount of phosphate in phospholipids, protein, and DNA based on the colourmetric reaction between malachite green, molybdate, and free orthophosphate under acidic conditions. The malachite green phosphomolybdate complex is measured at an A_{620nm}. Samples were measured in triplicate and compared against a plotted standard curve of serial diluted dibasic potassium phosphate (K_2HPO_4).

2.5.3 OMV concentration calculations to adjust for culture volumes

In Chapter 3, to appropriately compare the protein- or phosphate-based OMV content measurements when comparing mutant and WT OMV production, all values were adjusted for the amount of bacterial cells in the culture according to the following two equations.

EQ1a: $[\text{Protein}]_{\text{Sample}} = (A_{562\ nm} - B) / A$

EQ1b: $[PO_4^{3-}]_{\text{Sample}} = (A_{620\ nm} - B) / A$

Equation 1 (EQ1) calculates the OMV sample's protein and phosphate concentrations based on standard curves of bovine serum albumin (BSA) protein (EQ1a) and potassium phosphate (EQ1b) titrations, where the sample OD unit value at the measured wavelength ($A_{562\ nm}$ or $A_{620\ nm}$) is subtracted from the respective absorbance y-intercept (B) value from the standard curve, which is divided by the slope of the respective standard curve (A).

EQ2a: Adjusted $[\text{Protein}]_{\text{Sample}} = [\text{Protein}]_{\text{Sample}}$ / original culture CFU/mL

EQ2b: Adjusted $[PO_4^{3-}]_{\text{Sample}} = [PO_4^{3-}]_{\text{Sample}}$ / original culture CFU/mL

Equation 2 (EQ2) adjusts for the number of cells in the original culture by dividing the OMV sample's protein or phosphate concentrations determined from EQ1 by the OD_{600nm} of the original culture converted to colony forming units (CFU) per mL that the OMV isolations were obtained from.

2.6 Tricine sodium dodecyl sulphate-polyacrylamide gel electrophoresis (Tricine SDS-PAGE)

In Chapters 3 and 4, OMV preparation protein profiles were compared to the WT OMVs using the following Tricine SDS-PAGE method. OMV preparations were denatured for 10 min at 65˚C in 2 X Laemmli buffer (100 mM dithiothreitol, 150 mM Tris (pH 7), 12% w/v SDS, 30% w/v glycerol, 0.05% w/v Coomassie Brilliant Blue G-250), cooled for 10 min, and separated by 12% Tricine SDS-PAGE gels. A broad-range protein marker (BioRad, USA) was loaded alongside the samples and electrophoresis was performed at 30 V for 30 min or until the dye front reached the separating gel, and then at 80 V for 1.5 hr or until the dye front ran completely off the gel. Proteins were visualized with 0.5% v/v 2,2,2-trichloroethanol (TCE) by ultraviolet detection (147) or by Coomassie Blue staining. Before staining, the gel was fixed for 1 h in a solution of 10% MeOH and 7% acetic acid, followed by staining with Coomassie blue overnight at 4˚C, and an additional 1 h of fixation. Coomassie proteins were detected under ultraviolet

(UV) light. To quantify proteins, band densities were densitometrically analyzed using ImageJ software version 1.51 (https://imagej.nih.gov/ij/) and quantified as described in (148).

2.7 Western blotting of outer membrane protein A

Following Tricine SDS-PAGE separation, protein sample were blotted onto a nitrocellulose membrane for 1 hour at 100 milliAmps using an electroblotting apparatus (Bio-Rad, USA) in the presence of transfer buffer. Protein samples for western blot were loaded with a Spectra Multicolor Broad Range Protein Ladder (Thermo Fisher Scientific, USA). After blotting, membranes were blocked with 5% (w/v) milk powder in TBS for 1 h. The nitrocellulose membrane blot was incubated with Anti-Gram-negative bacterial OmpA primary rabbit antibody at 1:25000 dilution (1.2 µg/mL; Antibody Research Corporation, Missouri, USA) overnight at 4˚C followed by incubation with goat anti-rabbit IgG (Heavy+Light) horseradish peroxidase (HRP) conjugate antibody at a 1:500 dilution (0.4 µg/mL; Life Technologies, USA) for 1 h. OmpA was detected using an enhanced chemiluminescence (ECL) detection system kit (Thermo Fisher Scientific, USA) according to the manufacturer's detection protocol. Blot band densities were densitometrically analyzed using ImageJ software version 1.51 (https://imagej.nih.gov/ij/) and quantified as described in (148).

2.8 Broth microdilution antimicrobial susceptibility testing (AST)

In Chapters 3 and 4, AST was carried out as follows. Cryopreserved bacterial stocks were grown overnight (18hr) in LB broth in three biological replicates. The next day, cultures were standardized to OD_{600nm} = 1.0 spectrophotometrically, and diluted 10^{-2} into NUNC 96-well plates (Thermo Scientific, USA) containing serial two-fold dilutions of antimicrobials in LB broth. Plates were incubated at 37˚C for 16 h with shaking at 160 RPM, and the optical density of cultures (OD_{600nm}) was read using a plate spectrometer (Multiskan^{TM} spectrum, Fisher Scientific, USA). MIC values were defined by the lowest concentration of antimicrobial with no observable growth ($OD_{600nm} \leq 0.05$), and results were represented graphically by the mean ± standard deviation (SD) of three biological replicates performed on the same day.

2.8.1 OMV supplementation AST

To evaluate whether OMVs have protective effects against CAs, we conducted MIC testing on WT and CA-adapted strains with exogenous supplementation of isolated OMVs. To accomplish this, we prepared 96-well plates with two-fold dilutions of CAs (prepared in 2X LB) and 1.0 µg/mL or 2.0 µg/mL OMVs in dH_2O. Except for the addition of OMVs to cultures, AST was performed and measured as described in Section 2.8 above.

2.9 NanoSight Nanoparticle tracking analysis

OMV quantity and size distributions were determined using a NanoSight NS500 nanoparticle tracking (NTA) instrument (Malvern Instruments Ltd., UK) equipped with a 488 nm blue laser and a complementary metal-oxide semiconductor image sensor camera. OMV samples were thawed to room temperature prior to analysis and diluted 10^{-3} in 50 mM HEPES buffer at pH 7.4. Polystyrene beads (100 nm diameter) and HEPES buffer alone were run as positive and negative control standards, respectively. Samples were infused into the NanoSight instrument using a syringe pump set at '20' speed setting (in arbitrary units). Measurements were captured in five 60 seconds reads at ambient room temperature (23.9–25.2°C), with instrument-optimized settings, where 'blur', 'minimum track length', and 'minimum expected size' options were set to "automatic" and viscosity was set to "water" (0.883–0.911 cP). Automated image setup (camera level and focus) was chosen whenever available for video enhancement. A total of 1498 frames per sample were analyzed with NTA software version 2.3 (Malvern Instruments Ltd., UK) with a detection threshold of 5 (in arbitrary units). Mean size (nm), mode size (nm), and concentration (particles/mL) were tabulated, and the average of five reads was calculated and plotted as particle size versus number of particles per mL.

2.9.1 OMV stability after repeated freeze-thaw cycles

To ensure that OMV sizes and quantities were not unduly altered if samples sat over time at room temperature or after multiple rounds of freeze-thawing, NTA was performed on WT OMV samples under

various conditions. This was important to determine the long-term integrity and stability of vesicles during repeated lengthy analyses and for laboratory storage (149–151). WT OMV samples were thawed (from -20˚C storage) to room temperature prior to analysis and diluted 10^{-3} in 50 mM HEPES buffer at pH 7.4. HEPES buffer alone was run as a standard. Samples were measured by NTA as described in section 2.9.0, and the results were compiled for particle size data and binned concentration data.

2.10 Dynamic Light Scattering

In Chapter 4, dynamic light scattering was used to determine the hydrodynamic radius (r_H) of OMV samples from WT and CA-adapted strains. OMV samples were isolated in triplicate by UF as described in Section 2.4 and 2.4.2 and were quantified by BCA assay as described in Section 2.5.1. OMV samples were diluted to a range of 200 - 500 μg/mL protein per sample (to obtain final particle concentrations of ~10^8-10^9 particles/mL) prior to sending OMVs to Wyatt Technology for analysis. All samples were measured at 10×, 100×, and 1000× dilution with provided HEPES buffer by Wyatt Technology. Each dilution was measured in triplicate. Measurements were performed using a DynaPro Plate Reader III (Wyatt Technology, Santa Barbara, California) at 25.0˚C in an Aurora 384-well plate (Wyatt Technology, Santa Barbara, California). Data processing including autocorrelation was automatically performed by the software supplied with the instrument (Dynamics v.8).

2.11 Cryo-transmission electron microscopy

In Chapters 3 and 4, samples for cryo-TEM were prepared as described above for OMV isolation, with the exception that CA-adapted and Δ*tolA* OMV samples were diluted 10-fold in 50 mM HEPES buffer (pH 7.4) due to their higher concentration of OMVs as compared to WT samples. All sets of samples were combined with 10 nm diameter BSA-labelled gold tracer in a 6:1 ratio to assist with automated focusing. With assistance from Dr. Dan Beniac, 3 μL of this suspension was applied to freshly glow-discharged Quantifoil R 2/2 grids (Quantifoil Micro Tools GmbH, Germany). This suspension was allowed to adhere to the grid, and the excess liquid was blotted with standard Vitrobot filter paper (Ted Pella Inc., USA) using

a Vitrobot Mark IV (Thermo Fisher Scientific, USA), operating at 5ºC and 100% humidity. Grids were then frozen in liquid ethane cooled by liquid nitrogen. Samples were transferred to a Tecnai F20 transmission electron microscope (Thermo Fischer Scientific, USA) using a Gatan 626.DH low-temperature specimen holder (Gatan Inc., USA), and images were recorded using an Eagle 4k CCD camera (Thermo Fisher Scientific, USA). Images were taken in low-dose imaging conditions (10 e/Å^2) at both 5,000X and 14,500X magnifications, and vesicle sizes and morphologies were analyzed using ImageJ software version 1.51 (152).

2.12 Protein quantification by nano LC-MS/MS

2.12.1 Sample preparation

In Chapters 3-4, samples used for proteomic analysis were prepared from 1 L cultures as described for the OMV isolation using the UF method (Section 2.4.2). Protein from isolated OMVs were quantified using a BCA protein assay kit, with BSA as the standard (Thermo Fisher Scientific, USA). SDS was added to 100 µg of OMV protein at a final concentration of 2% (w/v), and then heated at 95ºC for 5 minutes. Upon cooling to room temperature, dithiothreitol was added to a final concentration of 100 mM, and heated at 95ºC for 5 minutes. Samples were frozen at -80ºC until ready for measurement. To generate peptides, protein samples were digested with trypsin (Promega, USA) overnight using a filter-assisted sample preparation method described previously (153) using Nanosep 30K Omega Centrifugal Devices (Pall Corporation, USA). A total of 100 µg of protein from each OMV sample was used for each digestion. Following digestion, all samples were dried down and reconstituted using mass spectrometry grade water to a final concentration of 0.5 µg/µL prior to mass spectrometry analysis.

2.12.2 Nano LC-MS/MS

Samples were each separately analysed using a nano-flow Easy liquid chromatography II system connected in-line to an linear trap quadripole Orbitrap Velos mass spectrometer with a nanoelectrospray ion source at 2.2 (Thermo Fisher Scientific, USA). Peptide samples (2 µL) were loaded onto a C18-reversed

phase trap column (3 cm long, 100 µm inner diameter, 5 µm particles) with 100% buffer A (2% acetonitrile, 0.1% formic acid) for a total volume of 30 µL, and then separated on a C18-reversed phase column (15 cm long, 75 µm inner diameter, 2.4 µm particles). Both columns were packed in-house with ReproSil-Pur C18-AQ resin (Dr. Maisch) and fritted with Kasil. Peptides were eluted using a linear gradient of 5-25% buffer B (98% v/v acetonitrile, 0.1% v/v formic acid) over 120 min, 25%-40% buffer B for 5 minutes, 40%-80% buffer B for 5 minutes and a wash at 80% B for 8 minutes at a constant flow rate of 250 nl/min. Total LC-MS/MS run-time was about 165 minutes, including the loading, linear gradient, column wash, and the equilibration.

Mass spectrometry data was acquired using the following settings: Dynamically choosing the top 10 most abundant precursor ions from each survey scan, each isolated with a width 2.0 m/z and fragmentation by collision-induced dissociation. The survey scans were acquired in the Orbitrap over m/z 300-1700 with a target resolution of 60,000 at m/z 400, and the subsequent fragment ion scans were also acquired in the iontrap at a normal scan rate. The lower threshold for selecting a precursor ion for fragmentation was 2000. Dynamic exclusion was enabled using a m/z tolerance of 15 ppm, a repeat count of 1, and an exclusion duration of 30 s.

2.12.3 MS data processing

All LC-MS/MS spectra were processed using MaxQuant (v1.6.7, Max Plank Institute) using the imbedded Andromeda search engine Searches were performed against a subset of the SwissProt database set to E. coli K12 (4519 sequences). The following search parameters were used: Carbamidomethyl (C) was selected as a fixed modification, Oxidation (M) and Acetyl (Protein N-term) as variable modifications, fragment ion mass tolerance of 0.5 Daltons (Da), parent ion tolerance of 20 ppm, and trypsin enzyme with up to 2 missed cleavage. False discovery rates were set up using 0.01 for peptides, 0.01 for proteins, and at least 1 razor peptide per protein. Label-free quantitation (LFQ) was enabled for MS/MS quantitation. The resulting LFQ intensities were imported into Perseus v1.6.5 (Max Plank Institute) software for analysis. In Perseus, the MS peptide data was Log2 transformed. Then all the proteins that did not have a least 3 valid

log2 LFQ intensities from identification analysis were filtered out and excluded from further analysis. Search results were imported into Scaffold Q+ (v4.11.0). Proteins were filtered using a 1.0% false discovery rate and assessed for significance using Fisher's exact test (p-value < 0.05). All significant proteins were annotated by their subcellular localization using the pSORTb algorithm (154). In Chapter 4, gene ontology (GO) enrichment analysis of proteins identified in WT and CA-adapted OMV samples was conducted by the Database for Annotation, Visualization and Integrated Discovery (DAVID) v.6.8 (https://david.ncifcrf.gov).

2.13 Statistical analysis

All data, excluding the proteomic LC-MS/MS data, was statistically analyzed using Graph Pad Prism 8 software (v8.4.2). The normality of data was assessed for cryo-TEM and NTA data using the Shapiro-Wilk and Kolmogorov-Smirnov test. Statistical significance for growth curve data was determined by the Mann-Whitney U test, and significance for cryo-TEM and NTA data was determined by the Student's *t*-test.

2.14 Data Visualization

Figures for all data, excluding the proteomic LC-MS/MS data, were created using Graph Pad Prism 8 software (v8.4.2) using line graph, bar graph, and scatterplot settings. Scale bars were added to cryo-TEM figures in ImageJ software version 1.51 (152) and vesicle type insets were created using Microsoft PowerPoint version 16.52. Venn diagrams in Figure 3.7 and Figure 4.9 were created using Microsoft PowerPoint version 16.52. String protein networks in Chapter 3 were generated using the StringApp v1.5.0 in Cytoscape version 3.8.0 software (155), where inside colours represent presence of protein in WT (blue), Δ*tolA* (green), or both (purple) vesicle samples, and border colours represent protein abundance, with dark green borders denoting upregulation of the protein in the Δ*tolA* sample, and dark blue borders denoting upregulation of the protein in the WT sample. Functional protein KEGG network maps shown in Chapter 3 were constructed using the ClueGo plugin (v2.5.6) add-in software for Cytoscape (v.3.8.0) with default settings (156), where default parameters were used for network

specificity. Bolded black terms below black nodes represent functional categories, and coloured nodes represent proteins with the colour of each node indicating the OMV sample it was found in. Connecting edge lines represent multiple functional categorizations of proteins. Heatmap images in Chapter 4 were made with “R” statistics software v.4.0.5 using the ggplot2 and heatmap functions, where proteins were sorted according to their annotated cellular locations and reordered by peptide mass intensity values. The gene ontology (GO) enrichment figure in Chapter 4 was created by exporting DAVID results into Graph Pad Prism 8 software (v8.4.2), and colour-coding functional categories.

Chapter 3. Comparative analysis of outer membrane vesicle isolation methods with an *Escherichia coli tolA* mutant reveals a hypervesiculating phenotype with outer-inner membrane vesicle content

The results and discussion portion of this chapter was recently published in the manuscript (1) in the journal Frontiers in Microbiology in February 2021. Shelby Reimer isolated the OMVs and performed growth curves, protein/phosphate assays, NTA and western blots. OMV samples for cryo-TEM were prepared by Shelby Reimer, where the preparation of cryo-TEM quantifoil was conducted by Dr. Dan Beniac (NML) in Dr. Timothy Booth's lab (Director of Viral Diseases Division, NML) with assistance from Shelby Reimer. All cryo-TEM imaging in this chapter was conducted by Shelby Reimer, with technical assistance from Dr. Dan Beniac, and Shannon Hiebert. OMV samples for proteomic analysis were prepared by Shelby Reimer, and protein sample preparation, nano LC-MS/MS and raw data collection and processing were performed by Drs. Patrick Chong and Stuart McCallister (Proteomics Core, NML) in collaboration with Dr. Garrett Westmacott's lab (Chief of Mass Spectrometry and Proteomics, NML). The mass spectrometry proteomics data have been deposited to the ProteomeXchange Consortium via the PRIDE partner repository with the dataset identifier PXD022786 and 10.6019/PXD022786. All data analysis and figure preparation was done by Shelby Reimer. Editing of this paper/section was done by Shelby Reimer and Dr. Denice Bay.

3.1 Aims, hypotheses and approaches

This goal of this study was to evaluate two of the most commonly used OMV isolation techniques, UC and UF with an *E. coli* K-12 BW25113 strain (WT) and JW0729 (Δ*tolA*), a mutant containing a single-gene deletion of TolA component in the Tol-Pal system. Δ*tolA* was selected for comparison as previous studies (85, 103) identified that this deletion mutant confers a hypervesiculating phenotype when compared to the WT *E. coli* strain. In our study, we compare OMVs isolated from both strains using UC and UF methods (Section 2.4) and measure the yield and size of vesicles with NTA (Section 2.9). NTA allows for

rapid analysis of nanoparticles in solution by combining laser light scattering microscopy with a charge-coupled device camera to visualize particles, then employing software to relate particles moving under Brownian motion to particle size according to the Stokes-Einstein equation (157–159). Using NTA is advantageous to other OMV quantification methods as it allows for direct measurement of polydisperse samples, while the flow mode allows a large number of particles to be measured in a small timeframe, resulting in more accurate measurements with less variance (157, 158). Growth curves (Section 2.3), protein and phosphate measurements (2.5), SDS-PAGE and western blotting techniques (Section 2.6-2.7) were also used to assess the production of OMVs in WT and Δ*tolA* strains. Cryo-TEM analysis (Section 2.11) was used to visually determine OMV morphology and verify OMV size and total quantity produced by each isolation technique. Comparing OMV isolations from a WT as well as a hypervesiculating Δ*tolA* strain allowed us to explore the limits of each technique. We also employed nano-LC-MS/MS proteomic analysis to compare the protein compositions of WT and Δ*tolA* vesicles (Section 2.12). The outcome of this analysis revealed that UC and UF methods are similar with the exception of OMV minimal size limits. It allowed us to provide the first in-depth characterization of Δ*tolA* mutant OMVs, which revealed not only an increase in Δ*tolA* OMV quantity but also Δ*tolA* vesicles with two (outer-IM vesicles; O-IMVs) or more membranes (multi-lamellar outer membrane vesicles; M-OMVs, grouped outer membrane vesicles; G-OMVs) by cryo-TEM visualization. Proteomic analysis of WT and Δ*tolA* OMVs demonstrated that Δ*tolA* OMVs possess more IM, PP, and CY proteins than WT, indicating that the loss of TolA may decrease linkages between the OM and IM and result in the formation of these unique vesicle morphologies, similar to phenotypes recently described in Δ*tolB* and Δ*tolR* mutants (107, 160).

3.2 Results

3.2.1 Comparison of vesicle production between ΔtolA and WT strains

The primary aim of this study was to compare two of the most commonly used UC and UF OMV isolation methods and in doing so, provide an opportunity to examine OMV production differences between an *E. coli* K-12 BW25113 strain and its hypervesiculating gene deletion Δ*tolA* mutant. Prior to UC and UF

OMV isolations, we wanted to ensure that OMV formation from WT and Δ*tolA* was proportional to the total quantity of cells grown in culture; this measurement was important to account for potential cell titre differences caused by in growth rate differences between the mutant and WT. To accomplish this, we measured the growth of each strain prior to OMV isolation (Figure 3.1). WT and Δ*tolA* growth rates were significantly different ($p < 0.05$) in OD at 600 nm (OD_{600nm}) unit values for all time points, and the maximum OD_{600nm} units for WT was 1.11 ± 0.03 and Δ*tolA* was 0.98 ± 0.02 after 24 h (Figure 3.1). Due to lower OD_{600nm} values of Δ*tolA,* we calculated OMV production yields based on total cells in CFU/mL from OD_{600nm} measurements of each culture in an effort to accurately compare WT and Δ*tolA* OMVs formation and quantity by UC and UF methods. For all comparisons made between UC and UF, a single large-scale bacterial culture was grown, and equally divided for UC and UF OMV isolations in order to minimize differences in OMV populations caused by batch growth effects.

After factoring in the cell growth differences of each strain, we compared differences in OMV production by each strain when isolated by UC and UF methods using NTA (Figure 3.2). NTA demonstrated statistically significant differences between WT and Δ*tolA* strains with respect to vesicle production. Both UC and UF methods confirmed greater Δ*tolA* OMVs quantities when compared to the WT based on particle/CFU calculations, corroborating previous studies on OMV production in Tol-Pal mutants (81, 103, 107, 160, 161). Specifically, UC had a 1.2-fold increase in Δ*tolA* OMVs compared to WT and UF had a 3.1-fold increase in Δ*tolA* OMVs compared to WT. NTA results also show fewer WT and Δ*tolA* OMVs were recovered by UC methods when compared to UF (WT; 24.8% reduction, Δ*tolA* 60.0% reduction; Figure 3.2C). Hence, isolating OMVs using UC and UF methods confirmed that the Δ*tolA* strain hypervesiculates when compared to WT grown under the same conditions, but UF methods recover more OMVs as compared to UC.

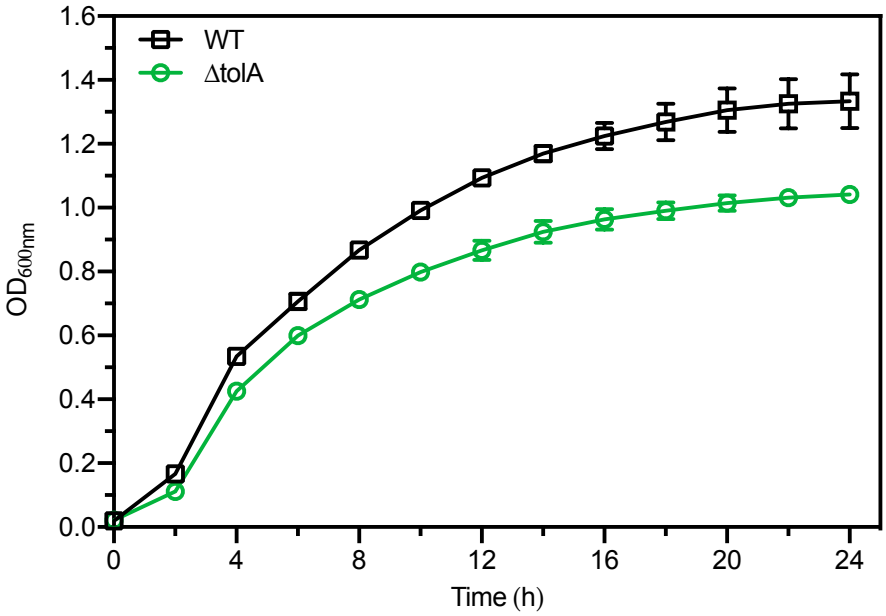

Figure 3.1. Growth curve analysis of *E. coli* BW25113 (WT) and JW0729 (Δ*tolA*) *E. coli* strains. $OD_{600\ nm}$ measurements (y-axis) are shown over time (h; x-axis) for WT (squares) and Δ*tolA* (circles) grown in LB broth at 37°C plates for 24 h at 37˚C. Growth curves represent the mean of two biological samples measured in triplicate (n=6), where error bars represent the standard deviation of the mean. WT and Δ*tolA* growth were significantly different for each time point except 0 h according to a Mann-Whitney U test ($p < 0.05$). Figure was reproduced from (1) with permission.

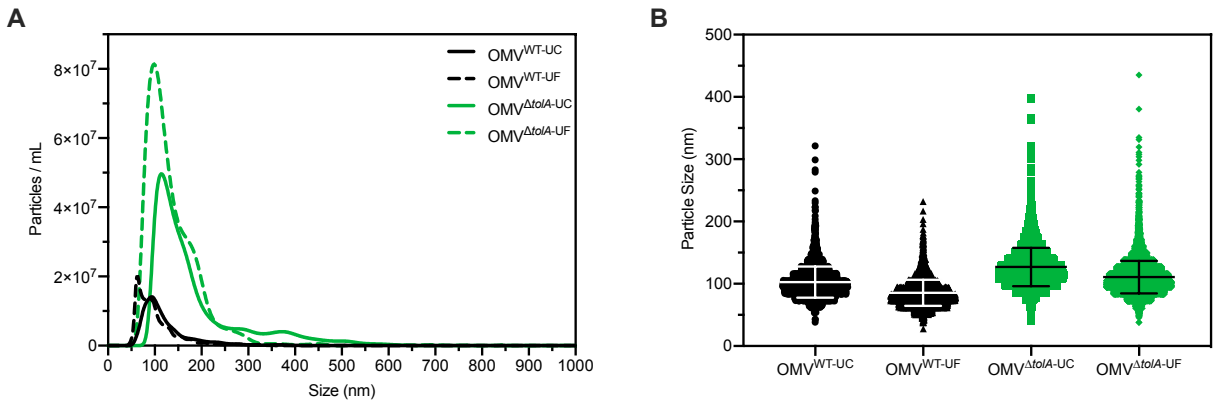

C

Sample	Mean Diameter ± SEM (nm)	Mode Diameter ± SEM (nm)	Concentration ± SEM (particles/mL)	Particles/CFU[a] ± SD
OMV$^{WT\text{-}UC}$	123.9 ± 1.6	97.1 ± 4.7	(8.20 ± 0.26) x 10^{11}	899.1 ± 164.4
OMV$^{WT\text{-}UF}$	104.7 ± 1.6	66.1 ± 2.8	(1.09 ± 0.02) x 10^{12}	1195.2 ± 232.8
OMV$^{\Delta tolA\text{-}UC}$	159.2 ± 1.3	110.2 ± 2.8	(2.86 ± 0.08) x 10^{12}	1945.6 ± 751.0
OMV$^{\Delta tolA\text{-}UF}$	138.8 ± 1.0	96.5 ± 3.0	(7.16 ± 0.05) x 10^{12}	4870.7 ± 484.0

[a] Calculated using the formula: particle/mL/CFU/mL; where WT = 9.12x10^8 CFU/mL and Δ*tolA* = 1.47x10^9 CFU/mL.

Figure 3.2. NTA measurements of OMVs isolated from WT and Δ*tolA* using either UC or UF methods. **A)** Concentration of OMVs from WT and Δ*tolA* as a function of their size. **B)** Scatter plot showing size of particles measured by NTA. **C)** A summary of NTA data collected, listing WT and Δ*tolA* mean vesicle size, mode size, concentration, and particles/CFU for each isolation method. OMVs isolated from WT and Δ*tolA* strains were diluted 1000-fold and measured using a Nanosight NS500. All data represent the means of triplicate experiments ± SEM. Figure was reproduced from (1) with permission.

3.2.2 OMVs isolated by UC and UF show no differences in OmpA abundance

To compare the differences in OMV content that may occur due to the isolation methods themselves, we performed Tricine SDS-PAGE analysis to determine if any OMV protein content was noticeably altered (Figure 3.3A). There were no significant differences in densitometry of stained protein bands between UC and UF OMV preparations for either strain. To determine if there were differences in key OM porins, Western blot analysis was performed to compare OmpA content ratios in OMVs. OmpA porin proteins are abundant and located in the OM, making them a reliable OMV detection marker (162). Based on this analysis, both UC and UF methods showed enrichment of OmpA in Δ*tolA* OMVs compared to WT based on net Δ*tolA* OmpA pixel density/ WT OmpA pixel density (UC; 1.27, UF; 1.85, Figure 3.3B), and no significant differences in OmpA protein abundance between UC and UF-isolated OMV samples for either Δ*tolA* or WT (Figure 3.3B). This suggests that OmpA protein expression on OMVs can be detected after both UC and UF isolation, and that isolation method does not influence the detection of vesicle protein content. This result also indicates that OmpA could be a reliable detection marker for OMV production as the ratio of OmpA present in WT and Δ*tolA* OMV samples was comparable to NTA analysis.

3.2.3 UC and UF isolated OMVs differ in protein and phosphate content

Next, UC and UF OMVs isolated from WT and Δ*tolA* cultures were quantified by total protein bicinchoninic acid (BCA), and total lipid phosphorous (Malachite Green) assays to determine if UC and UF methods influence total protein or lipid phosphate contents in OMVs. Total protein and lipid assays are routinely used to enumerate OMVs and to quantify protein-lipid content ratios of OMVs (85, 113, 129). Discordant results for WT and Δ*tolA* total protein and total phosphate were noted for UC and UF methods (Figure 3.3C). Significantly higher protein ($p < 0.005$) and phosphate ($p < 0.00005$) concentrations were detected in the UC-isolated Δ*tolA* sample as compared to Δ*tolA* OMVs isolated by UF, indicating greater protein and phosphate content in OMVs from these preparations (Figure 3.3C). The UF-isolated WT samples had significantly higher protein concentration ($p < 0.05$) than the UC-isolated WT, but no significant concentration differences between UC and UF WT isolations for phosphate concentration

(Figure 3.3C). When considered with NTA data (Figure 3.2), these results suggest that UF OMV isolation may enhance vesicle isolation yields as compared to UC but may also affect the WT and Δ*tolA* total protein and phosphate content.

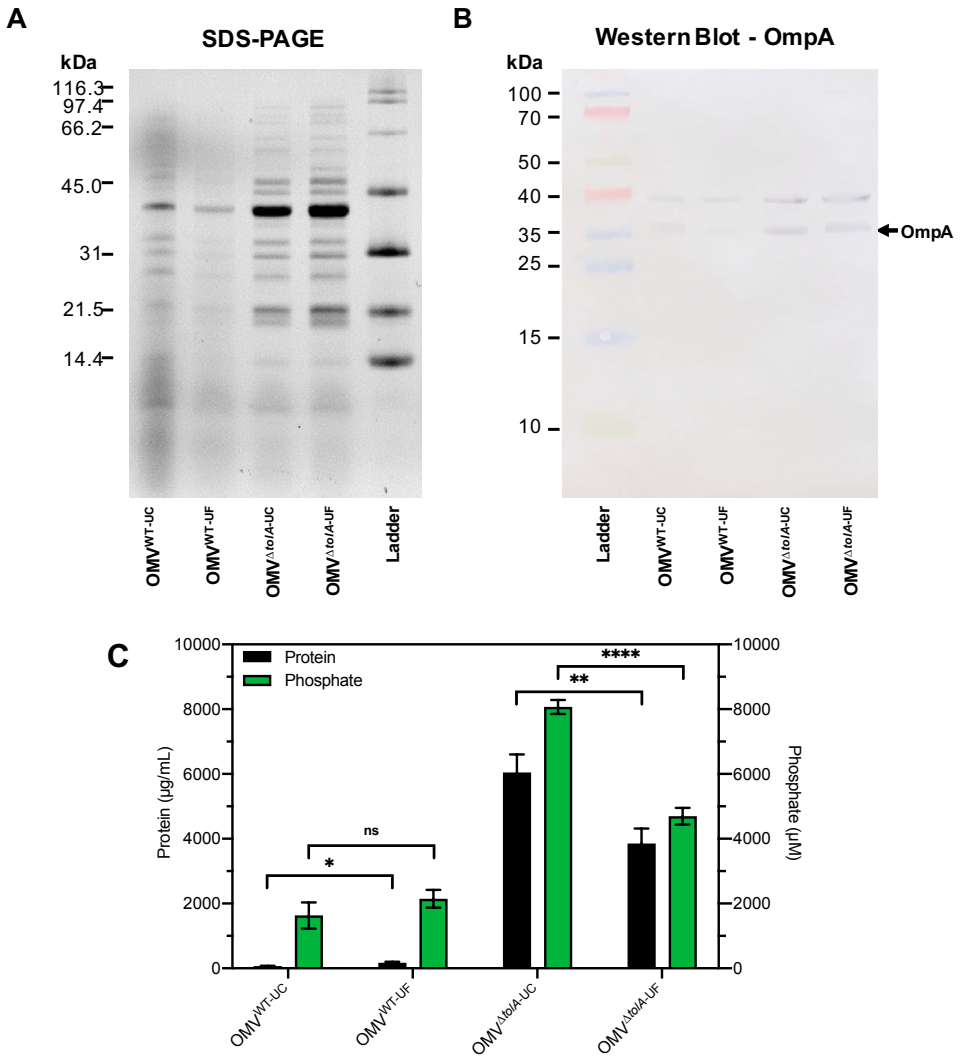

Figure 3.3. Protein and phosphorous profiles of isolated OMVs. **A)** 12% acrylamide Tricine SDS-PAGE gel image of UC and UF OMV isolations for WT and Δ*tolA E. coli* strains detected with TCE. **B)** Western blot of isolated OMV samples from WT and Δ*tolA E. coli* strains detected with anti-OmpA antibodies (1:25000). **C)** OMV sample total protein and total phosphorous content for each OMV isolation method. Values were obtained by BCA assay (protein) or malachite green assay (phosphate) and adjusted based on dilution factor and $OD_{600\ nm}$ of the original culture. All data represent the mean of triplicate measurements, and error bars represent standard deviation. Significant differences between WT and Δ*tolA* samples or between UC and UF samples were determined using the Mann-Whitney U test at *p*-values of < 0.05 (*), < 0.005 (**), < 0.00005 (****). Figure was reproduced from (1) with permission.

3.2.4 UC and UF methods differ in concentration and sizes of recovered OMVs

Next, we determined the average vesicle sizes of WT and Δ*tolA* by NTA to determine if either method significantly altered the size of OMVs recovered in nm diameter (dia; nm, Figure 3.2B-C). The average size of UC-isolated OMVs was 123.9 ± 1.6 nm (mean ± standard error of the mean (SEM)) in dia for WT and 159.2 ± 1.3 nm dia for Δ*tolA*. UF-isolated OMVs had smaller average sizes of WT and Δ*tolA* vesicles at 104.7 ± 1.6 nm dia and 138.8 ± 1.0 nm dia, respectively. Thus, OMVs formed by the Δ*tolA* strain were larger in size as compared to the WT control by both methods (Figure 3.2B, $p < 0.0001$). When analyzing OMV particle size distributions, we also noticed that all UF-isolated OMV samples had a larger proportion of smaller sized vesicles sizes, when compared to vesicles isolated by UC which enriched larger sized vesicles. OMVs with diameter sizes between 0-100 nm were greatly enriched in UF isolations (WT UF; 74.3%, Δ*tolA* UF; 50.4%) as compared to UC (WT UC; 58.1%, Δ*tolA* UC; 38.3%; Figure 3.4A-B). The opposite was true for UC-isolated vesicles, which had vesicles predominating at larger sizes between 200-550 nm (Figure 3.4A-B). OMVs with diameters over 100 nm corresponded to 41.9% of the total OMVs in UC-isolated WT samples and 61.7% in UC-isolated Δ*tolA* samples, whereas this range was 25.7% in UF-isolated WT samples and 49.6% in UF-isolated Δ*tolA* samples. These findings indicate that a size isolation bias exists for each method, where UF enriches for smaller sized particles when compared to the UC method.

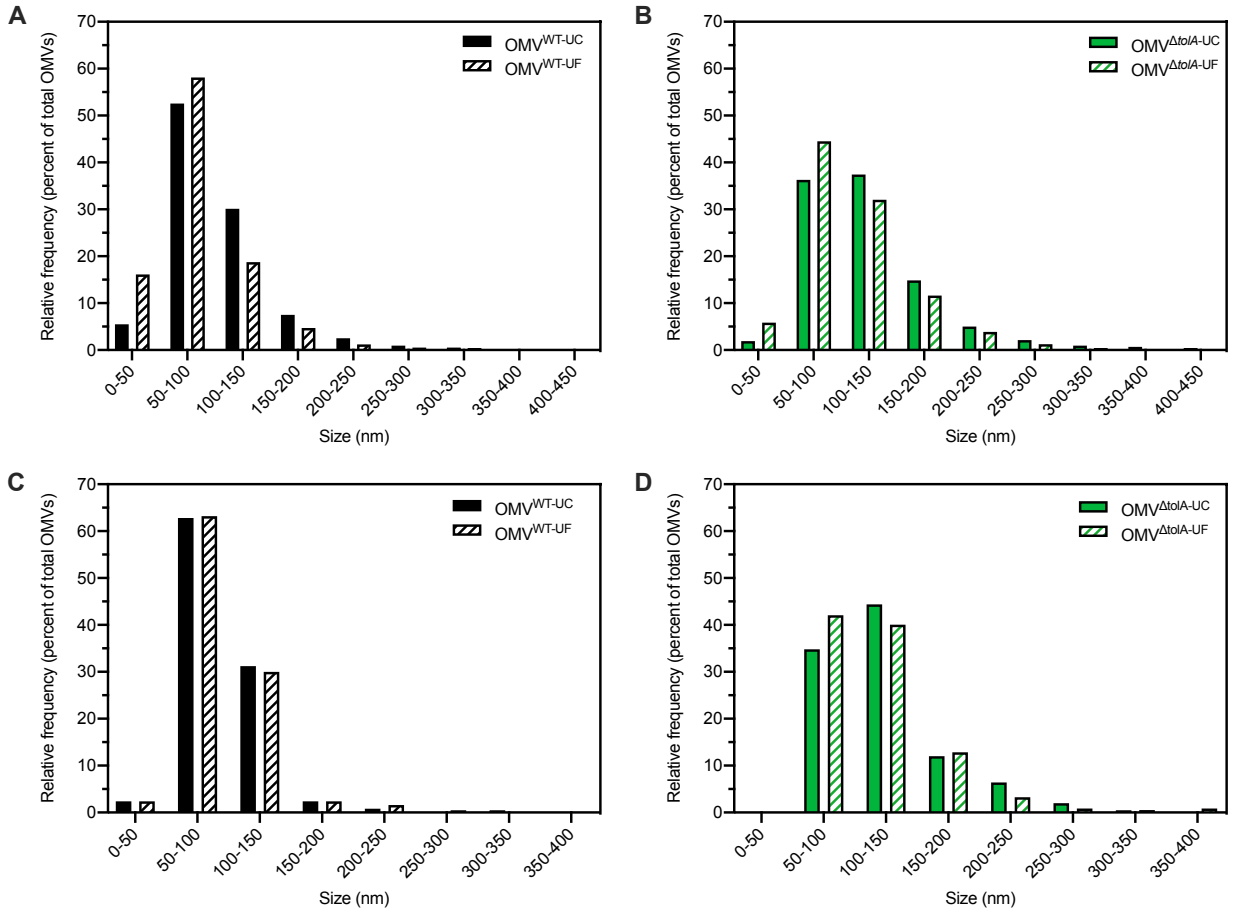

Figure 3.4. Sizes of isolated OMVs by NanoSight NTA and cryo-TEM. OMVs isolated from WT **(A,C)** and Δ*tolA* **(B,D)** were binned into 50 nm size ranges and represented as a percentage of the total OMV population. **A)** Size distributions of WT OMVs isolated by UC and UF methods as measured by NTA. **B)** Size distributions of Δ*tolA* OMVs isolated by UC and UF methods as measured by NTA. **C)** Size distributions of WT OMVs isolated by UC and UF methods as measured by cryo-TEM. **D)** Size distributions of Δ*tolA* OMVs isolated by UC and UF methods as measured by cryo-TEM. Figure was reproduced from (1) with permission.

3.2.5 Cryo-TEM of ΔtolA OMVs reveals distinct morphological differences from WT OMVs

Analysis of OMV morphology for each vesicle isolation method and strain type was performed using cryo-TEM analysis to establish any vesicle size and heterogeneity alterations (Figure 3.5, Figure 3.4C-D). Statistical analysis of OMV measurements from cryo-TEM photomicrographs of WT and Δ*tolA* strains revealed significant differences in vesicle size (Figure 3.6). Measurements from cryo-TEM vesicles images identified a range of OMV sizes (40-400 nm dia) for each strain and methodology used, supporting our NTA findings (Figure 3.2, Figure 3.4C-D). However, based on cryo-TEM vesicle image analysis, all OMVs isolated by either UC or UF had a smaller size distribution range when compared to the same preparations analyzed by NTA (Interquartile range (IQR); WT UC; 72.3-107.8 nm, WT UF; 75.7-107.7 nm, Δ*tolA* UC; 93.1-141.4 nm, Δ*tolA* UF; 86.2-133.7 nm; Figure 3.4). Additionally, cryo-TEM imaged vesicle diameters of Δ*tolA* isolated by UC and UF methods demonstrated significant differences in size, where average vesicle size of UC-isolated Δ*tolA* OMVs was 125.2 nm and UF-isolated Δ*tolA* OMVs was 116.7 nm (p = 0.0097; Figure 3.4C-D). Cryo-TEM average measurements of WT OMV diameters from either isolation method were not significantly different (UC; 93.55 nm, UF; 95.58 nm, p = 0.3123; Figure 3.6B). Hence, NTA and cryo-TEM measurements are generally in agreement with respect to UC and UF OMV size ranges and size averages, but when comparing vesicle size distributions by NTA and cryo-TEM techniques (Figure 3.4), cryo-TEM measurements suggest smaller diameter vesicle sizes and averages for both WT and Δ*tolA* by both isolation techniques. This disparity is likely due to differences in the number of vesicles counted by each method, and may indicate that NTA is more precise due to the quantity and range of particle sizes that are accurately measurable.

Lastly, cryo-TEM highlighted stark differences between WT and Δ*tolA* OMVs with respect to their overall morphology. WT OMV morphologies were characteristic of previously described OMVs by either UC or UF methods (107, 134, 163); based on cryo-TEM images nearly all WT OMVs had a single membrane, presumably composed of the OM bilayer (Figure 3.5A,C). In contrast, the Δ*tolA* mutant had OMVs with variable single and multi-membranous structures when isolated by either UC or UF technique

(Figure 3.5B,D). The Δ*tolA* strain had a high proportion of OMVs with two or more membranes by both methods (UC; 39.6, UF; 42.4%; Figure 3.6), which included double-bilayer outer-inner OMVs (O-IMVs), multi-layered vesicles (M-OMVs) (≥3 layers), as well as grouped encapsulated OMVs surrounded by a larger extramembrane layer (G-OMVs). These altered vesicle morphologies produced by the Δ*tolA* mutant likely account for the larger average sized vesicles detected by NTA. Δ*tolA* vesicles with multiple membranes had a significantly larger average size (UC; 146.7 nm, UF; 143.2 nm) than WT OMVs when measured by cryo-TEM (UC; 110.5 nm, UF; 98.5 nm; Figure 3.6B). Taken altogether with the results from total protein/ total phosphorous, NTA size distributions, and our cryo-TEM vesicle morphology analyses, we can state that tolA mutations considerably alter OMV formation and morphology. These analyses also reveal that neither UC or UF significantly altered the recoverable amount of WT and Δ*tolA* OMV content or morphology, highlighting both as useful OMV isolation techniques.

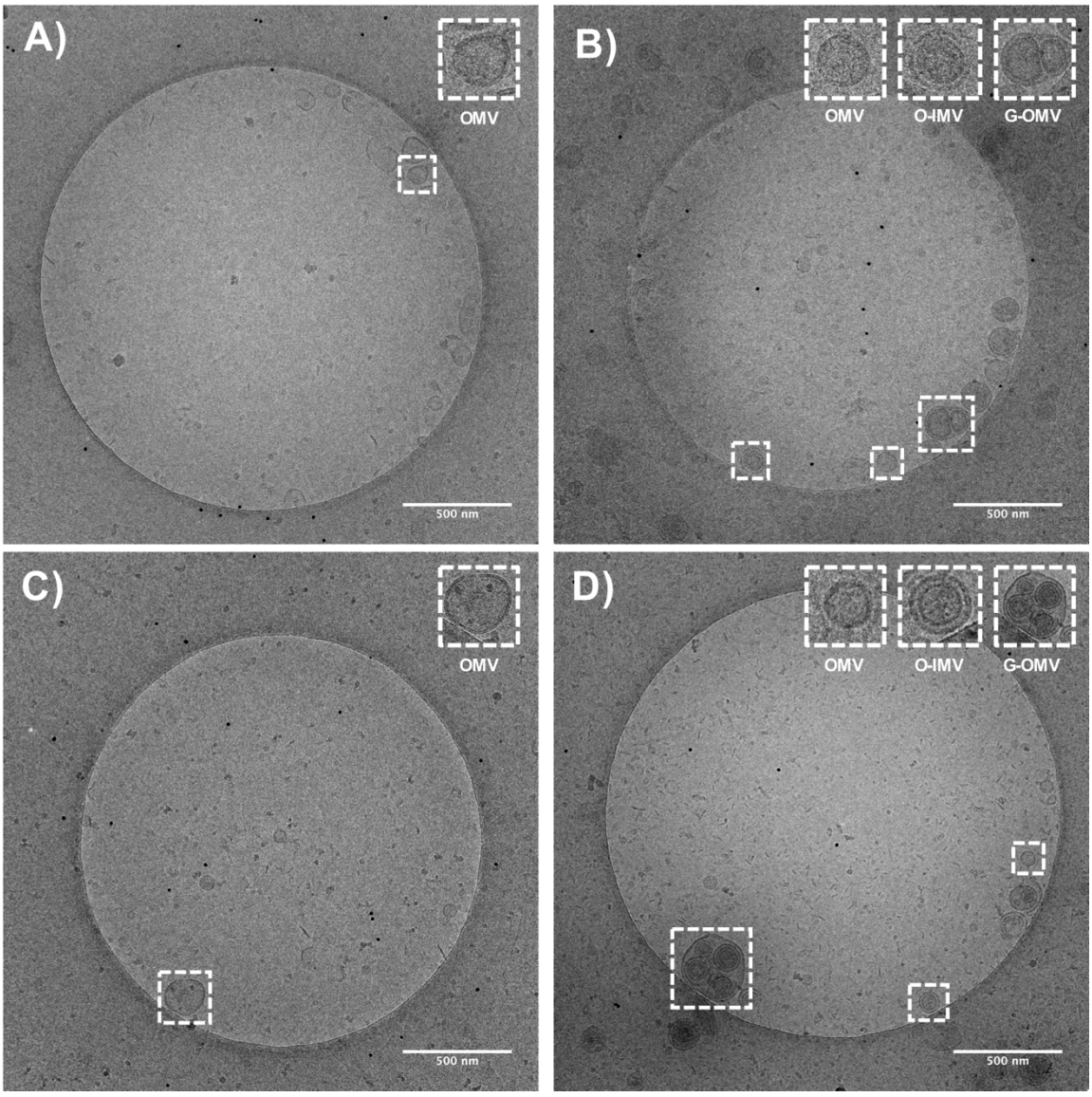

Figure 3.5. Cryo-TEM images of vesicles in WT and Δ*tolA* strains. Representative cryo-TEM images at 14,500X magnification of **(A)** WT OMVs isolated by UC, **(B)** WT OMVs isolated by UF, **(C)** Δ*tolA* OMVs isolated by UC, **(D)** Δ*tolA* OMVs isolated by UF**.** In each panel, enlarged images of representative OMVs frequently observed in WT and Δ*tolA* are highlighted as inset panel images in dashed boxes in the upper right-hand corner. Conventional OMVs as well as vesicles with two membranes (O-IMVs) and multi-layered vesicles (G-OMVs) are shown in these inset images in panels A-D. Figure was reproduced from (1) with permission.

A

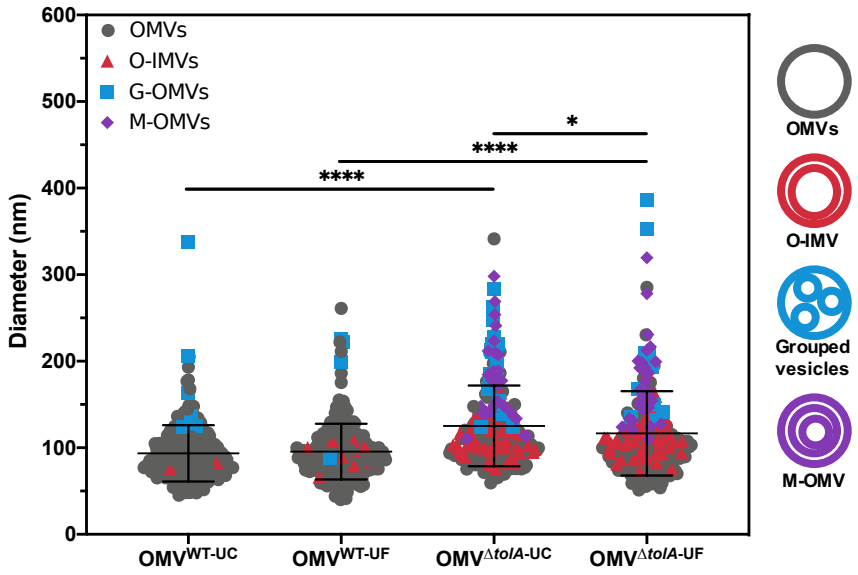

B

Membrane Architecture	OMV^{WT}		$OMV^{\Delta tolA}$	
	UC	UF	UC	UF
OMVs	96.4%	94.8%	57.6%	60.4%
O-IMVs	1.2%	3.6%	22.4%	23.6%
G-OMVs	2.4%	1.6%	8.0%	4.4%
M-OMVs	0.0%	0.0%	12.0%	11.6%

Figure 3.6. Quantification of size and vesicle types in WT and Δ*tolA* strains from cryo-TEM images. **A)** Scatter plot summaries of vesicle diameters measured from cryo-TEM images of OMVs isolated from the WT and Δ*tolA* strains using either ultracentrifugation (UC) or ultradiafiltration (UF) at N = 250 vesicles/ strain. Lines on each plot represent the mean value, and error bars represent standard deviations. Diameters of vesicles from cryo-TEM images were measured using ImageJ particle analysis software. Shape and colour of data points represent the types of vesicle visualized (refer to in panel legend). Significance was determined using Mann-Whitney U test (* p<0.01, ** p<0.0001, N=250 vesicles). **B)** Summary table of membrane vesicle architectures manually identified from cryo-TEM images using ImageJ. Values listed in the table represent the percent total number of vesicles manually assessed representing each shape/ architecture type (N=250 vesicles/ strain). Figure was reproduced from (1) with permission.

*3.2.6 Proteomic analysis identifies IM proteins in Δ*tolA* OMVs which were absent from the WT*

In an effort to confirm the membrane contents of both WT and Δ*tolA* OMVs we used a proteomic approach to identify altered or unique OMV proteins (Figure 3.7). We performed nano-LC MS/MS analysis on WT and Δ*tolA* UF OMV preparations since these preparations produced greater yields of OMVs, at size ranges also present in UC methods. A total of 109 proteins were identified in this proteomic analysis, where 31 proteins were over-accumulated in both the WT and the *tolA* mutant (Figure 3.7A, Table 3.1). Only 5 proteins were exclusively over-accumulated in WT OMVs, whereas 73 proteins were exclusively enriched in Δ*tolA* OMVs (Figure 3.7A; Table 3.1). This initial analysis indicates that the mutant has a larger number of proteins sequestered in its vesicles as compared to WT, as we expected from its M-OMV morphology visualized in cryo-TEM images (Figure 3.5, Figure 3.6).

To determine the membrane location of each identified protein we detected in each strain OMV preparation, we annotated the identified proteins and predicted their subcellular localization using the pSORTb algorithm (154), as shown in Figure 3.7B. 61% of the proteins we identified in both strains were classified as either OM proteins (37 proteins) or periplasmic proteins (29 proteins), whereas a smaller proportion of proteins from the IM (10 proteins) and CY (21 proteins) were detected primarily in Δ*tolA* mutant vesicles (Figure 3.7B). Of the remaining 10% of subcellularly localized proteins, 3 were predicted to be secreted proteins, and 8 had an unknown localization. From this analysis, we noted that all proteins associated with the IM and the extracellular space were exclusively identified in Δ*tolA OMVs* and at 2-3 fold higher quantities than in WT OMVs (Figure 3.7B). This strongly supports the presence of greater IM, periplasmic, and extracellular protein carryover in Δ*tolA* OMVs, in agreement with our cryo-TEM multi-lamellar vesicle images. Additionally, many the overlapping proteins identified in both WT and Δ*tolA* vesicle proteomes were located in the OM, including porins (OmpA, OmpC, OmpF), lipoproteins (LolB, Lpp, RcsF, RlpA, SlyB), and membrane assembly proteins (BamB, LpoA) (Figure 3.7C, Table 3.1). Membrane integrity proteins (Pal, TolB) as well as stress-related proteins (Dps, HdeB, OsmY) were noted in both WT and Δ*tolA* OMV proteomes (Table 3.1), indicating that membrane components involved in

stress and membrane maintenance were present even in the WT vesicles. Some of the proteins we detected were previously identified in other OMV proteomic studies (59, 120, 121, 164, 165), as well as others implicated in studies pertaining to OMV formation (85, 104, 105). Such proteins included periplasmic chaperone/protease DegP and the OM-anchored lipoprotein NlpE, which were found exclusively in the Δ*tolA* OMV sample (Table 3.1).

Functional analysis of OMV proteomes from WT and Δ*tolA* strains was performed using the Kyoto Encyclopedia of Genes and Genomes (KEGG) database (Figure 3.8). This analysis revealed enrichment of a number of proteins associated with two-component regulatory systems, flagellar proteins, ribosomal proteins as well as several metabolic pathways, predominantly from the Δ*tolA* OMV sample (Figure 3.8). Together, this proteomic analysis shows that both WT and Δ*tolA* strains produce vesicles enriched with proteins that are highly membrane-associated, that are responsible for membrane trafficking and assembly, and play a role in membrane integrity and bacterial stress response. It also verifies that deletion of Δ*tolA* results in OMV formation with much greater periplasmic, IM and extracellular content carryover than WT OMVs as suggested by cryo-TEM imaging.

Table 3.1. List of proteins identified by proteomic analysis in WT and Δ*tolA* OMVs isolated by UF. Table was reproduced from (1) with permission.

UniProtKB AC/ ID	Gene	Protein	Protein Detection in Strain(s)	Fisher's Exact Test (*p*-value): ($p < 0.05$)	Fold Change	Fold Increase in Strain
		CYTOPLASM				
P0A9G6	*aceA*	Isocitrate lyase	BOTH	< 0.00010	1.1	Δ*tolA*
P06959	*aceF*	Dihydrolipoyllysine-residue acetyltransferase component of pyruvate dehydrogenase complex	Δ*tolA*	0.015	INF	Δ*tolA*
P0A9Q7	*adhE*	Aldehyde-alcohol dehydrogenase	Δ*tolA*	< 0.00010	78	Δ*tolA*
P0ABB0	*atpA*	ATP synthase subunit alpha	Δ*tolA*	0.011	INF	Δ*tolA*
P0ABD3	*bfr*	Bacterioferritin	WT	< 0.00010	0	WT
P0ABT2	*dps*	DNA protection during starvation protein	BOTH	< 0.00010	0.3	WT
P0A953	*fabB*	3-oxoacyl-[acyl-carrier-protein] synthase 1	BOTH	< 0.00010	0.8	WT
P0A9B2	*gapA*	Glyceraldehyde-3-phosphate dehydrogenase A	Δ*tolA*	0.00094	INF	Δ*tolA*
P0C8J6	*gatY*	D-tagatose-1,6-bisphosphate aldolase subunit GatY	Δ*tolA*	< 0.00010	INF	Δ*tolA*
P0A6F5	*groL*	60 kDa chaperonin 1	BOTH	< 0.00010	0.4	WT
P09373	*pflB*	Formate acetyltransferase 1	Δ*tolA*	0.022	INF	Δ*tolA*
P0A7L0	*rplA*	50S ribosomal protein L1	Δ*tolA*	0.00023	INF	Δ*tolA*
P0A7R1	*rplI*	50S ribosomal protein L9 OS=Escherichia coli	WT	0.00065	0	WT
P0A7J3	*rplJ*	50S ribosomal protein L10	WT	0.0001	0	WT
P02413	*rplO*	50S ribosomal protein L15	Δ*tolA*	0.011	INF	Δ*tolA*
P0AG44	*rplQ*	50S ribosomal protein L17	BOTH	0.011	2.4	Δ*tolA*
P0A7K6	*rplS*	50S ribosomal protein L19	Δ*tolA*	0.022	INF	Δ*tolA*
P0A7V0	*rpsB*	30S ribosomal protein S2	BOTH	0.011	2.5	Δ*tolA*
P0A7S3	*rpsL*	30S ribosomal protein S12	Δ*tolA*	0.0019	INF	Δ*tolA*
P0ADZ4	*rpsO*	30S ribosomal protein S15	Δ*tolA*	0.0091	INF	Δ*tolA*
P0CE47	*tufA*	Elongation factor Tu 1	BOTH	< 0.00010	2	Δ*tolA*
		EXTRACELLULAR				
P75937	*flgE*	Flagellar hook protein FlgE	Δ*tolA*	< 0.00010	INF	Δ*tolA*
P33235	*flgK*	Flagellar hook-associated protein 1	Δ*tolA*	0.022	INF	Δ*tolA*
P04949	*fliC*	Flagellin	Δ*tolA*	< 0.00010	INF	Δ*tolA*
		INNER MEMBRANE				
P0AE06	*acrA*	Multidrug efflux pump subunit AcrA	Δ*tolA*	0.015	INF	Δ*tolA*
P0AB98	*atpD*	ATP synthase subunit beta	Δ*tolA*	0.026	INF	Δ*tolA*
P0ABA0	*atpF*	ATP synthase subunit b	Δ*tolA*	0.0091	INF	Δ*tolA*
P11557	*damX*	Cell division protein DamX	Δ*tolA*	0.031	INF	Δ*tolA*

P0AEH5	*elaB*	Protein ElaB	Δ*tolA*	< 0.00010	INF	Δ*tolA*
P00363	*frdA*	Fumarate reductase flavoprotein subunit	Δ*tolA*	0.044	INF	Δ*tolA*
P63235	*gadC*	Probable glutamate/gamma-aminobutyrate antiporter	Δ*tolA*	0.00039	INF	Δ*tolA*
P0ACD8	*mbhL*	Hydrogenase-1 large chain	Δ*tolA*	0.0027	INF	Δ*tolA*
P0AEX3	*kgtP*	Alpha-ketoglutarate permease	Δ*tolA*	0.031	INF	Δ*tolA*
P0AC41	*sdhA*	Succinate dehydrogenase flavoprotein subunit	Δ*tolA*	0.0013	INF	Δ*tolA*
P77804	*ydgA*	Protein YdgA	Δ*tolA*	0.015	INF	Δ*tolA*
		OUTER MEMBRANE				
P77774	*bamB*	OM protein assembly factor BamB	BOTH	< 0.00010	23	Δ*tolA*
P0A903	*bamC*	OM protein assembly factor BamC	Δ*tolA*	< 0.00010	INF	Δ*tolA*
P0AC02	*bamD*	OM protein assembly factor BamD	Δ*tolA*	< 0.00010	INF	Δ*tolA*
P0A901	*blc*	OM lipoprotein Blc	Δ*tolA*	0.013	INF	Δ*tolA*
P06129	*btuB*	Vitamin B12 transporter BtuB	Δ*tolA*	0.0012	31	Δ*tolA*
P10384	*fadL*	Long-chain fatty acid transport protein	Δ*tolA*	< 0.00010	79	Δ*tolA*
P13036	*fecA*	Fe(3+) dicitrate transport protein FecA	Δ*tolA*	< 0.00010	INF	Δ*tolA*
P05825	*fepA*	Ferrienterobactin receptor	Δ*tolA*	0.00094	INF	Δ*tolA*
P06971	*fhuA*	Ferrichrome-iron receptor	Δ*tolA*	< 0.00010	INF	Δ*tolA*
P0A6S0	*flgH*	Flagellar L-ring protein	Δ*tolA*	< 0.00010	INF	Δ*tolA*
P39180	*flu*	Antigen 43	Δ*tolA*	< 0.00010	41	Δ*tolA*
P02943	*lamB*	Maltoporin	BOTH	< 0.00010	28	Δ*tolA*
P25894	*loiP*	Metalloprotease LoiP	BOTH	< 0.00010	43	Δ*tolA*
P61320	*lolB*	Outer-membrane lipoprotein LolB	BOTH	< 0.00010	35	Δ*tolA*
P45464	*lpoA*	Penicillin-binding protein activator LpoA	BOTH	< 0.00010	19	Δ*tolA*
P69776	*lpp*	Major OM prolipoprotein Lpp	BOTH	< 0.00010	3.3	Δ*tolA*
P31554	*lptD*	LPS-assembly protein LptD	Δ*tolA*	< 0.00010	INF	Δ*tolA*
P0ADC1	*lptE*	LPS-assembly lipoprotein LptE	Δ*tolA*	< 0.00010	INF	Δ*tolA*
P0A908	*mipA*	MltA-interacting protein	Δ*tolA*	< 0.00010	28	Δ*tolA*
P28224	*mliC*	Membrane-bound lysozyme inhibitor of C-type lysozyme	Δ*tolA*	< 0.00010	INF	Δ*tolA*
P0A935	*mltA*	Membrane-bound lytic murein transglycosylase A	Δ*tolA*	0.026	INF	Δ*tolA*
P0ADA3	*nlpD*	Murein hydrolase activator NlpD	Δ*tolA*	< 0.00010	89	Δ*tolA*
P40710	*nlpE*	Lipoprotein NlpE	Δ*tolA*	0.028	2.9	Δ*tolA*
P0A910	*ompA*	OM protein A	BOTH	< 0.00010	2.2	Δ*tolA*
P06996	*ompC*	OM protein C	BOTH	< 0.00010	3.9	Δ*tolA*
P02931	*ompF*	OM protein F	BOTH	< 0.00010	21	Δ*tolA*
P09169	*ompT*	Protease 7	BOTH	0.00021	14	Δ*tolA*
P0A917	*ompX*	OM protein X	Δ*tolA*	< 0.00010	INF	Δ*tolA*
P0A912	*pal*	Peptidoglycan-associated lipoprotein	BOTH	0.023	4	Δ*tolA*
P69411	*rcsF*	OM lipoprotein RcsF	BOTH	0.00014	14	Δ*tolA*
P10100	*rlpA*	Endolytic peptidoglycan transglycosylase RlpA	BOTH	0.0014	9.7	Δ*tolA*

P0A905	*slyB*	OM lipoprotein SlyB	BOTH	< 0.00010	2.2	Δ*tolA*
P02930	*tolC*	OM protein TolC	Δ*tolA*	< 0.00010	INF	Δ*tolA*
P46130	*ybhC*	Putative acyl-CoA thioester hydrolase YbhC	Δ*tolA*	0.0017	20	Δ*tolA*
P0AA91	*yeaY*	Uncharacterized lipoprotein YeaY	Δ*tolA*	< 0.00010	INF	Δ*tolA*
Q46798	*ygeR*	Uncharacterized lipoprotein YgeR	Δ*tolA*	< 0.00010	INF	Δ*tolA*
P37665	*yiaD*	Probable lipoprotein YiaD	Δ*tolA*	0.0017	30	Δ*tolA*
		PERIPLASM				
P19926	*agp*	Glucose-1-phosphatase	BOTH	0.032	8.9	Δ*tolA*
P00805	*ansB*	L-asparaginase 2	BOTH	< 0.00010	22	Δ*tolA*
P66948	*bepA*	Beta-barrel assembly-enhancing protease	Δ*tolA*	0.015	INF	Δ*tolA*
P33363	*bglX*	Periplasmic beta-glucosidase	Δ*tolA*	0.0023	INF	Δ*tolA*
P08331	*cpdB*	2',3'-cyclic-nucleotide 2'-phosphodiesterase/3'-nucleotidase	Δ*tolA*	0.0091	INF	Δ*tolA*
P45955	*cpoB*	Cell division coordinator CpoB	Δ*tolA*	< 0.00010	64	Δ*tolA*
P0C0V0	*degP*	Periplasmic serine endoprotease DegP	Δ*tolA*	< 0.00010	INF	Δ*tolA*
P39099	*degQ*	Periplasmic pH-dependent serine endoprotease DegQ	Δ*tolA*	0.00094	INF	Δ*tolA*
P23847	*dppA*	Periplasmic dipeptide transport protein	Δ*tolA*	0.00025	19	Δ*tolA*
P23827	*eco*	Ecotin	Δ*tolA*	0.0045	INF	Δ*tolA*
P39176	*erfK*	Probable L,D-transpeptidase ErfK/SrfK	Δ*tolA*	0.0027	INF	Δ*tolA*
P45523	*fkpA*	FKBP-type peptidyl-prolyl cis-trans isomerase FkpA	Δ*tolA*	0.0061	20	Δ*tolA*
P0AEQ3	*glnH*	Glutamine-binding periplasmic protein	Δ*tolA*	0.04	19	Δ*tolA*
P0AET2	*hdeB*	Acid stress chaperone HdeB	BOTH	< 0.00010	1.2	Δ*tolA*
P61889	*mdh*	Malate dehydrogenase	BOTH	< 0.00010	0.8	WT
P33136	*mdoG*	Glucans biosynthesis protein G	Δ*tolA*	0.0091	INF	Δ*tolA*
P33937	*napA*	Periplasmic nitrate reductase	Δ*tolA*	0.00039	INF	Δ*tolA*
P0AFH8	*osmY*	Osmotically-inducible protein Y	BOTH	< 0.00010	2.3	Δ*tolA*
P0AGC3	*slt*	Soluble lytic murein transglycosylase	Δ*tolA*	< 0.00010	INF	Δ*tolA*
P0ABZ6	*surA*	Chaperone SurA	Δ*tolA*	0.0014	24	Δ*tolA*
P0A855	*tolB*	Protein TolB	BOTH	0.0057	7	Δ*tolA*
P77717	*ybaY*	Uncharacterized lipoprotein YbaY	BOTH	< 0.00010	1.7	Δ*tolA*
P0AAV6	*ybgS*	Uncharacterized protein YbgS	Δ*tolA*	< 0.00010	INF	Δ*tolA*
P0AAX8	*ybiS*	Probable L,D-transpeptidase YbiS	Δ*tolA*	0.009	12	Δ*tolA*
P77318	*ydeN*	Uncharacterized sulfatase YdeN	Δ*tolA*	0.0064	INF	Δ*tolA*
P0ADS6	*yggE*	Uncharacterized protein YggE	Δ*tolA*	< 0.00010	INF	Δ*tolA*
P0ADT2	*ygiB*	UPF0441 protein YgiB	Δ*tolA*	0.044	INF	Δ*tolA*
P0ADU5	*ygiW*	Protein YgiW	WT	0.016	1.8	Δ*tolA*
P64596	*yraP*	Uncharacterized protein YraP	BOTH	0.039	9.1	Δ*tolA*
		UNKNOWN				
P0ADE6	*kbp*	Potassium binding protein Kbp	Δ*tolA*	0.037	INF	Δ*tolA*
P77562	*yaiW*	Uncharacterized protein YaiW	Δ*tolA*	0.00028	INF	Δ*tolA*

P0ADA5	*yajG*	Uncharacterized lipoprotein YajG	BOTH	< 0.00010	1.2	Δ*tolA*
P75818	*ybjP*	Uncharacterized lipoprotein YbjP	BOTH	0.017	9.5	Δ*tolA*
P76177	*ydgH*	Protein YdgH	Δ*tolA*	< 0.00010	INF	Δ*tolA*
P0ADM4	*yidQ*	Uncharacterized protein YidQ	Δ*tolA*	0.0091	INF	Δ*tolA*
P0AF70	*yjeI*	Uncharacterized protein YjeI	Δ*tolA*	0.00013	29	Δ*tolA*

Abbreviations: AC; accession number, ID; identification number, INF; infinity value as the denominator in the fold change equation is zero.

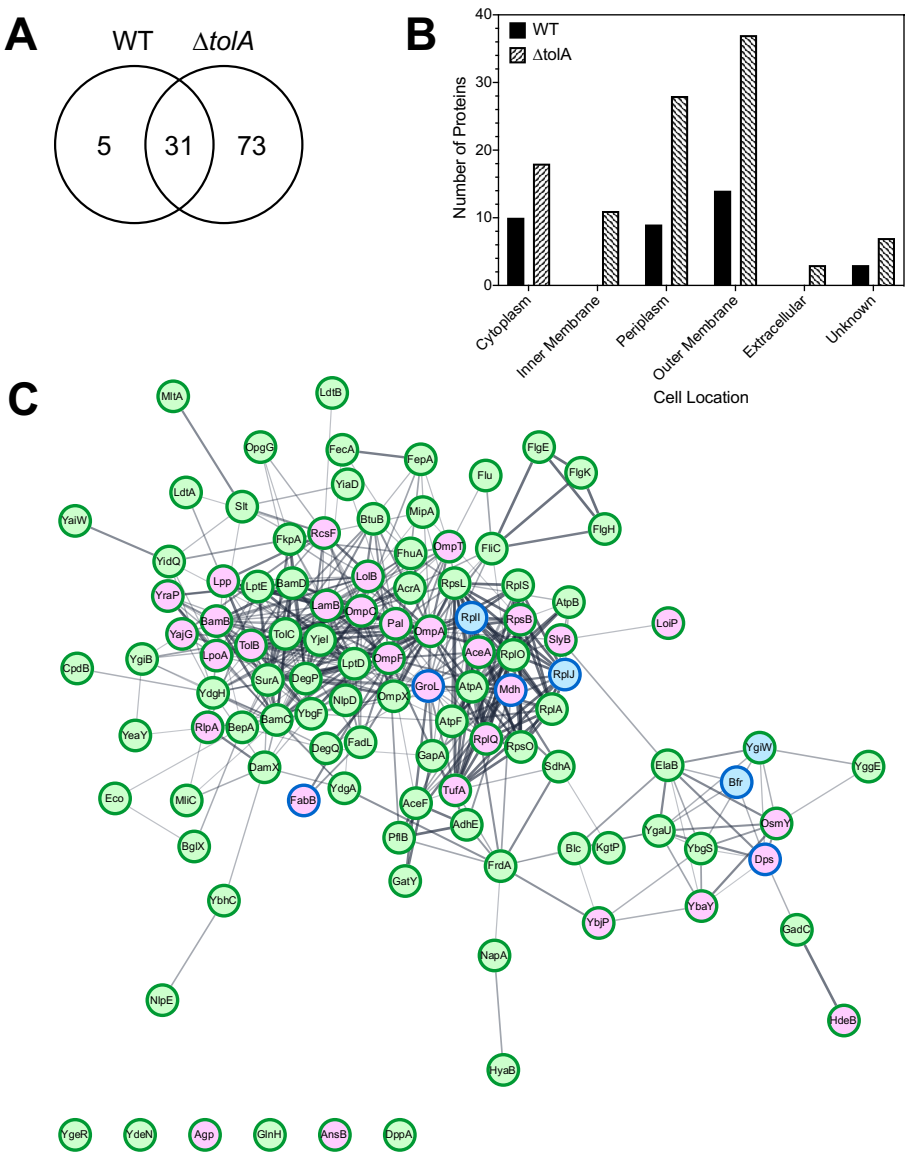

Figure 3.7. Proteomic characterization of WT and Δ*tolA* vesicles isolated by UF. **A)** Venn-diagram of identified proteins showing overlap between WT and Δ*tolA* vesicle samples. **B)** Cellular localization of identified proteins from WT (black) and Δ*tolA* (white) vesicle samples. **C)** String network of interacting proteins from WT (blue), Δ*tolA* (green), or both (purple) vesicle samples. Border colours represent protein abundance, with dark green borders denoting upregulation of the protein in the Δ*tolA* sample, and dark blue borders denoting upregulation of the protein in the WT sample. The network diagram was generated using the StringApp v1.5.0 in Cytoscape v.3.8.0 (155). All data used in this analysis are summarized in Table 3.1. Figure was reproduced from (1) with permission.

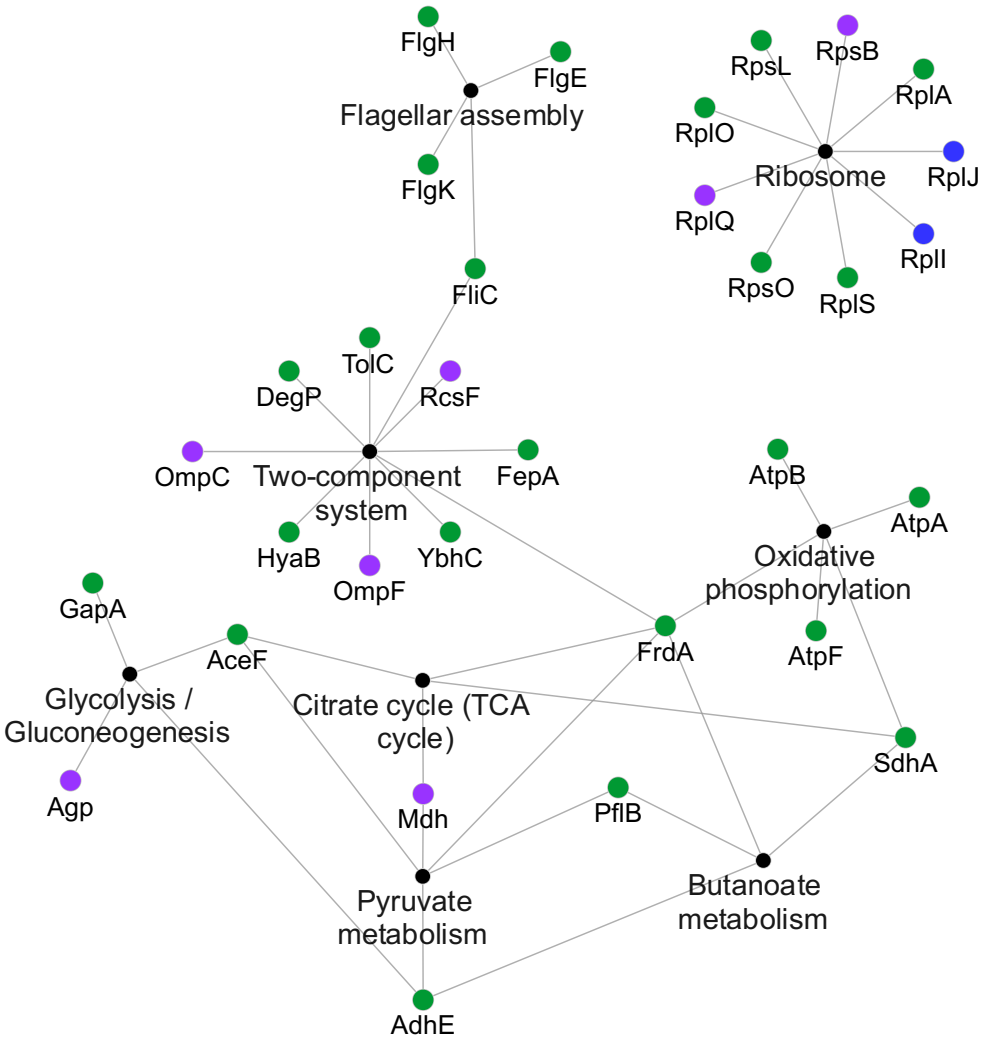

Figure 3.8. KEGG network of WT and Δ*tolA* OMV-associated proteins. Proteins were functionally annotated using the ClueGO (v.2.5.6) add-in software for Cytoscape (v.3.8.0) (156). Bolded black terms below black nodes represent functional categories, and coloured nodes represent proteins with the colour of each node indicating the OMV sample it was found in. Proteins were exclusive to WT (blue), Δ*tolA* (green) or present in both samples (purple). Connecting edge lines represent multiple functional categorizations of proteins. Default parameters were used for network specificity. Figure was reproduced from (1) with permission.

3.3 Discussion

3.3.1 Discussion of UC and UF isolation methods

From these results, we determined that both UC and UF OMV isolation methods were effective for isolating intact OMVs, as both methods yielded comparable WT and Δ*tolA* vesicle populations. Our analyses revealed that UC and UF vesicles differed when we compared their ability to isolate specific OMV size ranges and size distributions (Figure 3.4). They also revealed some differences in total protein and phosphorous content quantifications of WT and Δ*tolA* OMVs (Figure 3.3). These findings are important when considering how any isolated OMVs will be experimentally studied. OMVs isolation is a time-consuming process that requires large volumes of culture to overcome lower yields of vesicles naturally produced by cultured bacteria. While several authors have sought to optimize current methods to achieve the highest yields of vesicles (135, 139, 166), to our knowledge this is the first study to directly compare two of the most widely used isolation methods for their experimental OMV analysis applications. Despite both methods isolating high purity OMVs, our findings show that UF improves the recovery of more OMVs as compared to UC isolations, without qualitatively altering vesicle contents or morphology. In addition, the UC approach is more time-consuming as compared to UF due to the duration of centrifugation runs and was shown in this study to reduce the recoverable quantity of smaller sized vesicles (Figure 3.4). However, it is important to note that UC did enhance isolation of larger sized vesicles (>100nm) (Figure 3.4). As a result, our study offers more insights into the benefits and limitations of each technique, which should be considered in future OMV isolation experiments.

3.3.2 Smaller sized vesicles are enriched by UF

The average vesicle size and size distribution as determined by NTA was in general agreement with the cryo-TEM analysis data for both UC and UF OMVs, but we did notice differences in the size of particles isolated by each method. Based on NTA results, UF-isolated vesicles from WT and Δ*tolA* had a higher proportion of smaller (<100nm) vesicles, while UC-isolated samples from WT and Δ*tolA* had a higher

proportion of vesicles of larger (>100nm) sizes (Figure 3.4A-B). This trend in size distribution was also observed when we compared the Δ*tolA* vesicles in cryo-TEM measurements, where UF samples had a smaller average size, however no significant differences were found between WT UC and UF sizes according to cryo-TEM images (Figure 3.4C-D). This result suggests that NTA may be detecting small fragments of particles rather than fully formed OMVs in the UF-isolated samples. In a previous study it was found that NTA can measure vesicles as small as ~50 nm (167), however, we noticed that smaller particles were being measured by the NTA NanoSight instrument in all UC and UF samples. Therefore, the smaller particles (0-50 nm in diameter) could be undissolved salts/ media components and/or cell debris particles that were carried over from cell cultures in UF isolations, potentially skewing the size distribution of vesicles in samples with more small contaminating particles. We suspect that the UF procedure may naturally bias isolation of smaller sized particles as the media is membrane filtered, and may be prone to some filter blockage by media components and culture carryover over time. Filter blockage may cause the MW cut-off to become lower over time and allow smaller sized particles, such as salt or cell debris, to build up and enrich in UF techniques. Sucrose-gradient cushions have been used in past experiments to help eliminate these carryover particles (168) but it is unclear if cushions further bias the recovery of heterogenous OMV populations.

Another explanation for why UF isolates smaller OMVs than UC methods is that UC methods may promote aggregation of vesicles due to repeated pelleting steps. Vesicle pelleting may result in larger average sized OMV distributions as we observed in our study. Aggregation of vesicles and contamination with extravesicular protein complexes or aggregates is a commonly reported UC occurrence (for examples see (169–172)). Due to the use of fixed-angle ultracentrifuge rotors during UC, material pelleting and deposition against the wall of the centrifuge tube may be physically damaging, potentially promoting vesicle aggregation, which favors the fusion of vesicles with weakened or altered membranes (135, 169). In our study, we detected a small fraction of UC vesicles larger than 450 nm by NTA, which suggests this form of aggregation was occurring, as the 0.45 μm filtration step prior to UC/UF should remove all particles

above this size. Thus, while UC and UF methods are both comparable, it appears that each method alters the size distribution of OMVs, with UF selecting for smaller particles and UC promoting the aggregation of vesicles into larger-sized particles.

*3.3.3 Δ*tolA* OMVs are multilamellar and enriched with IM-associated proteins*

Mutations of the *tol-pal* system genes have been well documented in OMV studies and mutants are often used study hypervesiculation phenotypes (81, 103). Our study is the first to examine the morphology and content of a *tolA* mutant in detail. Our study determined that the Δ*tolA* strain not only produced more OMVs as compared to the WT strain, but that these vesicles were larger in size and displayed M-OMV, G-OMV, and O-IMV membrane morphology as observed for *tolB* mutant of *B. agrestis* in a recent study (160). Additionally, we determined that the Δ*tolA* vesicles with multiple membranes were larger in size than WT OMVs. The presence of these unique O-IMV and multi-lamellar vesicle types (M-OMV, G-OMV) has also been observed many Gram-negative species such as *E. coli* Nissle 1917, *H. pylori* strain 60190, *P. aeruginosa* PAO1, *A. baumannii* AB41, and *N. gonorrhoeae* DSM15130 strains, but their functional significance to these species has yet to be determined (107, 173, 174). This altered Δ*tolA* vesicle morphology suggests that the loss of TolA in *E. coli* promotes the carryover of IM, possibly to compensate for loss of membrane integrity caused by reduced Tol-Pal inter-membrane connections. Tol-Pal mutants have been previously shown to cause cell division impairments, resulting in increased distance between the IM and the peptidoglycan layer and enhancing defects in peptidoglycan-cleaving enzymes (160, 175). Our proteomic data reveals that the peptidoglycan degrading enzymes NlpD, MltA, Slt, and RlpA were significantly enriched in the Δ*tolA* strain (Table 3.1), supporting the idea that the Tol-Pal system plays a role in promoting glycan cleavage. Similar to the recent Δ*tolB* study (160), we suspect that increased OMV formation by the Δ*tolA* mutant is the result of incomplete tethering of the IM and OM, which would result in IM and cytoplasmic proteins being carried over into vesicles more frequently. This is supported by our proteomic analysis, which determined that more cytoplasmic proteins were detected in Δ*tolA* than WT, and IM proteins were found exclusively in the Δ*tolA* vesicles (Figure 3.7B).

Our isolated Δ*tolA* vesicles also appeared to be enriched with structural OMPs, cell membrane assembly proteins, and cell division proteins. Our proteomic analysis determined that Δ*tolA* OMVs were enriched with proteins involved in membrane biogenesis and degradation were enriched, including the OM assembly proteins (BamC, BamD), LPS assembly proteins (LptD, LptE, FadL), cell division proteins (CpoB, DamK, NlpD), and murein degrading proteins (MltA, MipA, Slt) (Figure 3.7C; Table 3.1). When compared to the WT, this suggests that the Δ*tolA* mutant may have to increase membrane biogenesis as well as membrane turnover or recycling, in order to keep up with the high levels of vesiculation and loss of both IM and OM to vesicles caused by Tol-Pal complex disruption. Our measurements of total phosphate and protein in the Δ*tolA* strain by both isolation methods indicated that more protein was detected relative to total lipid phosphate, which further supports this explanation. Additionally, many envelope stabilizing proteins were also enriched in Δ*tolA*, specifically NlpE, OmpX, and TolC, which support increased membrane biogenesis in *tolA* mutant vesicles (Figure 3.7C; Table 3.1). The increased prevalence of these proteins in Δ*tolA* OMVs is not surprising, as previous studies have shown that mutations in *tolA* can be partially compensated by expressing other OM-associated proteins that act to stabilize the OM in the absence of TolA (107, 125, 176). An increase in the amount of stabilizing proteins in the OM could conceivably compensate for the increased vesiculation in mutant strains and is worth further study. We also observed that the Δ*tolA* strain grows slower than the WT (Figure 3.1A), which underscores the fitness costs associated with loss of TolA and inter-membrane integrity in *E. coli*.

3.3.4 The role of the tol-pal system in vesicle production

The modulation of cell envelope intermembrane layer crosslinks is a strong correlate of increased OMV production in Gram-negative species. Proteins intricately involved in linking the OM to the IM include: i) OmpA, an OM porin that spans the periplasmic space and can bind to peptidoglycan. ii) The Tol-Pal complex, a cell-division component that aids in invagination of the OM and membrane stability. iii) Lpp, an OM lipoprotein that covalently crosslinks with the peptidoglycan (97). Studies have shown that mutants of *E. coli, Salmonella,* and *A. baumannii* lacking OmpA display increased OMV production (84,

97). Mutations in the Tol-Pal genes are associated with increased vesicle production in *E. coli* and *Salmonella*, specifically deletions in *pal, tolA,* and *tolB* (84, 101, 106). Our study corroborates these findings, with OmpA, Lpp, TolB and Pal all enriched in the Δ*tolA* mutant (Table 3.1), suggesting that the hypervesiculation phenotype exhibited by our Δ*tolA* strain is a result of generalized membrane instability and incomplete membrane linkage.

Proteomic analysis of Δ*tolA* OMVs also identified the involvement of σ^E and Cpx envelope stress response pathways (Figure 3.7C, Table 3.1). In the presence of misfolded proteins and extracellular stress, the σ^E response is activated, and contributes to DNA repair, metabolism, OM biogenesis, and periplasmic homeostasis (177). σ^E-regulated chaperones and proteases (SurA, FkpA, DegP) and several members of the BAM complex (BamB, BamC, BamD) were all significantly enriched in Δ*tolA*, indicating that this pathway is highly active in the Δ*tolA* mutant. The chaperone Skp was also found in both WT and Δ*tolA*, although we did not significantly detect over-accumulation in either sample. The Cpx envelope stress response is crucial for mitigating envelope stress caused by misfolded proteins in the PP, and Cpx regulated members are involved in protein folding and degradation primarily within the IM (178–180). NlpE, an activator of this system, was found to be significantly enriched in Δ*tolA* only (Figure 3.7C, Table 3.1). DegP, a periplasmic serine protease was the only significantly enriched protein regulated by the Cpx regulon. It is important to note, that the Cpx regulon has been associated with IM-associated proteins and functions (181), as was seen in our Δ*tolA* proteomic dataset. Together, this suggests that mutations in the Tol-Pal system are intricately involved with envelope stress responses as a compensatory mechanism against envelope instability.

3.4 Concluding Remarks

The study of OMVs is a rapidly expanding research area, so understanding the isolation method limitations improves our ability to modulate OMV production using the fewest genetic alterations. Better understanding of OMV recovery by common vesicle isolation methods aids ongoing and future biotechnological OMV applications, helping to standardize and improve efforts to enhance the overall

recovery of OMVs from bacterial cultures. Our analyses suggest that UF may be an improved method for isolating OMVs, due to its faster isolation time and higher yield of smaller and averaged-sized vesicles. Depending on the OMV sizes desired, UC applications may be a desired methodology and both methods should be carefully considered based on the type of downstream experimental analysis needed. Our study also provides the first in-depth characterization of Δ*tolA* OMVs, which revealed a multi-lamellar membrane morphology similar to recent studies of *tolB* (160). Our proteomic analysis highlighted the impact that the Tol-Pal system has on cell membrane content released into secreted vesicles and identified protein components worth following up on in future studies.

Chapter 4. Cationic antimicrobial-adapted *E. coli* K-12 produce greater amounts of OMVs with altered proteomic and lipidomic patterns that confer specific protective effects when supplemented to *E. coli*

The contents of this chapter will be submitted to 2 journals according to antimicrobial class (CET- and CHX-OMVs as one study, and COL-OMVs as one study); BBA-Biomembranes and the Biophysical journal. All the CA-adapted strains tested in this chapter were generated by Dr. Nicola Cartwright, and their intial AST tests for CA-adapted strains were conducted by former students Dr. Nicola Cartwright and Kari Green. Shelby Reimer designed, performed, and analyzed all data from growth rate measurement experiments, all OMV isolations, protein and phosphate quantification assays, SDS-PAGE, Western blotting, NTA, and MIC determination assays with OMV supplementation, detailed in this results sections. Additionally, DLS samples were prepared by Shelby Reimer for experimental analysis by Wyatt Technology Corporation. OMV samples for cryo-TEM were prepared by Shelby Reimer, where the preparation of cryo-TEM quantifoil was conducted by Dr. Dan Beniac (NML) in Dr. Timothy Booth's lab (Director of Viral Diseases Division, NML) with assistance from Shelby Reimer. All cryo-TEM imaging in this chapter was conducted by Shelby Reimer, with technical assistance from Dr. Dan Beniac and Shannon Hiebert. OMV samples for proteomic analysis were prepared by Shelby Reimer, and protein sample preparation, nano LC-MS/MS and raw data collection and processing were performed by Dr. Patrick Chong and Stuart McCallister (Proteomics Core, NML) in collaboration with Dr. Garrett Westmacott's lab (Chief of Mass Spectrometry and Proteomics, NML). All proteomic data analysis and interpretation was done by Shelby Reimer and Denice Bay. All remaining data analysis and figure preparation was done by Shelby Reimer. Editing of this paper/section was done by Shelby Reimer and Dr. Denice Bay.

4.1 Aims, hypotheses, and approaches

This aim of this chapter and study was to examine the effect of CA exposure on *E. coli* OMV production, and to test the hypothesis that CA-tolerant strains demonstrate increased production of OMVs. OMV production is believed to provide an additional AMR mechanism that enables bacteria to remove and

survive higher CA concentrations, and previous studies of Gram-negative species exposed to antimicrobials such as β-lactams, quinolones, and polymyxins have shown that bacteria can increase the production of OMVs to shield or potentially absorb antimicrobials as a defensive AMR mechanism (59, 86, 128, 182). At the time this study was initated in 2018, it was not known how membrane-active and disruptive antiseptics (CET or CHX) or antibiotics such as colistin (COL) influence OMV formation and production (183). To test this hypothesis, we selected the model organism *E. coli* K-12 BW25113, which our lab previously adapted to three different CA classes using a gradual antimicrobial exposure method (51), producing lab-strains that were tolerant to CET (CETR), CHX (CHXR), and COL (COLR) (143, 144, 184). Each CA-adapted *E. coli* BW25113 strain was selected for study to represent different classes of CAs (CET; QAC, CHX; bisbiguanide, COL; polymyxin), and allowed for a comparison of different membrane disrupting CAs. We grew these strains along with unadapted *E. coli* K-12 BW25113 to early stationary phase and exposed each adapted strain to selective concentrations of their respective CA. OMVs from each CA-adapted strain (CA-OMVs) were isolated from culture supernatants by an ultradiafiltration method optimized in our lab (1) and detailed in Chapter 3. The UF method was selected as it was faster and equally efficient in collecting WT-OMVs as compared to the UC method (Chapter 3). These purified CA-OMVs were further characterized for their size distributions and relative concentrations in comparison to WT-OMVs using DLS or NTA techniques. CA-OMV morphologies were assessed using cryo-TEM. The proteomic contents and alterations specific to each CA-OMV in comparison to unadapted *E. coli* OMVs (WT-OMVs) were elucidated using nano-LC-MS/MS. Lastly, broth microdilution AST was used to determine MIC values when isolated WT-/ CA-OMVs were added to exogenously to *E. coli* cultures. These assays assessed the protective capabilities of each CA-adapted OMV against the unadapted and CA-adapted strains in the presence of their respective CA. The findings from this study showed that each CA-adapted strain produced more OMVs than WT, validating our hypothesis. It also highlighted that CA-adapted *E. coli* produce OMVs with unique morphological and proteomic differences that conferred different antimicrobial protective abilities when added to various *E. coli* cultures (CA-adapted strains and WT).

These differences highlight key features related to genetic alterations associated to *E. coli* adaptation to each CA and likely reflect differences in their specific mechanisms of membrane disruption.

4.2 Results

4.2.1 The addition of CAs to each CA-adapted E. coli culture to maintain their CA selection phenotypes reduced their overall final cell yield as compared to unadapted cultures

Prior to CA-OMV characterization and analysis, it was important to determine and compare the overall growth and fitness of each CA-adapted (CETR, CHXR, and COLR; Table 2.1) strain, so we perfomed broth microtitre plate growth curves as described in Section 2.3. As discussed in Chapter 3, cell culture growth yields can influence the quantification of OMVs released into the culture, so we determined final growth curves and yields for each CA-adapted strain using optical density growth curve measurements. AST MIC values for each CA-adapted strain were determined previously (Table 2.1); CA selective concentrations used in the growth curve analyses were based on the lowest MIC values determined for each CA-adapted strain as described in Section 2.8 deemed to be selective against WT. CA-adapted strains had increased tolerance (≥2-fold increase in MIC value) to the respective CA they were adapted to and as compared to the unadapted *E. coli* (Table 2.1). The first growth curve experiment examined each CA-adapted strain incubated with a respective CA selective-MIC concentration (CHX; 2.4 µg/mL, CET; 40 µg/mL, COL; 100 µg/mL) to maintain CA-tolerant phenotypes and prevent phenotypic reversion. Phenotypic reversion (also known as phenotypic stability) was noted to occur in previous studies after 10 days without CA selection (144, 184). When the CA-adapted strains were grown for 24 h in rich LB media with CA selection, their growth and final OD_{600nm} values were significantly different from the WT (WT OD_{600nm} = 1.15 ± 0.03, CETR OD_{600nm} = 0.69 ± 0.05, CHXR OD_{600nm} = 1.38 ± 0.01, COLR OD_{600nm} = 0.88 ± 0.06, *p*-values < 0.0001) (Figure 4.1A). Significant differences in OD_{600nm} were noted using a two-way ANOVA with Dunnett's multiple comparisons tests at 2 h time points collected during the 24 hr growth curves for each CA-adapted strain versus the WT with CA selection. Lower OD_{600nm} values were noted for CETR at all timepoints, and significant differences were found for CHXR at 0 hr and 4 h in lag phase, and

COLR at 0 hr, 12-18hr in late-log/ early stationary phase growth (Figure 4.1A). This indicated that any CA-OMV extraction and purifications from the supernantant from 18 h cultures of each CA-adapted *E. coli* strain grown with CA selection would need to be normalized for OD_{600nm} when determining OMV final yields per culture.

Growth curves of CA-adapted strains in LB medium without CA selection demonstrated that each CA-adapted strain grew differently without CA exposure, with CHXR having significantly increased OD_{600nm} values and CETR having signficantly reduced OD_{600nm} values when compared to WT at nearly all timepoints (Figure 4.1B). Without CAs, each CA-adapted strain also had significantly higher final OD_{600nm} values as compared to the same strain grown with CA selection (CETR $OD_{600nm} = 1.01 \pm 0.016$, CHXR $OD_{600nm} = 1.37 \pm 0.01$, COLR $OD_{600nm} = 1.08 \pm 0.02$; *p*-values <0.05) (Figure 4.1

Figure 4.1B). The increased growth of CHXR as compared to WT grown without selection was recently described and published in a study by the Bay lab (144) and was associated with deleterious mutations in the OM lipoprotein *mlaA;* in this study *E. coli Δmla* mutants also increased OD_{600nm} final growth after 24 hrs in LB without CHX selection when compared to WT growth. Together, these results show that CA adaptation comes at a fitness cost when bacteria are incubated with selective concentrations of CAs. To account for these growth differences when CA-adapted cultures were grown with CA selection, we have applied the same OMV yield growth correction calculations described in Chapter 3 when determining the total OMV yields/ culture.

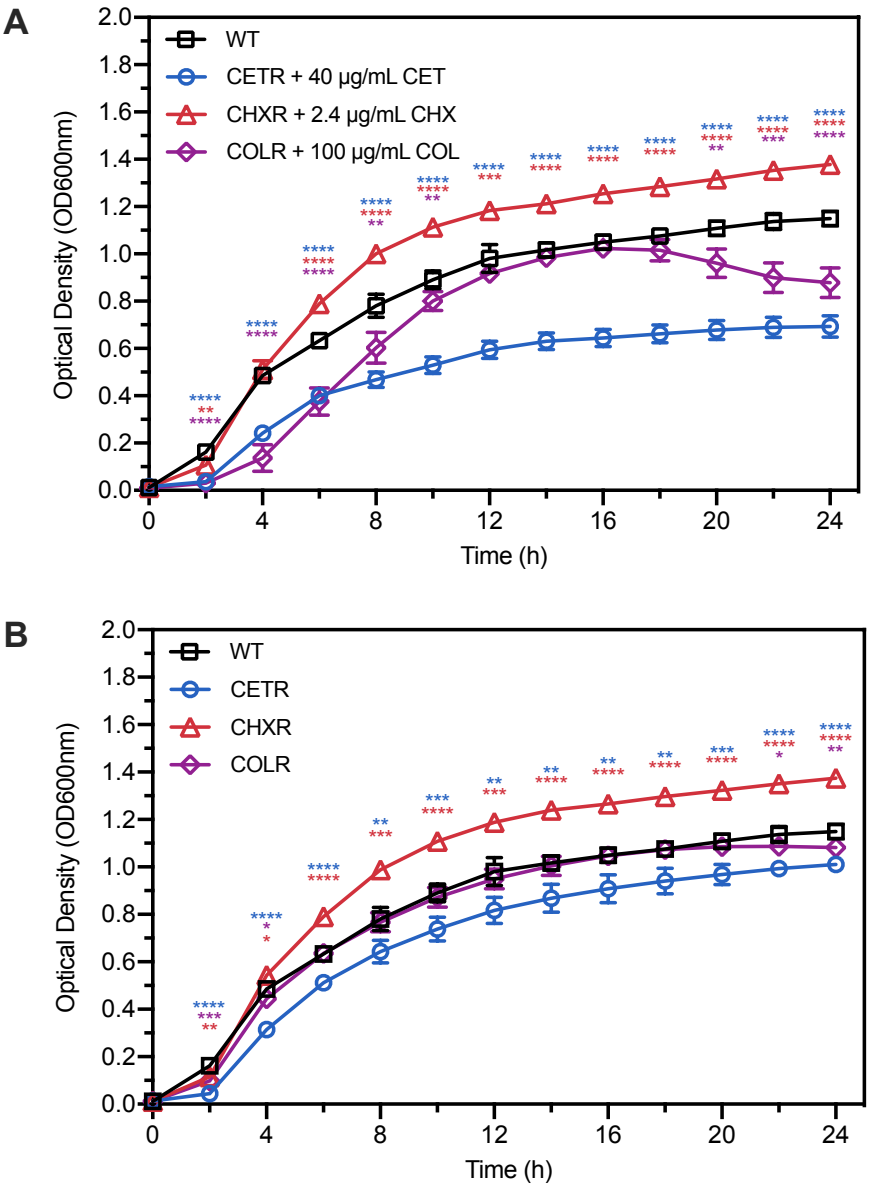

Figure 4.1. Growth curve of WT and CA-adapted bacterial strains with and without CA selection. **A)** OD_{600nm} of CA-adapted strains (CETR, CHXR, COLR) in LB with CA selection (40 µg/mL CET, 2.4 µg/mL CHX, 100 µg/mL COL) grown in microtitre plates over 24 h and compared to unadapted WT without added CA. **B)** OD_{600nm} of WT and CA-adapted bacterial strains (CETR, CHXR, COLR) in LB over 24 h without antimicrobial selection.

4.2.2 OMV production is significantly increased in all three CA-adapted strains using NTA and DLS analyses.

Prior to quantifying how CA-adaptation influences OMV production as compared to WT-OMVs, we performed some initial analyses on purified WT-OMVs using a NanoSight NS300 NTA system to ensure that the conditions used for CA/WT-OMVs extraction, storage, and handling did not bias OMV size distributions. Briefly, OMVs were harvested from 1 L cultures of each WT or CA-adapted strain grown at 37ºC with CA selection after 18 h of growth. The optical density of cultures was measured to estimate growth cell yields in CFU/mL. The culture supernants were collected after centrifugation to separate the cells, filtered (0.45 μm) and subsequently concentrated in an ultradiafiltration chamber under vacuum using a molecular weight cutoff filter disk of 500 kDa. The concentrated solutions were ultracentrifuged and resuspended in HEPES buffer for further analysis (Sections 2.4, 2.4.2). To ensure that freeze-thawing of the isolates did not affect vesicle size and shape, we conducted NTA on repeatedly frozen and thawed WT-OMV samples (Figure 4.2A-B). NTA analyses of repeatedly freeze-thawed OMV samples (1-5 times) showed no major differences in particle size or distributions, so freezing conditions were adopted for OMV storage in this study (Figure 4.2A-B). Furthermore, to test the durability/ stability of purified OMV samples over time, we left WT-OMV samples at room temperature for 9 days and then measured the particles in solution using NTA (Figure 4.2C-D). These preparations remained relatively stable in size (day 1; 129.3 ± 1.6 nm (mean ± SEM), day 3; 130.0 ± 1.8 nm, day 9; 131.6 ± 1.1 nm), but were significantly different in calculated concentration (day 1; $9.41 \times 10^8 \pm 2.19 \times 10^7$ particles/mL, day 3; $8.13 \times 10^8 \pm 6.12 \times 10^7$ particles/mL, day 9; $5.81 \times 10^8 \pm 2.33 \times 10^7$ particles/mL) (Figure 4.2C-D). OMVs were resistance to rupture and aggregation as demonstrated by nearly identical size distribution and calculated concentration after being left at room temperature or after multiple rounds of freeze-thawing. Given the stability of our vesicles under varied conditions, we were confident in our ability to determine OMV yields from the CA-adapted strains by calculating the relative particles/ CFU of each culture.

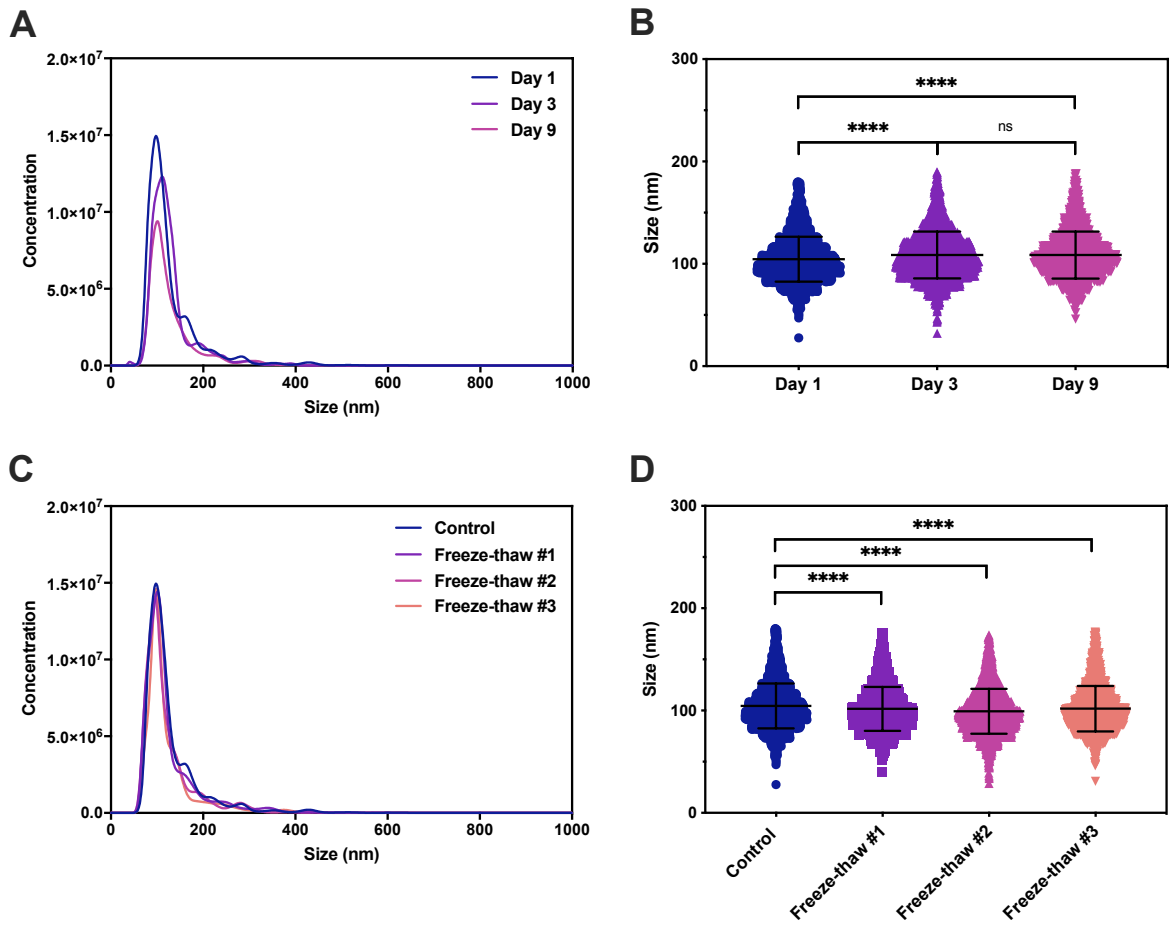

Figure 4.2. Stability of WT-OMVs at room temperature or after multiple rounds of freeze-thawing measured by NTA. Panels **A)** and **C)** show binned WT-OMV particle size data (x-axes) and their relative concentrations (y-axes). Panels **B)** and **D)** represent the WT-OMV particle size distributions (x-axes) after prolonged incubation at room temperature in days **(B)** or after 3 freeze-thawing attempts **(D)**. In panels B and D, vertical bars show mean size values ± standard devation, . Horizontal lines in panels B-D indicate significant differences in compared variables based on a Student's *t*-test (**** = $p < 0.0001$).

Using the same procedures as for WT-OMV isolation and measurement in Chapter 3, we proceeded to determine if CA-adapted strains produced more OMVs than WT. All purified OMVs preparations were examined by NanoSight NS300 NTA and a DynaPro Plate Reader III DLS system to determine and compare sample particle sizes and size distributions. Since OMVs have been assessed in past studies using either NTA or DLS techniques (157, 185), we chose to perform both techniques to ensure there were no significant differences in vesicle sizes or a size bias when using one technique over another. Both NTA and DLS assess particle sizes by measuring the light scatter from particles in solution undergoing Brownian motion, and both techniques calculate sizes based on the diffusion coefficient of particles in solution (186). However, these techniques differ in how they measure light scatter; NTA tracks the trajectories of individual scattering objects using a microscope and calculates their displacement related to each particle's size. In contrast, DLS analyzes intensity fluctuations in scattered light related to the diffusion of particles (158, 186). Due to these discrepancies, DLS is able to measure a wider size range than NTA, while NTA offers greater insights into particle resolution as compared to DLS (158). As a result, both techniques can be used to complement one another and provide information on OMV particle size distributions.

Initial analysis of CA-adapted OMV samples indicated they were highly concentrated, therefore CA-adapted OMVs were diluted prior to their measurement by NTA or DLS (Section 2.9-2.10). To measure light scattering on both systems, all OMV samples required dilution 1/1000 – 1/10,000 to obtain solutions with particle concentrations in the range of 10^8 – 10^9 mL^{-1}. It was noted that OMV particle sizes decreased with dilution for all samples, this effect could be due to viscosity changes or the inability of the instruments to separate closely interacting vesicles in highly concentrated samples. Our DLS and NTA results both demonstrated that CA-adapted strains produced more OMVs as compared to WT as summarized in tables shown in Figure 4.3 and Figure 4.4. After correcting for growth using the particles/ CFU calculations as described in Chapter 3 (Section 3.2.1), both DLS and NTA demonstrated that CHXR produced the highest concentration of particles (8 to 134-fold change from WT), when compared to CETR (7 to 16 fold change)

or COLR (2 to 7 fold change) by both light scattering measurements (NTA; Figure 4.3, DLS; Figure 4.4). This validates the hypothesis that CA-adaptation increases OMV production.

Both DLS and NTA techniques also demonstrated that OMVs formed by each CA-adapted strain were significantly larger in size as compared to WT-OMVs. However, both NTA and DLS techniques differed in their measurement of the average size of OMVs: the particle size diameters (nm) measured by NTA for WT-OMVs was 122.8 ± 1.4, CETR-OMVs was 260.7 ± 6.4 nm, CHXR-OMVs was 171.4 ± 0.6 nm, and COLR-OMVs was 268.5 ± 7.1 nm (Figure 4.3). For DLS measurements, particle size diameters for WT-OMVs was 154.6 ± 20.0nm, CETR-OMVs was 327.4 ± 65.5 nm, CHXR-OMVs was 200.6 ± 20.6 nm, and COLR-OMVs was 211.4 ± 86.0 nm (Figure 4.4). Specifically, DLS size measurements were generally larger than NTA, with fold change values (DLS/NTA) as follows; 1.26 for WT-OMVs, 1.26 for CETR-OMVs, 1.17 for CHXR-OMVs, and 0.79 for COLR-OMVs.

Additionally, the particle size dispersions within each OMV sample differed for each CA-adapted strain using both light scatter measurement techinques. By NTA, WT and CHXR had a monodisperse population of vesicles where the majority of vesicles were within 100-175 nm sizes (Figure 4.3, Figure 4.4). In contrast, CETR and COLR strains produced OMVs that were polydisperse in size, where particle sizes ranged more broadly from 120-200 nm for CETR-OMVs and 100-250 nm for COLR-OMVs. These particle size measurements may explain the larger average sizes of particles for CA-adapted vesicles, and indicate that CET and COL-adapted strains produce greater numbers of mixed small and large vesicle populations. Lastly, the COLR-OMV samples were the most diverse in particle size ranges, and this resulted in issues during NTA and DLS measurements as the OMVs increased the viscosity of the solution, and resulted in poor autocorrelation functions as some particles were too large for particle concentration calculations. NTA results for COLR-OMV sample analyses indicated that the average size of particles were 268.5 ±7.1 nm (mean ± SEM) in diameter, while DLS calculated the diameter to be 211.4 ± 86.0 nm (mean ± SD), however, given COLR's properties, we believe that this underrepresents the larger populations of vesicles which were unable to be measured by either NTA or DLS. Altogether, these results suggest that CA-adapted

strains produce more OMVs compared to WT, and that these strain's OMV properties are distinct from one another, warranting further investigation into the contents of these vesicles and their overall morphology.

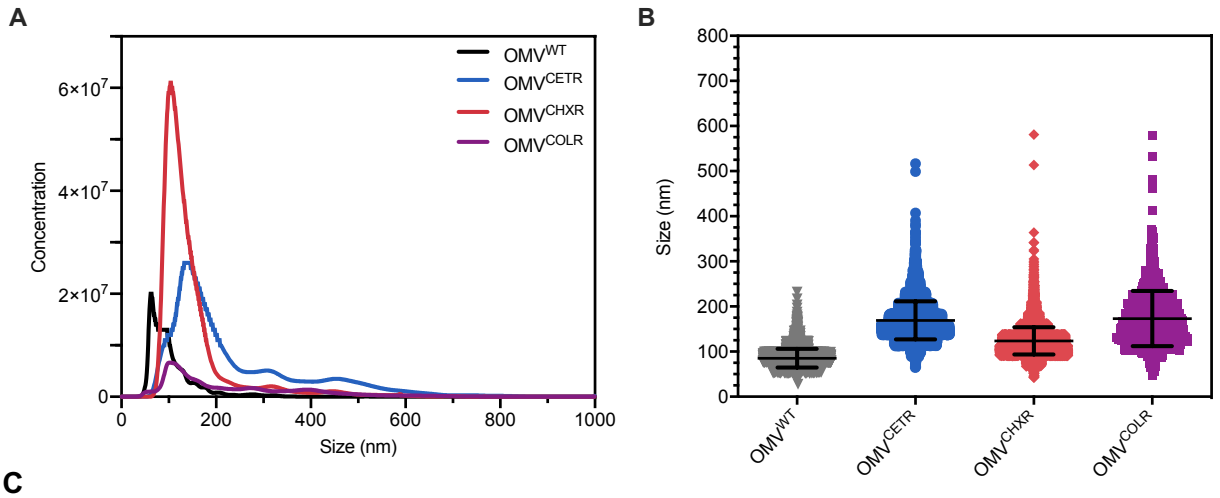

C

Sample	Mean Diameter ± SEM (nm)	Mode Diameter ± SEM (nm)	Concentration ± SEM (particles/ mL)	Particles/CFU[a] ± SEM
OMV^{WT}	122.8 ± 1.4	86.3 ± 2.7	(5.45 ± 0.08) x 10^{10}	28.9 ± 0.45
OMV^{CETR}	260.7 ± 6.4	156.0 ± 16.5	(8.54 ± 0.19) x 10^{11}	459.1 ± 10.30
OMV^{CHXR}	171.4 ± 0.6	125.0 ± 4.0	(5.82 ± 0.12) x 10^{12}	3880.0 ± 78.67
OMV^{COLR}	268.5 ± 7.1	132.2 ± 20.8	(1.51 ± 0.03) x 10^{11}	188.8 ± 3.46

[a] Calculated using the formula: particle/mL/CFU/mL; where WT = 1.88x10^9 CFU/mL, CETR = 1.86x10^9 CFU/mL, CHXR = 1.50x10^9 CFU/mL, and COLR = 8.00x10^8 CFU/mL.

Figure 4.3. Particle size and concentration of WT and CA-adapted OMVs measured by NTA. **A)** Particle concentration as a function of particle size for WT and CA-adapted OMVs (CETR; blue, CHXR; red, and COLR; purple). **B)** Particle size scatter dot plot for WT and CA-adapted OMVs. Bars represent the mean size ± SD. **C)** Summary calculations for size and particle concentration of WT and CA-adapted OMVs measured by NTA. OMV samples were measured in triplicate experiments (except for COLR, which was measured in duplicate experiments), with five independent runs using the NanoSight NS300, and error is represented by SEM.

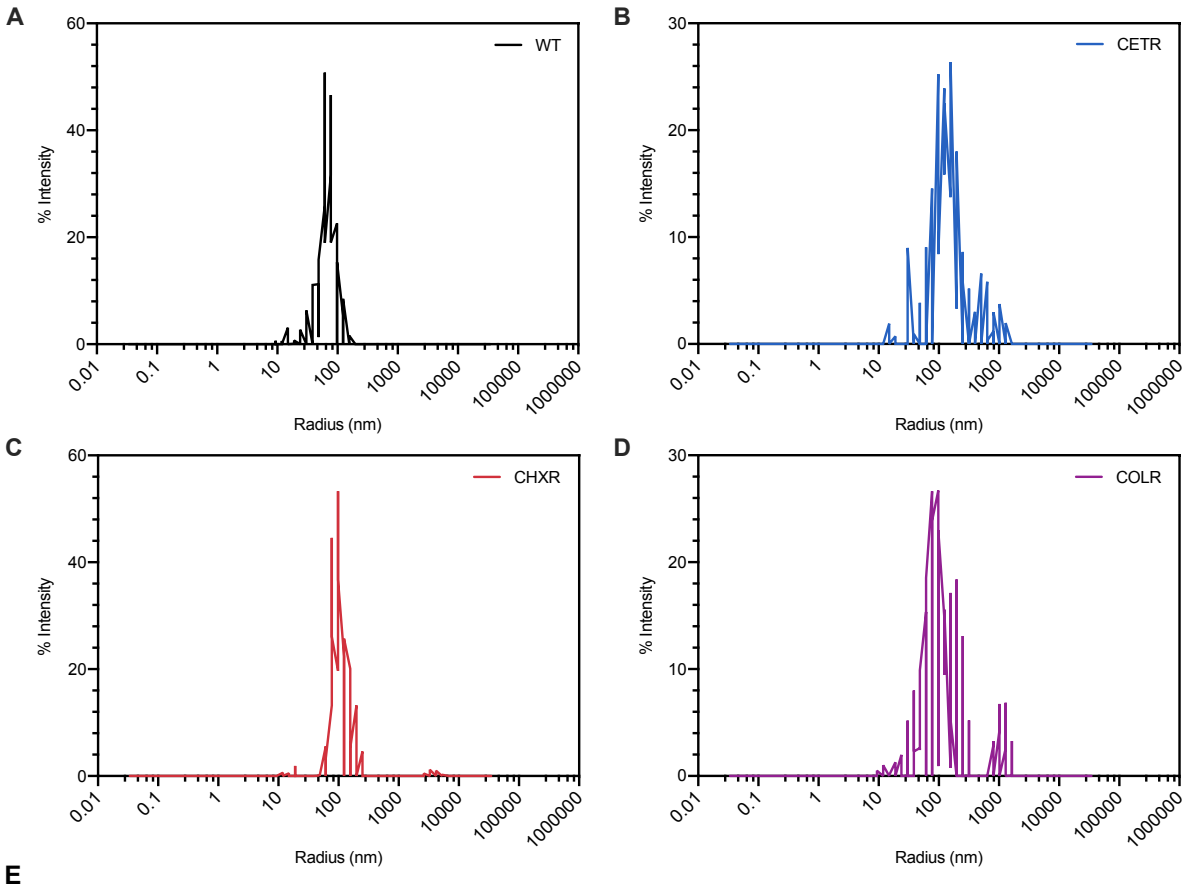

E

Sample	Hydrodynamic Radius (nm)		Concentration (particles/ mL)		Particles/CFU[a] ± SD
	Mean ± SD	Relative SD	Mean ± SD	Relative SD	
OMV^{WT}	77.3 ± 10.0	13%	(2.22 ± 1.11) x 10^{11}	50%	155.6 ± 75.14
OMV^{CETR}	163.7 ± 33.7	21%	(8.29 ± 3.62) x 10^{11}	44%	1120.7 ± 381.08
OMV^{CHXR}	100.3 ± 10.3	10%	(1.60 ± 0.24) x 10^{12}	44%	1302.0 ± 573.05
OMV^{COLR}	105.7 ± 43.0	39%	(2.32 ± 1.60) x 10^{11}	54%	382.3 ± 201.32

[a] Calculated using the formula: particle/mL/CFU/mL; where WT = 1.42x10^9 CFU/mL, CETR = 7.40x10^8 CFU/mL, CHXR = 1.23x10^9 CFU/mL, and COLR = 1.21x10^9 CFU/mL.

Figure 4.4. Particle size radii and concentration of WT and CA-adapted OMVs measured by DLS. Intensity-weighted particle size radius distributions and peak sizes for **A)** WT-OMVs, **B)** CETR-OMVs, **C)** CHXR-OMVs, and **D)** COLR-OMVs. **E)** Summary calculations table of particle sizes and concentrations of WT and CA-adapted OMVs measured by DLS. All OMV samples were measured in triplicate under two dilution conditions using the DynaPro Plate Reader III, and error was calculated as SD.

4.2.3 OMV protein and phosphate profiles differ between CA-adapted and WT OMVs samples

To determine relative amounts of total protein and lipids present in CA-OMVs, BCA assays (Section 2.5.1) and malachite green phosphate assays (Section 2.5.2) were performed on each OMV preparation to quantify their protein and phosphate levels, respectively (Figure 4.5). The results of these assays demonstrated that the ratios of proteins to lipids in OMVs differed between CA-adapted strains. BCA assays revealed that the CA-adapted strains produced OMVs with greater total protein content as compared to WT (CETR; $p < 0.0005$, CHXR; $p < 0.05$, COLR; ns), but CETR-OMVs had the greatest total protein content overall as compared to WT-OMVs (

Figure 4.5A). Malachite green phosphate assay results generally agreed with BCA results, demonstrating that CETR-OMVs and CHXR-OMVs contained significantly greater amounts of total phosphate content ($p < 0.0001$) than WT. The total phosphate amounts in COLR-OMV showed greater levels than WT-OMVs but these values were not statistically significant. Interestingly, CHXR-OMVs had a much higher ratio of total phosphate to total protein than all of the other CA-OMVs tested (Figure 4.5C), and appeared to be in good agreement with particle size concentration findings from NTA and DLS analyses (Figure 4.3, Figure 4.4). These assay results indicate there are notable differences in OMV composition in each CA-OMV preparation, reflecting changes in the amounts and proportions of proteins and phosphate (lipids) in these assays.

In an effort to further expand CA-OMV total protein and phosphate assessments, the protein profiles of each CA-adapted OMVs were investigated with Tricine SDS-PAGE gels and Western blotting to detect OmpA (

Figure **4.6**A-B). Tricine SDS-PAGE showed that numerous proteins were detectable in each CA-OMV and WT-OMV sample, however, the abundance of certain proteins in different OMV samples appeared to differ depending on the CA-adapted strain examined. In particular, protein bands between 35 kDa and 40 kDa, which are known to correspond to common OM proteins (OmpA = 37 kDa, OmpF = 39 kDa, OmpC = 40kDa) were noticably distinct between samples. Densitometry performed on OmpA Western blots of

the CA-adapted strains showed an increase in OmpA abundance in all strains as compared to WT-OMVs (fold increase; CETR; 1.28, CHXR; 1.21, COLR; 1.40) (

Figure **4.6**C). However, given that protein and phosphate levels appear to differ in the various CA-OMV samples, it is important to note that our efforts to compare protein and phosphate contents to WT-OMVs are more complicated and caution should be taken when using only these metrics to determine OMV concentrations. Overall, CHXR-OMVs, CETR-OMVs, and COLR-OMVs all appear to have unique distributions of proteins and phosphate levels when compared to WT-OMVs suggesting CA-adaptation promotes substantial changes in *E. coli* OMV composition and content.

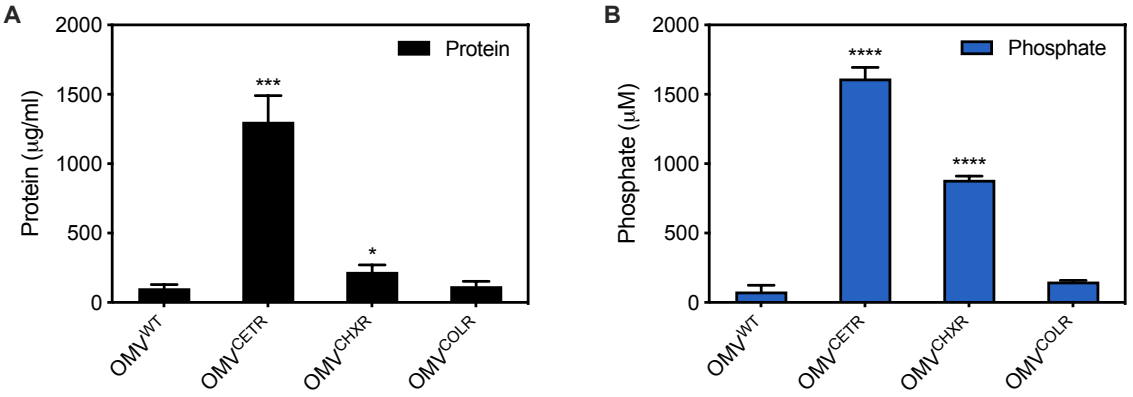

C

Sample	Protein (µg/mL)	Phosphate (µM)	Phosphate: Protein Ratio
OMV^{WT}	102.11 ± 27.39	78.94 ± 46.01	0.77
OMV^{CETR}	1302.94 ± 188.61	1613.37 ± 81.15	1.24
OMV^{CHXR}	221.28 ± 49.46	884.77 ± 25.48	4.00
OMV^{COLR}	117.51 ± 35.10	150.53 ± 8.63	1.28

Figure 4.5. Protein and phosphate profiles of CA-adapted OMVs. **A)** Total protein was measured by BCA assay, adjusted based on dilution factor and OD_{600nm} of the original culture. **B)** Total phosphate was measured by malachite green assay, adjusted based on dilution factor and OD_{600nm} of the original culture. **C)** Summary calculations for OMV protein and phosphate data, as well as phosphate to protein ratios. Data listed represents the mean of triplicate measurements, and error bars represent SD. In Panels A-B, significant differences between WT-OMV and CA-OMV samples were determined using the Mann-Whitney U test at *p*-values of < 0.05 (*), < 0.0005 (***), < 0.0001 (****).

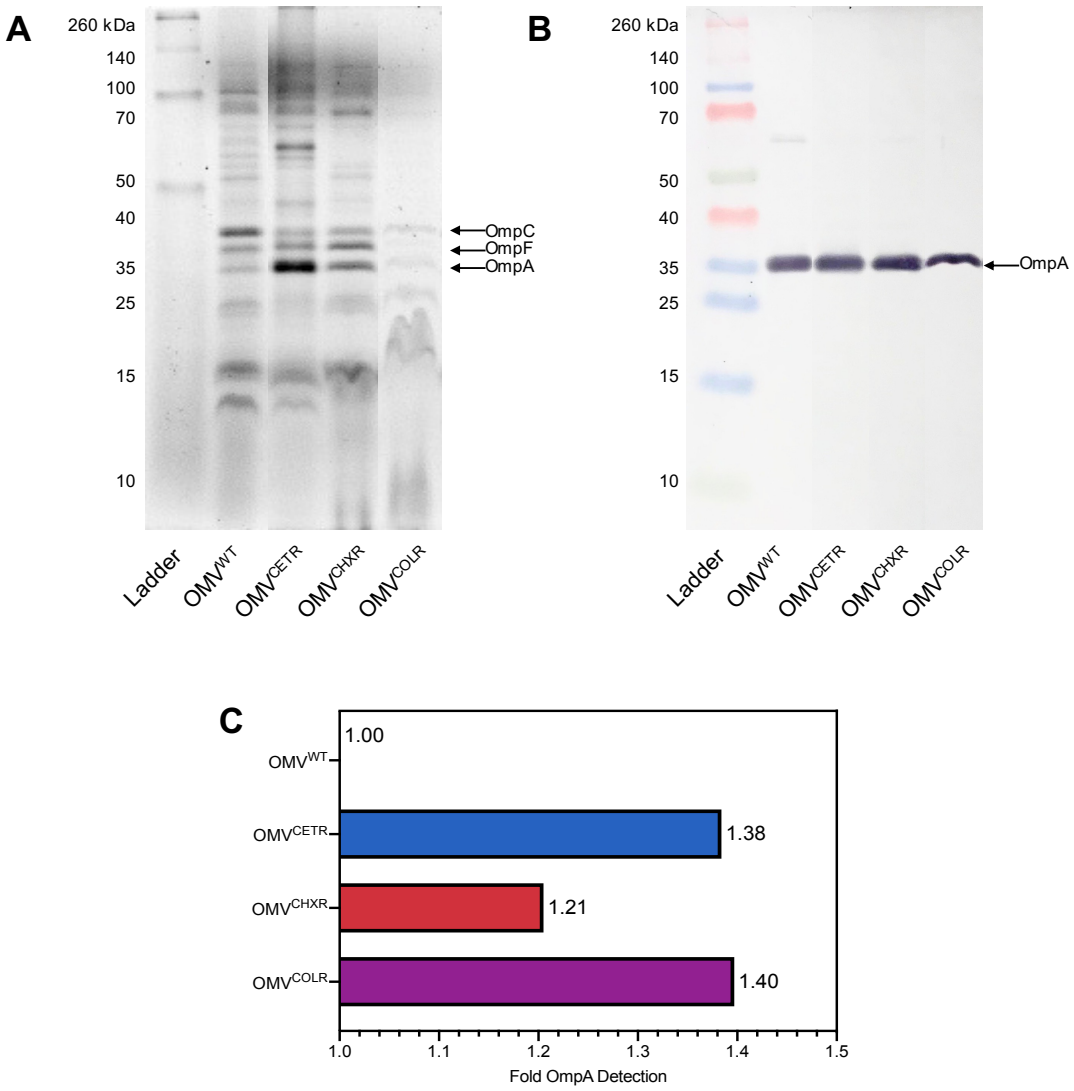

Figure 4.6. Tricine SDS-PAGE and Western blotting for proteins in CA-adapted OMVs. **A)** 12% Tricine SDS-PAGE gel of WT and CA-adapted OMVs (CETR, CHXR, COLR). In each gel lane, 10 µg of total OMV protein was loaded along with Spectra Multicolor Broad Range Protein Ladder (Thermo Fisher Scientific, USA) and samples were visualized under ultraviolet light using a 0.5% (v/v) TCE gel staining method (147). **B)** A Western blot of each CA-adapted OMV sample and WT-OMV using anti-OmpA primary antibody and HRP secondary antibody. **C)** A summary of OmpA densitometry calculations performed from OmpA protein Western blots using ImageJ software (v. 1.51). All values were compared to the WT-OMV sample in order to calculate fold-change using the equation: sample inverted pixel density / control inverted pixel density (148).

4.2.4 The morphologies of the CA-adapted OMVs imaged by cryo-TEM show distinctive vesicle types and shapes unique to each antimicrobial as compared to unadapted WT

Based on NTA and DLS findings shown in Figures 4.3-4.4, we suggest that each CA-adapted strain produces different vesicle morphologies based on their particle size distributions and broad size ranges. To examine if CA-adaptation resulted in different ultrastructural changes to each CA-OMVs, WT and CA-adapted OMVs were examined and compared using cryo-TEM imaging (Figure 4.7). Visual analysis of cryo-TEM images verified that all of the CA-adapted strains produced more OMVs when compared to WT-OMVs, corroborating NTA and DLS particle/ CFU results (Figure 4.3, Figure 4.4). Furthermore, cryo-TEM images revealed that the morphologies of each CA-OMVs were unique and each strain produced a population of vesicles with distinct morphologies (Figure 4.7). As expected from previous analysis, WT-OMVs had the standard 'single-bilayer' OMVs predominating, whereas for CA-OMVs other multi-lamellar phenotypes were observed to dominate or equally populate OMV morphological distributions (Figure 4.7). Double-layered O-IMVs, multi-layered M-OMVs, and grouped G-OMVs were visualized in images of CETR, CHXR, and COLR (Figure 4.7). In addition, the cryo-TEM images of CETR-OMVs showed additional low-density external material surrounding some vesicles, which appeared to encase 3-5 OMVs, forming vesicle aggregates (Figure 4.7B). Comparatively, CHXR-OMVs appeared to be relatively dispersed within the field of view and have higher proportions of M-OMVs and G-OMVs than other CA- or WT-OMVs (Figure 4.7C). COLR-OMVs were the most unique of all the OMV samples visualized (Figure 4.7D). At first glance, we thought some kind of extrapolymeric substance covered aggreated vesicles in cryo-TEM fields of view similar to the CETR samples, however, upon inspection of numerous images, we discovered COLR-OMVs were elongated, large (50-500 nm) amorphous vesicle structures of varying sizes, with some vesicles large enough to fill the field of view entirely (Figure 4.8). Some COLR vesicles were long and tubular, others bulbous, and still others so convoluted in shape they defied classification. Together, the results from cryo-TEM analysis suggest that adaptation to different CA classes affects bacterial OMV formation and morphology in unique ways.

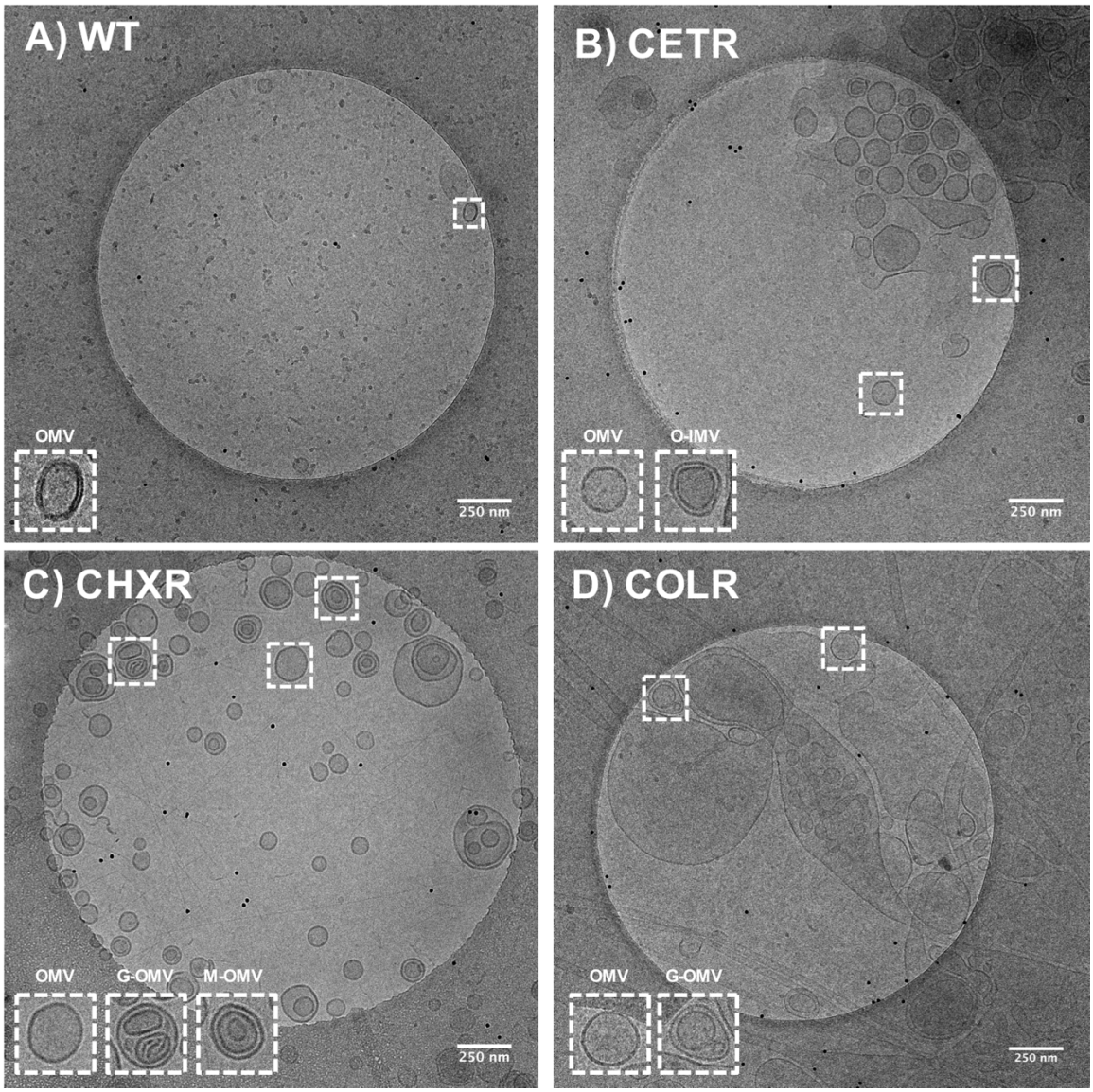

Figure 4.7. Representative cryo-TEM images at 14,500X magnification of WT and CA-adapted OMVs. **A)** WT-OMVs **B)** CETR-OMVs **C)** CHXR-OMVs **D)** COLR-OMVs. In each panel, enlarged images of representative OMVs frequently observed are highlighted as inset panel images in dashed boxes in the bottom left-hand corner. Conventional OMVs as well as vesicles with two membranes (O-IMVs) and multi-layered vesicles (M-OMVs, G-OMVs) are shown in these inset images in panels A-D. Scale bars represent 250nm.

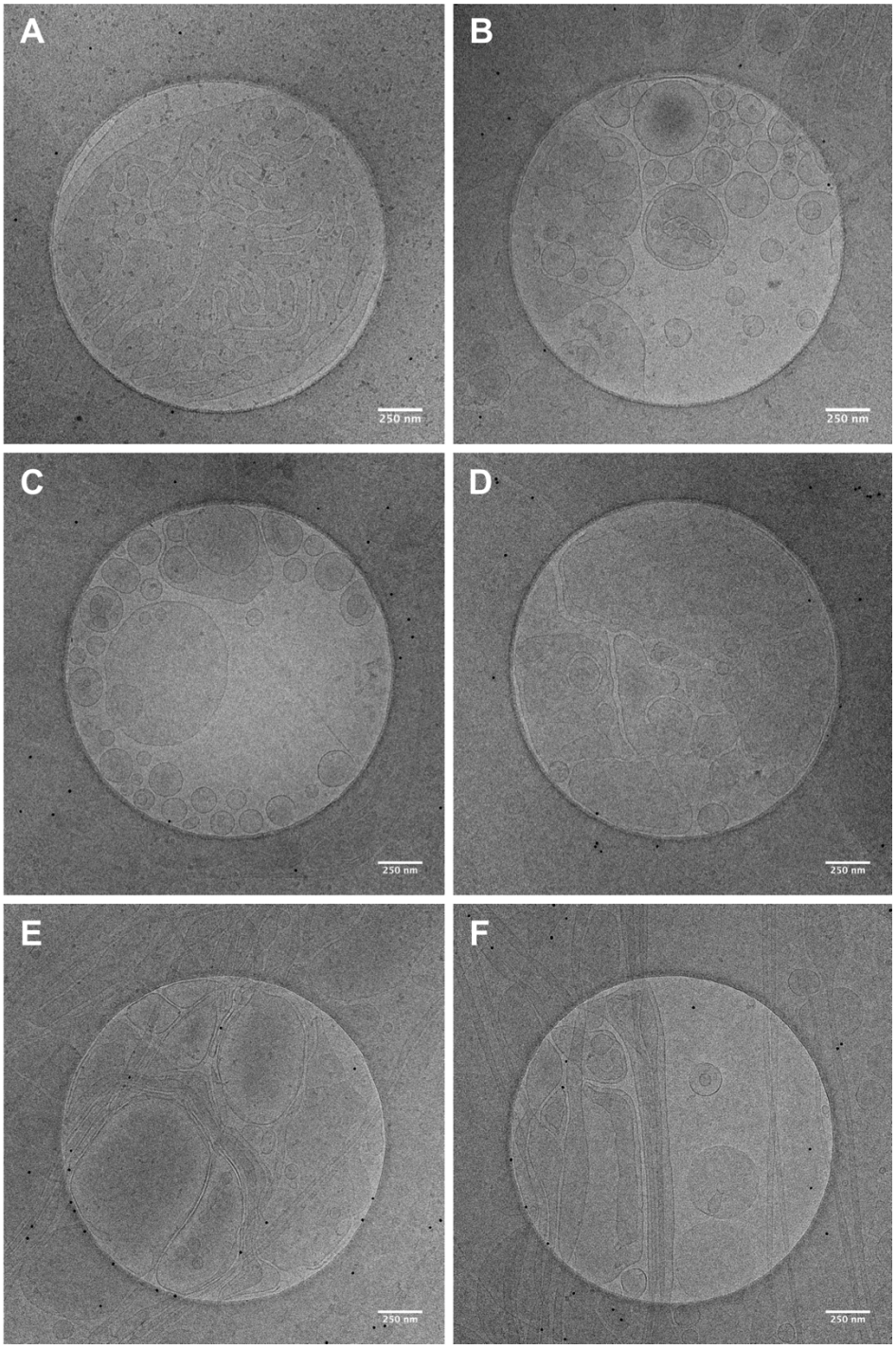

Figure 4.8. Additional examples of COLR-OMV cryo-TEM images at 14,500X magnification to highlight variable vesicle morphologies. Vesicles that fill the entire field of view are visible in **A) D)** and **E)**, conventional OMVs and multi-lamellar vesicles are visible in **B)** and **C)**, and tube-shaped vesicles are visible in **E)** and **F)**. Scale bars shown in panels represent 250nm.

4.2.5 Comparative analysis of OMV proteomes from CA-adapted strains reveal unique proteomic signatures reflecting additional cell compartment carryover.

Based on the findings from our BCA protein assays and significant differences in vesicle morphology, we predicted that OMVs from each CA-adapted strain would have unique protein compositions. To characterize the OMV proteomes in more detail, we performed nano-LC-MS/MS on WT and CA-OMV samples. This proteomic analysis identified a total of 209 proteins from the WT and the CA-adapted strains OMVs (Appendix Dataset; Figure 4.9A). Venn diagram plots of the 209 proteins revealed that WT-OMVs had the fewest unique or shared proteins identified, followed by CHXR, CETR, and COLR-OMVs (Figure 4.9A). These proteomic results agree with the complex and unique morphologies observed for each CA-adapted vesicle preparation, and support the hypothesis that each CA-adapted OMV has different compositions from the WT.

Identification of the protein contents for each OMV sample revealed that 48 total proteins were detected in WT-OMVs, 75 proteins were detected in CHXR-OMVs, 155 proteins were detected in CETR-OMVs, and 197 proteins were detected in COLR-OMVs (Figure 4.9A). Of these, 9 proteins were unique to CETR-OMVs, 45 proteins were unique to COLR-OMVs, and no proteins were unique to either the WT- or the CHXR-OMVs (Figure 4.9A). Remarkably, only 30 proteins of the 209 total proteins were identified in all four OMV proteomes and are listed in Table 4.1. As expected the majority (46.6%) of these 30 commonly identified OMV proteins in all of four vesicle proteomes were located in the OM, and fewer proteins were predicted to be localized to the PP (13.3%), CY (20.0%) and IM (16.6%) (Table 4.1). In addition, more than half of the 30 shared proteins have been identified in previous OMV studies, showing good agreement with previous OMV proteomic characterization studies (Table 4.1).

Since all OMVs isolated for this analysis were harvested from cells at stationary growth phases, it is important to note that growth phase could increase the carryover of vesicles with altered architectures such as O-IMVs and M-OMVs, containing OM+PP+IM+CY content as reviewed by Toyofuku *et al*. 2019 (75). As we show from our cryo-TEM and proteomic analyses (Figure 4.6), our WT-OMVs appear to have

a small proportion of alternative vesicle morphologies such as O-IMVs and M-OMVs that likely explain the CY and IM protein carryover (Figure 4.9B). It is important to note that many studies, including some of the earliest reports of *E. coli* OMVs in 1966, have reported the presence of additional O-IMVs and M-OMVs when isolated from stationary phase cultures (187).

To characterize OMV proteins based on their subcellular localization, we analyzed our WT and CA-adapted proteome datasets using pSORTb (v3.0.3) (https://www.psort.org/psortb/) (Figure 4.9B). Protein localization analysis revealed that CY proteins were the largest constituent in vesicles. This was followed by OM proteins and PP proteins (Figure 4.9B), as would be expected for vesicles produced by the OM. When comparing WT-OMV protein locations to each CA-OMV proteome, CETR, CHXR, and COLR-OMVs, all OMVs demonstrated significant increases in OM, PP, IM and CY proteins as well as unknown proteins. Two extracellular proteins were identified in our proteomic analysis; FliC, a flagellar filament structural protein identified in all OMVs, and YggN, a polypeptide with unknown function known to be upregulated in biofilm formation and detected in CETR and COLR-OMVs. Some proteins were unable to be categorized by subcellular localization by pSORTb, however, nearly all of these proteins have multiple cell location identifiers (e.g. a protein detected in OM and PP or IM, PP, and CY, etc.) and as such, were sorted into the 'unknown' category in Figure 4.9B. The heatmaps displayed in Figure 4.10A-D indicate unknown proteins with multiple locations in bolded lettering.

The bioinformatic database DAVID with GO annotations (https://david.ncifcrf.gov) was used to functionally classify OMV proteins and the results from this analysis are summarized in Figure 4.9C. This analysis revealed that most proteins were associated with lipid biosynthesis, membrane assembly, protein transport and efflux, stress response and protein folding/secretion. Importantly, while our localization results suggested that we had the greatest amount of CY proteins in our samples, the most enriched functions were associated with OM biogenesis and assembly, indicating that the OMVs were selective for OM and PP proteins (Figure 4.9C).

To gain more insight into OMV composition from the proteomic dataset, we compared peptide relative intensity differences in MS/MS detection for CA-OMV protein content to WT-OMV proteins, with results summarized in heatmaps shown in Figure 4.10A-D. Heatmap plotting of OM-localized OMV proteins indicating their GO functions revealed that that all three CA-adapted OMVs had a greater number of protein folding and secretion proteins (Slp, BamACD), cell wall organization and peptidoglycan biosynthesis proteins (MltA, LpoB, YbhC), as well as porin (OmpX) and transporter proteins (LamB, BtuB, FepA, FadL) (Figure 4.10A). In OM-OMV heatmap plots, CETR, CHXR, and COLR also had unique protein profiles associated with lipid biosynthesis and transport proteins (Blc, LptDE) as well as porins (OmpF) and OM transporters (Figure 4.10A). CA-OMV proteins localized to the PP had more proteins when compared to WT, although the CHXR and WT profiles were very similar (Figure 4.10B). CETR and COLR had unique OMV PP protein profiles that had increased detection of associated transporter proteins (ModA, GlnH, MglB, FliY) and protein folding (Skp, FkpA, DegP, DsbA) proteins when compared to WT. All three CA-adapted OMV PP proteomes contained the acid stress chaperone HdeB, the cell division and peptidoglycan synthesis coordinator CpoB, and the chaperone SurA, involved in the correct folding and assembly of OM proteins, such as OmpA, OmpF and LamB. The IM-OMV heatmap plots demonstrated that WT had far fewer IM proteins compared to the CA-adapted strains. All three CA-adapted strain OMVs only shared six IM proteins in common, four of which were also present in the WT OMV proteome (AtpF, YifL, OsmE, YajG) and two of which are were associated with stress response (OsmE, BorD; Figure 4.10C). The greatest number of IM proteins were associated with COLR-OMVs, including several transporter proteins (CydC, SecAD, PstB), the murein degrading enzyme MltB, and the cell division proteins DamX and FtsZ (Figure 4.10C) supporting observations that cell division proteins may be altered in these amorphous vesicles (Figure 4.7). Finally, the CY-OMV heatmaps highlighted the largest number of cytoplasmic proteins in the WT and CA-adapted strain vesicles (Figure 4.10D). Specifically, COLR had the greatest number of CY proteins, followed by CETR, CHXR, and lastly WT. A large number of these proteins had functions associated with carbohydrate metabolism/energy generation (WT; 6 proteins, CHXR; 4 proteins, CETR; 28 proteins, COLR; 21 proteins), protein synthesis and translation (WT; 3

proteins, CHXR; 7 proteins, CETR; 11 proteins, COLR; 17 proteins), and (RNA transcription/ transcriptional regulators (CHXR; 1 proteins, CETR; 3 proteins, COLR; 9 proteins) (Figure 4.10D). Several proteins involved in lipid biosynthesis were also detected in the CY-OMV proteome, in CETR and COLR (KdsA), in CHXR and WT (GlmM), as well as CY proteins exclusively in COLR (HldD, Ugd, FabZ), and in CETR (FabB). Of note, mutations in *hldD* and *ugd* have been found previously to contribute to increased polymyxin sensitivity (188, 189). This may suggest that, in response to mutations in key LPS genes, the CA-adapted strains may alter the expression of other critical systems involved in lipid biosynthesis and modification in order to compensate for alterations in membrane structure. Altogether, these OMV proteomic analyses have confirmed the carryover of proteins from various cellular compartments that may be useful biomarkers indicative of each CA-adapted strain and may aid determination of OMV form and function.

Following subcellular location and functional proteomic analyses, we wanted to assess how many OMV proteins were involved in processes associated with known intrinsic CA-tolerance mechanisms. The dominant IM efflux pump protein AcrA was found exclusively in the CETR- and COLR-OMV samples, and the general diffusion porin OmpF was found exclusively in the CHXR- and COLR-OMV samples. Cell wall-regulating OM lipoprotein protein LpoB which forms a complex with penicillin binding protein 1B was also noted to be present in only CETR and COLR proteomes (190). Also, the globomycin-sensitive OM lipoprotein Blc which binds fatty acids and phospholipids in the OM (191) was also noted in only CHXR and COLR-OMV proteomes (Figure 4.10A). In the COLR-OMV proteome, we also identified one protein associated with polymyxin resistance, the phosphoethanolamine transferase EptC (192, 193). EptC is responsible for modifying the lipid A structure of LPS by the addition of a pEtN group (194). In addition to known AMR genes, lipid biosynthesis and transport proteins FadL, LptD, LptE were identified in all CA-adapted OMVs (Figure 4.10). Lipid modifications and composition alterations may also contribute to enhanced AMR by altering drug permeability across the membrane (195, 196). Lastly, we also identified a number of periplasmic chaperones associated with stress response that were exclusive to CA-adapted

OMVs. Specifically, SurA and HdeB were found in CETR-, CHXR- and COLR-OMVs, whereas DegP, Skp, FkpA were found only in CETR and COLR-OMVs (Figure 4.10). Changes in the expression of protein folding chaperones such as *skp* when combined with AcrAB-TolC efflux pump mutations have been shown to alter *Salmonella* AMR phenotypes (197), and Skp and DegP have also been shown to be associated with increased OMV biogenesis (97).

To investigate proteins that contribute to OMV biogenesis, we focused on proteins detected in WT and all three CA-adapted OMV samples (Table 4.1). Among the 30 proteins identified in all OMV samples, many were previously identified and shown to participate in OMV biogenesis mechanisms (80, 84, 97, 113). Specifically, OM assembly complex proteins (BamB, BamC), OM porins (OmpA, OmpC, OmpW), proteins associated with osmotic stress responses (OsmE, OsmY) and oxidative stress response proteins (AdhE, FtnA) (Table 4.1). We also detected a number of Tol-Pal proteins involved in maintaining membrane integrity (TolB, TolC, Pal, Lpp), which have been implicated in OMV biogenesis and increase OMV formation when altered (85, 103, 106, 108, 160) (Table 4.1). Since we identified these proteins in all OMV samples, they likely represent important OMV biogenesis proteins that are vital for vesicle production even in the more variable CA-adapted strains.

Together, this proteomic data shows CA-adaptation significantly influences the protein contents of *E. coli* OMVs. Our analysis has revealed the presence of many additional IM and CY proteins in all samples, especially CA-OMVs which may be useful as biomarkers in future analyses. Many proteins associated with previous OMV studies in *E. coli* were noted (Table 4.1) and many unique protein profiles were identified (Figure 4.10A-D) that are involved in various aspects of cell membrane morphology, AMR, lipid and cell wall biogenesis that will be worth pursuing in future studies.

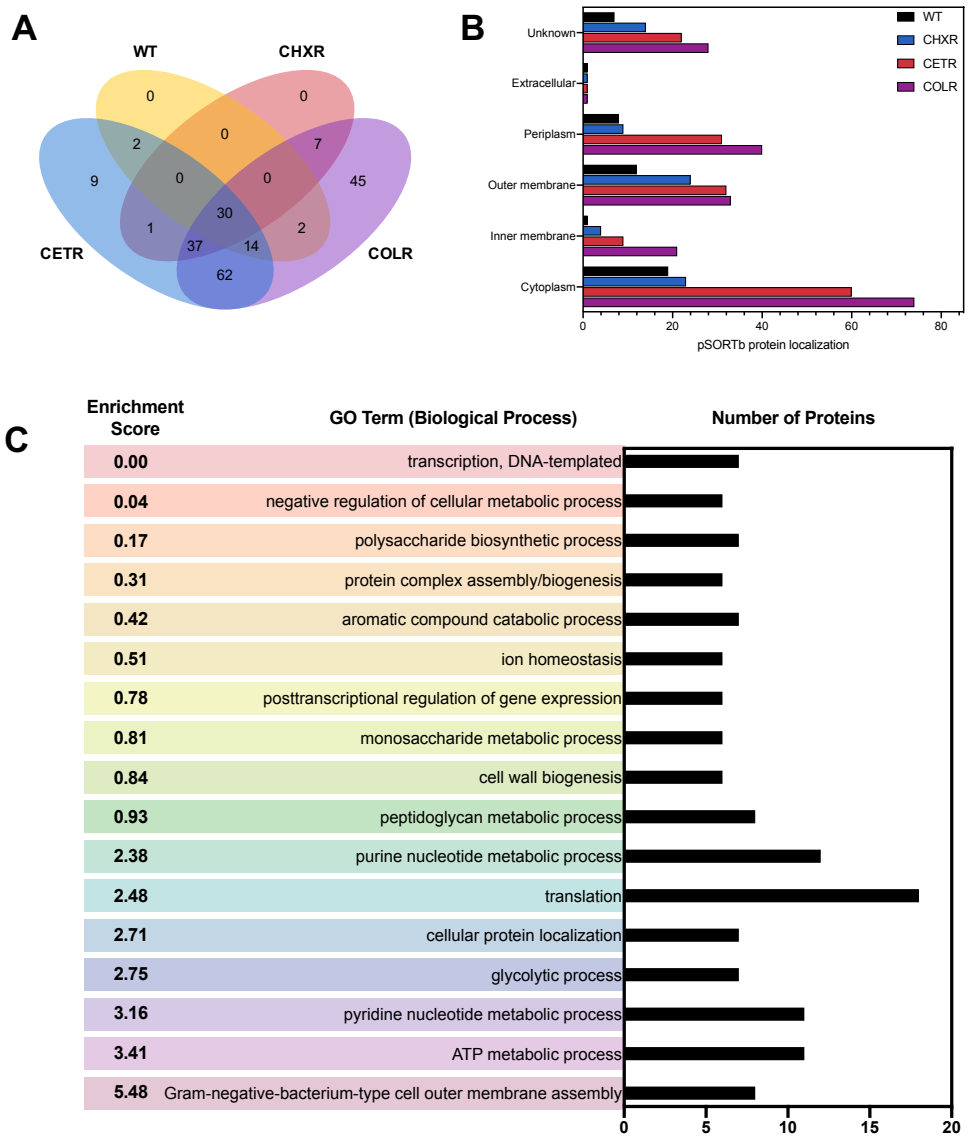

Figure 4.9. Proteins detected in CA-adapted OMVs as identified by LC-MS/MS. **A)** Venn diagram of the number of unique and shared proteins detected in each strain's OMVs. **B)** Cellular localization of proteins from CA-adapted OMVs as determined by pSORTb v.3.0.2 (https://www.psort.org/psortb/). **C)** Gene ontology enrichment analysis of the biological processes of proteins identified in WT and CA-adapted OMV samples by DAVID v.6.8 (https://david.ncifcrf.gov).

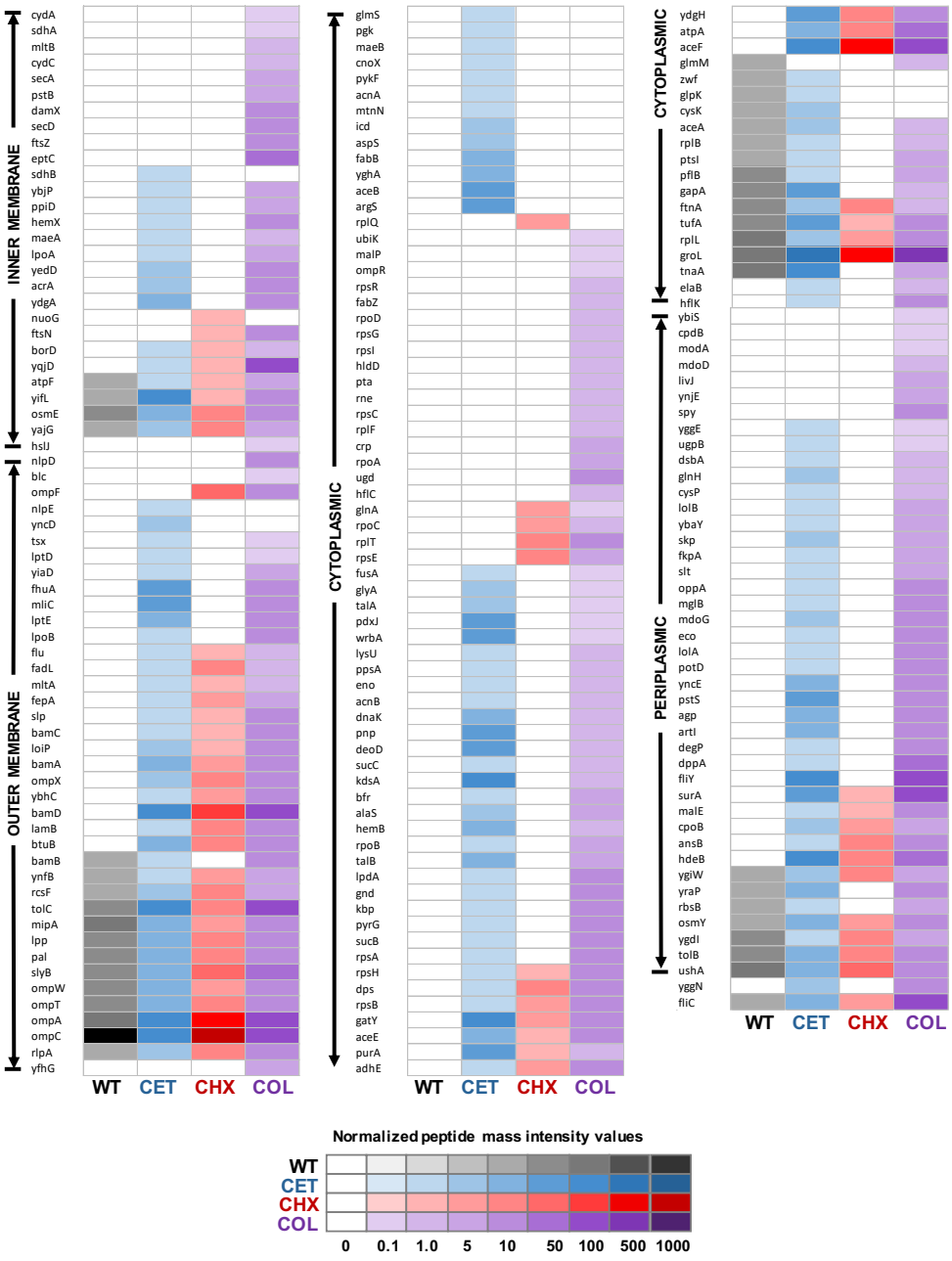

Figure 4.10. Heatmap diagram of WT and CA-adapted OMVs proteomes as identified by LC-MS/MS. Heatmap coloring is shown in the bottom panel legend, and highlights protein presence by color, as well as shading which represents the normalized peptide mass intensity values. Proteins were sorted by cellular localization using pSORTb v.3.0.2 (https://www.psort.org/psortb/). The heatmap image was made with "R" statistics software v.4.0.5 using the ggplot2 and heatmap functions, where proteins were sorted according to their annotated cellular locations and reordered by peptide mass intensity values.

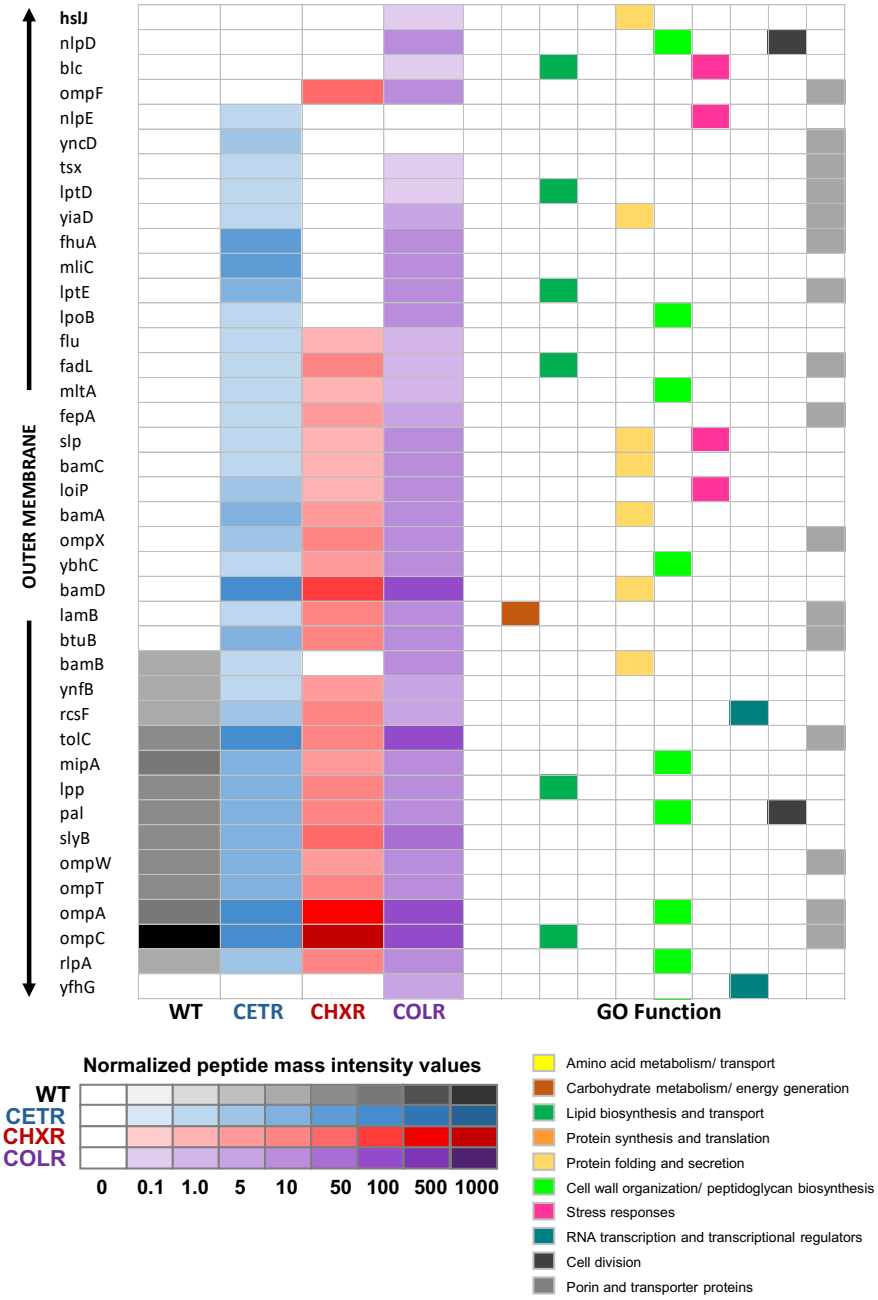

Figure 4.10 A. Heatmap summary of OM annotated proteins identified from WT and CA-adapted vesicle proteomes. Each CA adapted OMV sample shown on the heatmap plots are color coded according to normalized peptide mass intensity values of each strain tested: WT; black, CETR; blue, CHXR; red, and COLR; purple. The GO functions of the proteins are plotted as a separate colorcoded heatmap based on presence (color) or absence of function (white). In all heatmaps, white signifies the absence of detectable protein or its protein function.

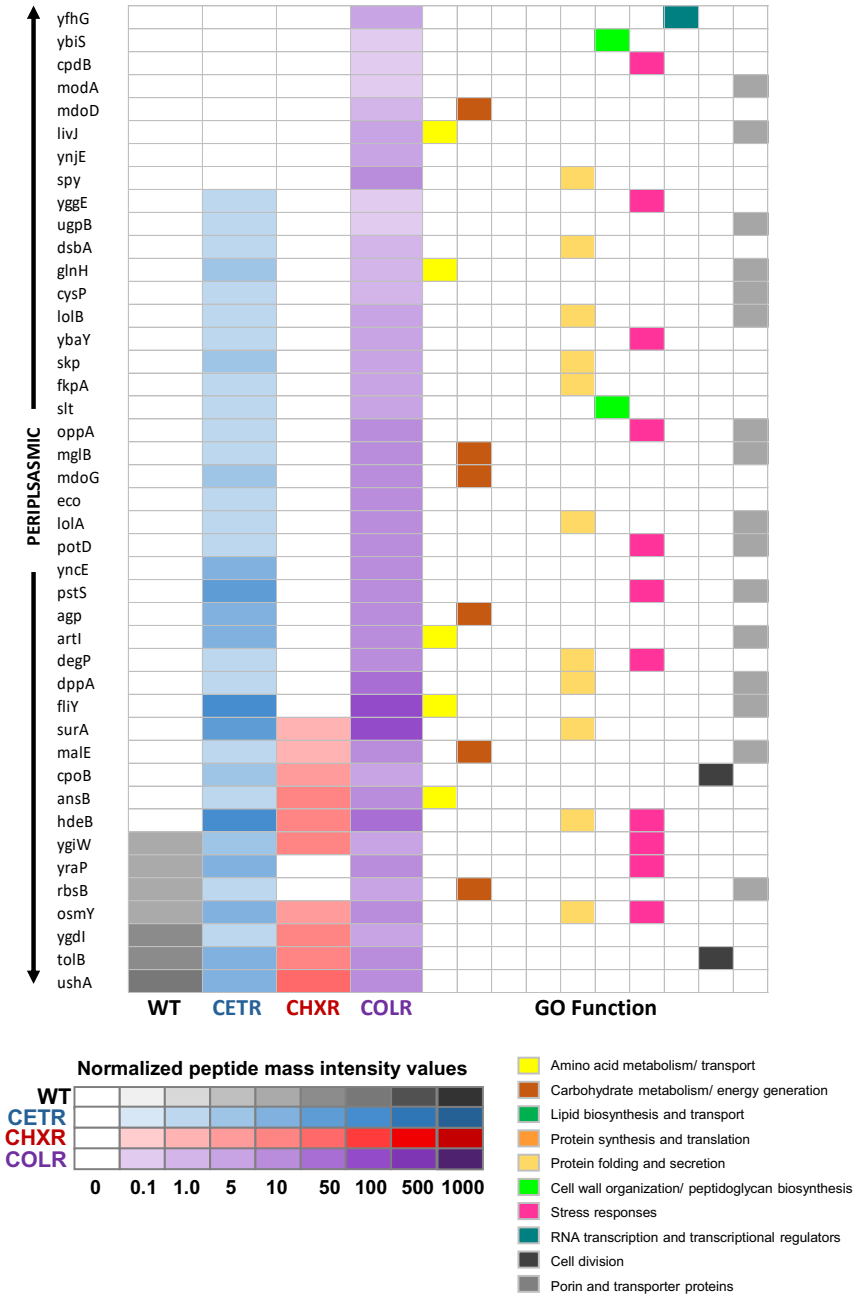

Figure 4.10 B. Heatmap summary of PP annotated proteins identified from WT and CA-adapted vesicle proteomes. Each CA adapted OMV sample shown on the heatmap plots are color coded according to normalized peptide mass intensity values of each strain tested: WT; black, CETR; blue, CHXR; red, and COLR; purple. The GO functions of the proteins are plotted as a separate colorcoded heatmap based on presence (color) or absence of function (white). In all heatmaps, white signifies the absence of detectable protein or its protein function.

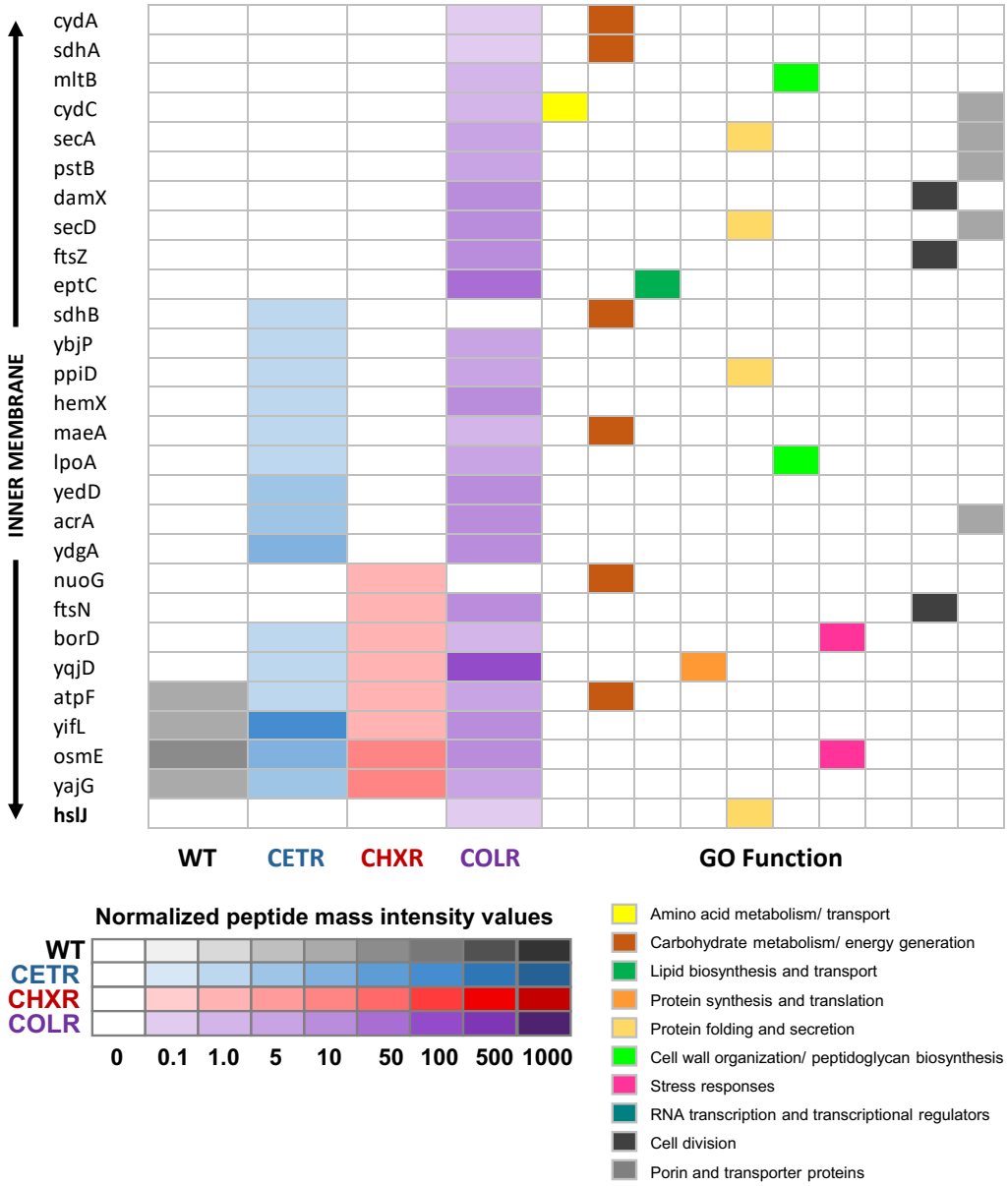

Figure 4.10 C. A heatmap summary of IM annotated proteins identified from WT and CA-adapted vesicle proteomes. Each CA adapted OMV sample shown on the heatmap plots are color coded according to normalized peptide mass intensity values of each strain tested: WT; black, CETR/ CET; blue, CHXR/CHX; red, and COLR/COL; purple. The GO functions of the proteins are plotted as a separate colorcoded heatmap based on presence (color) or absence of function (white). In all heatmaps, white signifies the absence of detectable protein or its protein function.

Figure 4.10 D. A heatmap summary of CY annotated proteins identified from WT and CA-adapted vesicle proteomes. Each CA adapted OMV sample shown on the heatmap plots are color coded according to normalized peptide mass intensity values of each strain tested: WT; black, CETR; blue, CHXR; red, and COLR; purple. The GO functions of the proteins are plotted as a separate colorcoded heatmap based on presence (color) or absence of function (white). In all heatmaps, white signifies the absence of detectable protein or its protein function.

Table 4.1.Proteins detected in OMV proteomes of WT, CETR, CHXR, and COLR.

UniProt ID	Entrez GeneID	Protein	Protein Name	pSORTb Localization	Molecular Mass (kDa)	Identified in other *E. coli* OMV studies
P0A9Q7	945837	AdhE	Aldehyde-alcohol dehydrogenase	CY	96 kDa	(59, 120)
P0ABA0	948247	AtpF	ATP synthase subunit b	IM	17 kDa	
P77774	946982	BamB	OM protein assembly factor B	OM	42 kDa	(59)
P0A903	946954	BamC	OM protein assembly factor C	OM	37 kDa	(164)
P04949	949101	FliC	Flagellin structural filament	EX	51 kDa	(59, 120)
P0A998	946410	FtnA	Bacterial non-heme ferritin	CY	19 kDa	
P0A9B2	947679	GapA	Glyceraldehyde-3-phosphate dehydrogenase A	CY	36 kDa	(59, 121)
P0A6F5	948665	GroL	60 kDa chaperonin	CY	57 kDa	(116, 120, 164)
P69776	946175	Lpp	Major OM prolipoprotein	OM	8 kDa	(59, 120)
P0A908	946301	MipA	MltA-interacting protein	OM	28 kDa	(59, 120, 164)
P0A910	945571	OmpA	OM protein A	OM	37 kDa	(59, 120, 164)
P06996	946716	OmpC	OM porin C	OM	40 kDa	(59, 120, 164)
P09169	945185	OmpT	Protease 7	OM	36 kDa	(59, 120, 164)
P0A915	945128	OmpW	OM protein W	OM	23 kDa	
P0ADB1	945305	OsmE	Osmotically-inducible putative lipoprotein	IM	12 kDa	
P0AFH8	948895	OsmY	Osmotically-inducible protein Y	PP	21 kDa	(164)
P0A912	945004	Pal	Peptidoglycan-associated lipoprotein	OM	19 kDa	(59, 120, 164)
P69411	949113	RcsF	OM lipoprotein	OM	14 kDa	(120)
P10100	945241	RlpA	Endolytic peptidoglycan transglycosylase	OM	38 kDa	(59)
P0A7K2	948489	RplL	50S ribosomal protein L7/L12	CY	12 kDa	
P0A905	946801	SlyB	OM lipoprotein	OM	16 kDa	(59, 120, 164)
P0A855	945429	TolB	Tol-Pal system protein	PP	46 kDa	(59, 120, 164)
P02930	947521	TolC	OM protein TolC	OM	54 kDa	(59, 120, 164)
P0CE47	947838	TufA	Elongation factor Tu 1	CY	43 kDa	(164)
P07024	947331	UshA	Protein UshA	PP	61 kDa	
P0ADA5	945521	YajG	Uncharacterized lipoprotein YajG	IM	21 kDa	(59, 120, 164)
P65292	947276	YgdI	Uncharacterized lipoprotein YgdI	IM	8 kDa	
P0ADU5	946051	YgiW	Protein YgiW	PP	14 kDa	
P0ADN6	1450304	YifL	Uncharacterized lipoprotein YifL	IM	7 kDa	
P76170	946119	YnfB	UPF0482 protein YnfB	OM	13 kDa	

Abbreviations: CY; cytoplasm, EX; extracellular, IM; inner membrane, OM; outer membrane, PP; periplasm.

4.2.6 OMV supplementation assays show that OMVs impact E. coli CA MICs differentially where some are protective and others antagonistic

As a final experiment following the results of the OMV quantification and phenotypic analysis, we wanted to explore whether OMVs isolated from different CA-adapted strains had an effect on WT and other CA-adapted strain's cell growth and MIC values when added to cultures exogenously. To accomplish this, a series of growth curve and antimicrobial susuceptibility testing experiments were conducted to test the effect of supplementing WT *E. coli* cultures with isolated OMVs derived from WT- and CA-adapted strains. For these experiments, OMVs isolated from WT and CA-adapted strains were quantified using BCA assays as described in Section 2.5.1 and supplemented into cultures based on protein concentration (0.4-2.0 µg/mL for growth cruves, 2.0 µg/mL for MICs), and at the same time as CA addition to cultures. Our results shown in Figure 4.11 indicate that supplementing WT *E. coli* with WT-OMVs both with and without sub-inhibitory CA exposure had no significant effects on cell growth at the OMV concentrations we tested (0.4-2.0 µg/mL OMV total protein) (Figure 4.11A, C, E). This indicated that WT-OMV supplementation was not toxic to cell growth and did not confer measureable advantages to culture growth with out without sub- inhibitory CA exposure. Similarily, CETR- and CHXR-OMV supplementation appeared to have no effect on the growth of WT *E. coli* cultures with exposure to sub-MIC concentrations of CET (15 µg/mL) and CHX (1.0 µg/mL), respectively (Figure 4.11B, D). At the highest concentration of CETR-OMV supplementation tested (2.0 µg/mL), significant differences in optical density (OD_{600nm}) values of WT *E. coli* growth were determined between 12-18 h, however, no other CET concentrations or time points grew significantly different from the control. In contrast, supplementing with COLR-OMVs had noticable effects on the growth of WT *E. coli*, and a concentration-dependent decrease in *E. coli* growth was noted as the concentration of COLR-OMVs increased (Figure 4.11F). Supplementing WT *E. coli* cultures with 0.4-2.0 µg/mL of COLR-OMVs significantly decreased the OD_{600nm} of cultures from 2-6 h growth timepoints ($p < 0.05$), and significant differences between the WT and the WT + 2.0µg/mL COLR-OMVs were determined

from 2-12 h of growth (Figure 4.11). This indicates that COL-OMV supplementation was moderately deterimental to WT *E. coli* growth at particular stages of growth.

To further assess whether OMVs could have protective effects, we performed AST to determine CA MIC values in the presence of OMV supplementation. In order to determine whether OMV supplementation affected previously determined CA MIC values of the WT and CA-adapted strains, we used the highest concentration of OMVs from the growth curve assays (2.0 µg/mL). These OMV concentrations were shown to have an effect on growth based on growth assays in Figure 4.11 and were the most feasible concentrations to test and properly dilute given the low concentrations of recoverable OMVs from litres of culture and stocks available. Supplementation of WT-OMVs had no effect on the WT *E. coli* MICs of CET and CHX, but was found to increase COL MIC values by 4-fold (Table 4.2). WT-OMV supplementation was also found to increase the COL MIC of COLR by 2-fold. Interestingly, supplementation of COLR-OMVs had the opposite effect on WT *E. coli*; when they were supplemented into cultures COL MIC values decreased by 2-fold (Table 4.2). However, when COLR-OMVs were supplemented into COLR cultures they increased MIC values by 2-fold (Table 4.2). This suggests that COLR-OMVs may be antagonistic towards WT *E. coli*, but give a protective influence on COL resistance in COLR strains. The addition of CETR-OMVs did not appear to signifcantly alter WT *E. coli* or CETR CET MIC values indicating that CETR-OMVs had little protective or antagonistic influences on QAC tolerance. Lastly, supplementation of CHXR-OMVs to WT cultures increased CHX MIC values by 2-fold as compared to WT *E. coli* without OMV supplementation (Table 4.2). In contrast, the addition of CHXR-OMVs to CHXR cultures did not confer any differences in CHX MIC values when compared to CHXR MIC values without OMV supplementation. This suggests that CHXR-OMVs may be more protective against CHX for WT cells that lack prior CHX adaptation. Together, these results provide greater insights into the functional roles these OMVs confer to cells, where some OMVs offer protective effects (WT and CHXR) to antimicrobials (CHX/ COL) while others confer antagonistic effects (COLR) and excerbate antimicrobial inhibition (COL). These differences in function likely reflect the unique shapes and

compositions of the vesicle released from WT and CA-adapted strains, and may offer more insights into the specific mechanisms of action and tolerance of each CA.

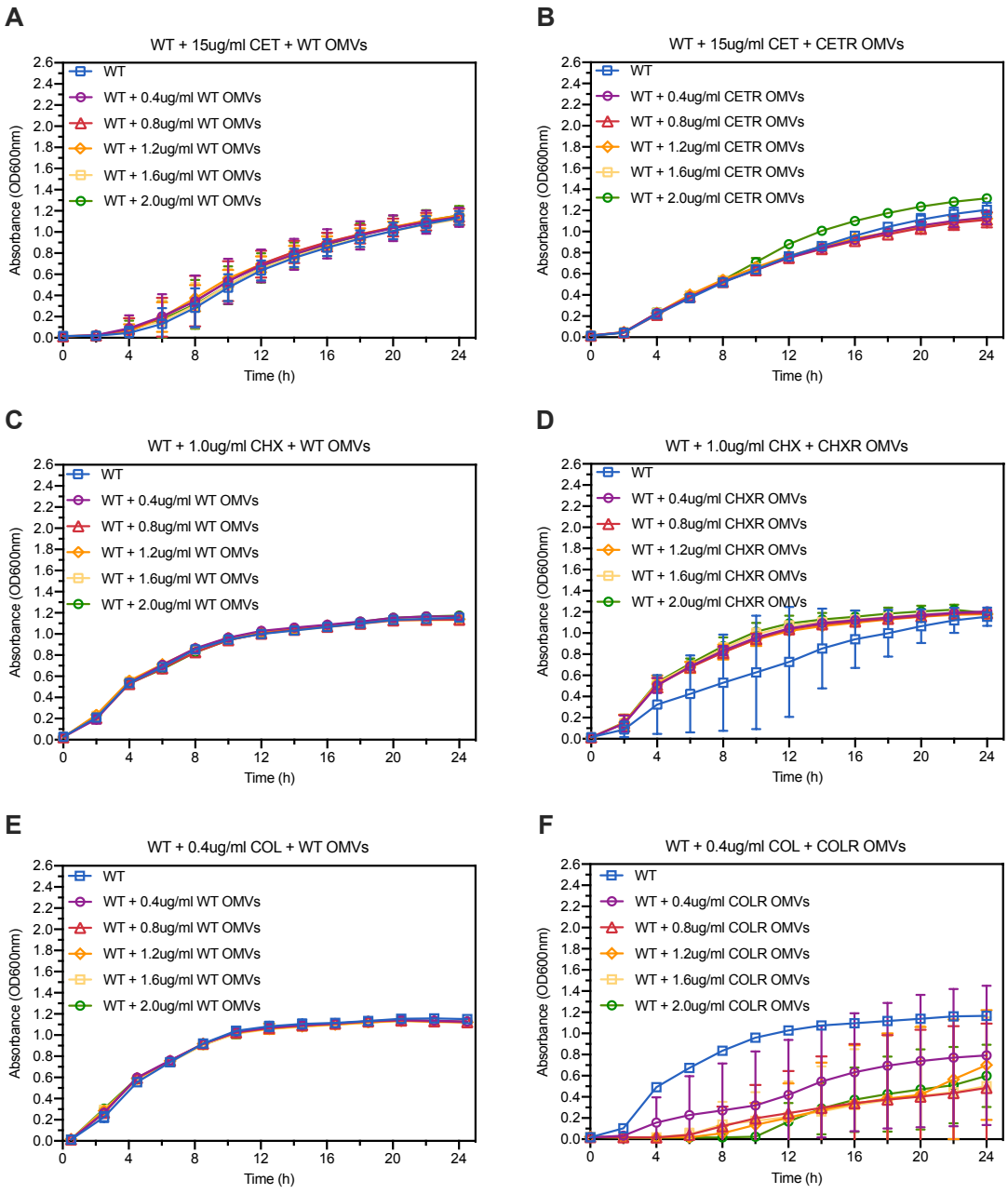

Figure 4.11. Growth curves of WT *E. coli* K-12 BW25113 supplemented with WT and CA-adapted OMVs and exposed to sub-inhibitory concentrations of CAs. **A)** Growth of WT cultures + 15 µg/mL CET with 0-2.0 µg/mL WT-OMVs. **B)** Growth of WT cultures + 15 µg/mL CET with 0-2.0 µg/mL CETR-OMVs. **C)** Growth of WT cultures + 1.0 µg/mL CHX with 0-2.0 µg/mL WT-OMVs. **D)** Growth of WT cultures + 1.0 µg/mL CHX with 0-2.0 µg/mL CHXR-OMVs. **E)** Growth of WT cultures + 0.4 µg/mL COL with 0-2.0 µg/mL WT-OMVs. **F)** Growth of WT cultures + 0.4 µg/mL COL with 0-2.0 µg/mL COLR-OMVs.

Table 4.2. Minimum inhibitory concentration values for WT and CA-adapted bacteria supplemented with OMVs against CET, CHX, and COL.

Sample	OMV Supplementation	CET MIC (μg/mL)	CHX MIC (μg/mL)	COL MIC (μg/mL)
WT	-	30	2	1
WT	2.0 μg/mL WT OMVs	30	2	**4**
WT	2.0 μg/mL CETR OMVs	30	-	-
WT	2.0 μg/mL CHXR OMVs	-	**4**	-
WT	2.0 μg/mL COLR OMVs	-	-	**0.5**
CETR	-	120	-	-
CETR	2.0 μg/mL WT OMVs	120	-	-
CETR	2.0 μg/mL CETR OMVs	120	-	-
CHXR	-	-	16	-
CHXR	2.0 μg/mL WT OMVs	-	16	-
CHXR	2.0 μg/mL CHXR OMVs	-	16	-
COLR	-	-	-	256
COLR	2.0 μg/mL WT OMVs	-	-	**512**
COLR	2.0 μg/mL COLR OMVs	-	-	**512**

4.3 Discussion

Antimicrobial adaptation over the course of many generations has been shown to result in global changes to cell physiology and function (51, 144, 184). Modifications to these systems cause widespread changes, such as the activation of stress response pathways, upregulation of efflux systems, downregulation of porins, modification of membrane lipids and production of OMVs (23, 69, 82). The findings presented in this chapter indicate that CA adaptation profoundly affects OMV production, morphology, size, and composition, and OMVs isolated from CA-adapted strains can alter antimicrobial susceptibility. These findings also offered novel insights into the role of OMVs in AMR, and reconfirm that OMVs have protective but also antagonistic influences against bacterial cells.

4.3.1 Adaptation to CAs and consequences for growth phenotypes and OMV biogenesis

Growth curve experiments conducted in this chapter were important to determine OMV particle/CFU values for each CA-adapted strain, however, these experiments also unexpectedly offered additional insights into OMV biogenesis and CA-tolerance mechansisms of these CA-adapted strains. Based on previous in-depth molecular characterization studies of the three CA-adapted *E. coli* K-12 strains generated in the Bay lab, we know that each of these strains possess a number of single nucleotide variants and in-frame deletions in a number of genes responsible for lipid biosynthesis and transport (CETR; *msbA, lpxL*, CHXR; *mlaA,* COLR; *lpxC, waaY, eptA*) and transcriptional regulators (CETR; *marR, rob* and COLR; *basS*) (38, 198–201). These genetic alterations were the consequence of prolonged, increasing CA exposure that resulted in >2-fold increased MICs against their respective CA after 20-40 subcultured generations (143, 144, 184). The genetic alterations accumulated in the final CA-adapted strains repetitively altered many LPS biosynthesis and/or LPS transporters genes (*msbA*, *lpxC*, *waaY*, *eptA*, *pqiB, mlaA*). Some CA-adapted strains also possessed mutated genes known to control lipid biosynthesis and transporter gene expression such as *basS* (202) in COLR, which is known to alter COL resistance, and *marR/ rob* which controls AMR efflux pump, porin and lipid gene expression as the *mar-sox-rob* regulon system (203). These strains were ideal candidates for exploring how intrinsically CA-tolerant, CA-adapted strains may influence

OMV production. Our NTA and DLS findings demonstrated that COL, CHX and CET-adapted strains all produced significantly greater quantities of OMVs as compared to their unadapted *E. coli* counterpart suggesting that OMV biogenesis may be altered. Additionally, these CA-adapted OMVs produced by the strains were morphologically altered compared to their unadapted WT counterparts. At first we believed OMV alterations would increase OMV production simply by their membrane damaging and disruptive effects (18), but this may not completely explain how intrinsically CA-tolerant *E. coli* produced such remarkable OMVs.

Previous studies have reported that AMR due to chromosomal mutations in the genes altered by each CA-adapted strains, some of which are essential genes (*lpxC, msbA*) are associated with fitness costs as measured by reduced growth rates compared to CA sensitive strains (204–206). In our study, we found that in the presence of CA selection, 2/3 of the CA-adapted strains had significantly reduced growth rates compared to WT (CETR and COLR), and the CHXR strain had a significantly higher growth rate compared to WT (

Figure 4.1). Reduced growth in the presence of antimicrobial was not unexpected however, the increased growth by CHXR in the presence of CHX was (Figure 4.1). A recently published study from our lab characterizing CHXR in-depth, identified that *mlaA* deletions present in CHXR strains, confer greater growth rates to *E. coli* when deleted (144), indicating that this phenotype is attributed to this gene alteration specifically. MlaA is part of a larger multi-partite intermembrane spanning complex known as the maintenance of outer membrane lipid asymmetry (MlaABCDEF) system responsible for removing phospholipids from the OM back to the IM to maintain LPS asymmetry in the OM (207). MlaA is also known to contribute to OMV biogenesis, where *mlaA/ vacJ* deletion mutants in *Haemophilus influenzae* and *V. cholerae* increase OMV production due to the accumulation of phospholipid build-up in the OM outer leaflet (113). As our recently published study of CHXR shows, Δ*mlaA* present in CHXR increase CHX MIC values by 4-8 fold, and is an excellent example of how increased OMV production may directly confer CA tolerance. Other LPS associated genes like essential gene *msbA,* an important LPS flippase in

the IM and essential gene *lpxC,* a lipid A biosynthesis enzyme likely also have an impact on OMV biosynthesis when altered, athough no OMV studies have examined these mutants to date.

Lastly, growth curve experiments conducted without CA selection showed similar growth curve trends for CA-adapted strains as compared to the WT strain. The final optical densities of each CA-adapted strain grown without selection were unexpectedly higher than in CA supplemented growth curves (Fugure 4.1). This result suggests that while these strains have undergone chromosomal mutations to lipid biosynthesis genes and their transcriptional regulators, these changes benefitted their fitness compared to WT. Future studies should examine OMV formation of CA-adapted strains grown without CA selection, as we may see even more differences in OMV morphology and size distribution. Together, these results confirm that CA adaptation has significant effects on fitness and growth, and highlight OMV biogenesis differences due to the mutations each CA-adapted strain possessed. These effects are dependent on the CA strain tested and reflect differences in their respective CA mechanism of tolerance.

4.3.2 CA-adapted strains produce more OMVs compared to WT with altered morphology and size

It is well documented that antimicrobial exposure can induce formation of OMVs as well as increase their production relative to control strains, therefore, it came as no surprise that our findings demonstrated each CA-adapted strain produced significantly more OMVs compared to WT. It was, however, interesting to note that there were profound differences in OMV production between strains, and that our CHXR strain had approximately 100 times as many particles/CFU as the other adapted strains as measured by NTA and DLS (Figure 4.3, Figure 4.4). As we discuss in Section 4.3.1, increased OMV production in all of our CA-adapted strains may suggest that OMV formation is linked to genetic alterations associated with their AMR and drug adaptation, as well as a result of antimicrobial exposure and membrane disruptive actions.

In terms of vesicle morphology, CA-adaptation and exposure resulted in different OMV phenotypes, implying that there are differences in the structure of the OM that likely influence OMV biogenesis. Studies of OMV biogenesis have shown that in strains with genetic alterations to membrane-integrity associated proteins (eg. Tol-Pal system), OMV formation primarily occurs at sites of membrane reorganization/turnover, sites of membrane deformation, or at sites of cell division (84, 163, 208, 209). Findings from our proteomic analysis of CA-adapted OMVs show significant increases in proteins corresponding to each of these categories in our CA-adapted OMVs (Figure 4.10A-D). In previous OMV studies, membrane disruption as well as antimicrobial exposure have been shown to be associated with presence of multi-layered vesicles (107, 163, 174, 210). This supports our cryo-TEM findings and suggests that the underlying genetic changes discussed in section 4.3.1 and/or antimicrobial exposure in the CA-adapted strains caused the variations in OMV morphology.

Our NTA and cryo-TEM findings (Figure 4.3, Figure 4.7) suggest that the CA-adapted strains also produced OMVs of a significantly greater size than WT, with COLR-OMVs being the largest. Given the morphology of vesicles from these strains, it is possible that a number of cell division proteins may be involved (as highlighted in Figure 4.10A-D), leading to OMV production from regions of cell division as a mechanism for membrane turnover. A previous study showed that large OMVs (~200-500nm in diameter) tended to form at sites of bacterial cell division, giving creedence to this theory (163). Alternatively, it is possible that the exposure to CAs during growth directly impacted membrane integrity and cell division, and that the increased amount and size of COLR-OMVs is the result of generalized membrane disruption. Of note, a recent study scanning electron microscopy study of *E. coli* and *P. aeruginosa* isolates exposed to COL showed significant changes in cell membrane morphology, where cells become fused and aggregated (27). Our observation of large amorphous COLR vesicles may reflect this fusion and highlight cell division and OMV biogenesis issues, and will be further explored in future studies. Together, this data shows that OMV production can be altered by adaptation to CAs, and further studies are needed to clearly elucidate the mechanisms of OMV biogenesis in these strains.

4.3.3 CA-adapted OMVs have altered contents compared to WT

We have previously characterized the genetic and proteomic changes in each CA-adapted strain (143, 144, 184). Whole genome sequencing identified mutations in genes involved in lipid biosynthesis, transport, and modification (CETR; *lpxL, msbA*, CHXR; *mlaA, yghQ*, COLR; *lpxC, waaY, basS*) as well as genes involved in AMR (CETR; *marR*, COLR; *sbmA, acrB*). Our hypothesis was that the CA-tolerant strains would make changes during CA adaptation that would modify the composition of their membrane, thus making them more impermeable to CAs. We suspected that these changes would also affect OMV production and composition, especially if such changes were made to genes associated with OM biosynthesis, modification, or transport.

The focus of our proteomic analysis of WT and CA-adapted OMVs was to ascertain whether the contents of vesicles were altered by comparison to the the originating unadapted WT *E. coli*, and to see whether any specific proteins associated with AMR were packaged into OMVs as a defense mechanism. Our results show that there were far more proteins detected in the CA-adapted strains as compared to WT, and that these proteins were enriched from numerous cell compartments, not just the OM and PP (Figure 4.9). As expected, we found a high abundance of OM structural proteins, such as OM porins, membrane integrity proteins, and proteins involved in membrane biogenesis and transport in CA-adapted strains (Figure 4.10). In addition, we found that the CA-adapted strains had more proteins associated with stress responses, including periplasmic chaperones and proteases. Extracytoplasmic stress has been shown to affect the release of OMVs by inducing the accumulation of envelope components, thus, activating a number of stress pathways and increasing OMV formation (104, 177). We noted several proteins involved in the σ^E and Cpx pathways in our OMV samples, and we also found that these proteins were only detected in the CA-adapted strains (144, 184). As many of these systems were identified in whole cell proteomic analyses of each CA-adapted strain, it is clear that stress repsonses many play an important factor in OMV biogenesis (144, 184).

Our results suggest that membrane disruption caused by CA exposure may be another important mechanism of increased vesicle formation in the CA-adapted strains. This is evident from the presence of multiple membranes and large amorphous vesicles in our cryo-TEM images, as well as the presence of proteins originating from the IM and the cytosol in our proteomic data. Previous genetic, proteomic, and microscopic studies in Gram-negative bacteria have indicated that the disruption of membrane integrity and the removal of specific proteins involved in connecting the IM and OM leads to increased formation of OMVs (84, 85, 103, 105–107). Recent studies of the membrane integrity of *E. coli* CETR, CHXR, and COLR using the impermeant dye propidium iodide have shown that these strains are more permeant than unadapted *E. coli* both with and without any added CA (144, 211). Further studies are needed to elucidate whether the genetic characteristics of the CA-adapted strains play a larger role in OMV formation, or whether this effect is the result of sub-inhibitory antimicrobial exposure during growth prior to OMV isolation.

4.3.4 Discussion of modifications in CA-adapted strains that impact their susceptibility

Following characterization of the CA-adapted OMVs, we wanted to determine whether or not isolated and purified OMVs allowed WT or CA susceptible strains to survive CA exposure at inhibitory concentrations (Figure 4.11). It has been previously reported that OMVs interact with host cells as well as bacteria, and these cell-OMV interactions facilitate immune activation and pathogenesis. Increased production of OMVs in response to stress such as antimicrobials has been documented in a variety of bacteria, and OMVs have enhanced bacterial survival against antimicrobial treatment in *E. coli*, *H. pylori,* and *P. aeruginosa* (59, 82, 86, 212). OMVs also offer protection by transferring antibiotic resistance genes or by acting as decoys that can bind to or adsorb antibiotics (59, 86, 97).

Our OMV supplementation experimental findings indicate that the protective effects of OMVs against CAs is significant (2-4 fold MIC increases), as well as CA-OMV and CA-strain specific (Figure 4.11; Table 4.2). Our results showed supplementation of WT cultures with OMVs dervived from CETR at the highest concentration tested (2.0 μg/mL) was the only condition that had a significantly increased

growth rate compared to the control (Figure 4.11). We did not detect a protective effect for any CETR conditions when we conducted MICs, but we did note a 2-fold increase in the CHX MIC for WT bacteria grown with 2.0 μg/mL CHXR-OMVs. In contrast, we discovered that COLR-OMVs had a detrimental effect on growth and survival of WT cells, causing a concentration-dependent decrease in fitness and survival, contrary to our initial hypothesis that OMVs would be protective against all membrane-acting antimicrobials. This result was further confirmed by OMV supplementation AST assays, where WT grown with 2 μg/mL COLR-OMVs had a 2-fold decrease in MIC value against COL (Table 4.2). In previous studies, the protective effects of OMVs have been attributed to the sequestration of antibiotics in solution, thus, preventing them from acting on the bacterial cells (59). This non-specific OMV-dependent mechanism would imply that regardless of the cell of origin, if the OMVs are able to interact with the antibiotic, there would be some protective abilities. However, our COLR-OMV results suggest not all OMVs are created equally, and another potential mechanism may be contributing. Reports that horizontal gene transfer can be mediated by OMVs have also been published, where the mechanism of the OMVs merging with the recipient cell's membrane can occur (78, 88–90). This OMV-cell fusion mechanism may be enhanced in COLR-OMVs (as discussed in section 4.3.2); therefore, when COLR-OMVs are exposed to WT cells, these OMVs could merge with lethal effects and transfer some of their membrane alterations to the WT cells that may in turn may make these cells weaker and less fit against COL. These COLR vesicles may themselves be an interesting antimicrobial adjuvant worth further study.

Together, our results suggest that there are protective and detrimental effects of OMVs on growth and survival in CAs, but the exact mechanism for these effects is unknown. Given the MIC results, we suggest that we may see more significant changes in the growth curves at CA concentrations closer to MIC values. This does make sense when considering only stressed cells, under the threat of being destroyed by CAs in growth media may experience the positive effect of OMVs as opposed to real environmental conditions beyond the lab. Future experiments could also look at supplementing with higher concentrations of OMVs, to see if this effect is further exacerbated by the concentration of OMVs.

4.4 Concluding Remarks

Taken together, these findings support our hypothesis that CA-adaptation affects OMV formation, morphology and protein content in unique ways, highlighting the differences between each CA's membrane disruptive mechanism of action and giving more insight into OMV biogenesis. Our results also show that CA-adapted OMV exposure has important implications for bacterial antimicrobial susceptibility, as COLR-OMVs appeared to be antagonistic for COL resistance by WT strain, whereas WT- and CHXR-OMVs were protective. This is important when considering that *E. coli* can exist in diverse environments (human/ animal hosts, aquatic or soil sources), they are often exposed to low-levels of antimicrobials, host defense systems and other species within these communities. Further work is needed to elucidate whether CA-adapted OMVs can protect bacteria against CA exposure, and whether OMV-mediated survival and growth promotion are biologically relevant *in vivo*. Our findings indicate that these stressors will greatly influence the formation of OMVs, with important consequences for survival and pathogenesis during infection.

Chapter 5. Discussion of Conclusions and Future Directions

In this thesis, we addressed two important knowledge gaps regarding Gram-negative bacterial OMs. The first study discussed in Chapter 3, addressed technical knowledge gaps by examining how OMVs isolated by UF and UC methods compared by testing OMVs produced by wildtype *E. coli* K-12 BW25113 and its hypervesiculating *E. coli* Δ*tolA* mutant. The second study described in Chapter 4, examined a knowledge gap related to how CAs and CA tolerance in *E. coli* alter OMV formation, morphology and function as it pertained to AMR in three *E. coli* K-12 strains adapted to different CA compound classes. In this section the main findings from both chapters of this thesis will be discussed and summarized in a broader context to present any overarching themes and conclusions regarding OMV production, biogenesis, and composition in CA-adapted *E. coli*. The contents of this chapter were written by Shelby Reimer with editing provided by Dr. Denice Bay.

5.1 What are the consequences of genetic changes and CA adaptation on OMV biogenesis?

As discussed in Section 1.5.3, we have categorized the mechanisms involved in OMV biogenesis into three main models, i) altered OM-IM crosslinking, ii) stress protein build-up in the PP, and iii) accumulation of lipids that enhance membrane curvature (97–100). In Chapter 3, it was demonstrated that the deletion of the IM protein *tolA* in *E. coli,* which is an integral part of the membrane integrity Tol-Pal system, resulted in increased vesicle formation and supports model (i) of OMV biogenesis. Disruption of membrane integrity by removing a component of the Tol-Pal system also had a profound effect on vesicle morphology, and we identified several lesser known Tol-Pal system phenotypes associated with Δ*tolA* in Chapter 3. We also characterized a new kind of vesicle that we coined grouped vesicles or "G-OMVs" from Δ*tolA* studies. Interestingly, similar multi-layered OMV morphologies were seen in our *E. coli* K-12 CA-adapted vesicles from CETR, CHXR, and COLR strains, and had significantly increased production as compared to WT-OMVs. For these CA-adapted strains, the mechanisms behind increased OMV production is less clear.

We believe that there are multiple mechanisms that may explain the increased OMV production observed in the CA-adapted strains. These include antimicrobial-induced stress pathway activation favoring model (ii) and genetic alterations to the membrane leading to atypical LPS structures favoring model (iii). Given what we know about the genetic alterations in the CA-adapted strains (see Section 4.3.1), we suggest that the third mechanism is most likely responsible for the increased OMV formation in these strains. Specifically, the CHXR strain has an increased buildup of phospholipids in its OM due to a deletion in *mlaA,* which normally functions to recycle phospholipids from the OM back to the IM, ultimately maintaining lipid asymmetry. The anticipated overabundance of phospholipids likely accounts for the disproportionate amount of OMVs produced by this strain. The CETR strain possesses mutations in *lpxL* and essential gene *msbA* which are responsible for lipid A biosynthesis and LPS transport; mutations to either LPS gene likely result in fewer properly formed lipid A and LPS molecules trafficked to the OM and possibly a greater amount of phospholipids. Finally, the COLR strain has mutations in *basS,* which acts as a transcriptional regulator that controls LPS biosynthesis. In addition to *basS*, COLR possessed mutations to *waaY* and essential gene *lpxC* which builds and modifies lipid A. Thus, all three COLR mutations likely reduce LPS synthesis and induce LPS modifications in the OM. Due to the pandemic, lipidomic analyses of lipid A and phospholipids from these strains to verify lipid alterations is ongoing and will ideally be completed later this year by the Bay lab. Ultimately, each of these CA-adapted strains is expected to decrease the amount of properly formed LPS and as a consequence increase the amount of phospholipids in the OM, consequently altering cell membrane curvature (favoring model iii) and likely inducing OMV formation. In fact, a recent study showed that membrane perturbations due to mutations that altered phospholipid composition resulted in 3-5 fold increased OMV production in the bacterium *Shewanella livingstonensis*, supporting the hypothesis that lipid-modifying mutations increase vesicle formation (213). Therefore, each CA-adapted *E. coli* strain appears to favor the third model of OMV biogenesis, however, each CA-adapted strain accomplishes phosphoplipid alterations in a unique way, highlighting the differences in CA adaptation related to each CA's specific mechanism(s) of action.

5.2 What insights were gained from these studies regarding CA mechanisms of action?

As discussed in Chapter 1, the mechanisms of action for each of the three CAs that were used in this thesis all focus on membrane disruption, however, the specific actions promoted by each CA differ. The CAs (CET, CHX, COL) act by binding to LPS in the OM, displacing divalent cations (Mg^{2+}, Ca^{2+}) and resulting in destabilization of the OM, allowing the CAs to gain access to the PP and IM but each CA disrupts and pertubs lipids differentially. Specifically, CET acts by associating with phospholipid head groups and integrating its hydrophobic tail into the hydrophobic interior of the bilayer, causing membrane distortion, lipid micellarization, and leakage of cytoplasmic material (32). CHX adsorbs to the membrane surface and alters membrane fluidity through displacement and lipid headgroup bridging (35). COL's mechanism of action is still unclear, although a recent study by Sabnis *et al.* 2021 suggested that COL interacts with LPS both the OM and in the IM that are awaiting transport to the OM, causing permeabilization of the IM and leakage of intracellular contents (183). Given the specific mechanisms of action by each CA studied, it could be assumed that when *E. coli* were exposed to each CA, the result would be increased membrane perturbation, leading to cytoplasmic protein leakage as well as carryover of IM and CY proteins into newly formed OMVs. Based on our findings in Chapter 4, we observed significant increases in CY and IM proteins in our CA-adapted strains as compared to WT (Figure 4.9B). This effect was most pronounced in the COLR strain, which had the highest amount of CY and IM proteins of all the strains we examined. In contrast, we noted very few IM proteins and CY proteins in CHXR compared to CETR and COLR. Interestingly, exposure to higher concentrations of CHX have been documented to cause coagulation of the cytosol, which could explain why we did not see as much cytoplasmic leakage and the contents of OMVs from this strain are similar to WT (214, 215). Finally, the amount of cytoplasmic proteins appears to be related to the size of vesicles, with the largest observed vesicles in the COLR strain having the greatest number of CY proteins, followed by CETR, CHXR, and then WT having the least. It is unclear whether the increased amount of CY proteins is directly responsible for the increased vesicle size (i.e. OMVs form around CY proteins leaking out of the IM), or whether the increased size of the vesicle is due

to the CA and cellular responses by vesiculation which increased the carryover of CY proteins as a coincidental effect. Ideally, future studies will elucidate how CAs increase OMV formation and content.

Furthermore, the mechanism of action for each CA in this study and how *E. coli* adapted to each CA, lends insight into OMV morphologies seen by cryo-TEM analysis in Chapter 4. For example, the actions and chemical properties of CET causes cells to lose osmoregulatory capabilities, increase oxidiative stress, and leak potassium ions and protons (18) in addition to membrane perturbations. Many CETR OMVs cryo-TEM images (Figure 4.7) appeared to be surrounded or encompassed by low-density emission external material. This additional material may explain why these CETR-OMVs had the least influence on *E. coli* OMV supplementation OMV antimicrobial susuceptibility testing (Table 4.2); perhaps OMV encapsulation in this material prevented their interaction with cells. More studies of this are necessary to determine what this encapsulating OMV material is in CETR preparations. Given the chemical structure and action of CHX, WT *E. coli* cells are believed to be less tolerant to the increased membrane rigidity caused by the inflexible compound bridging headgroups of adjacent phospholipids (18). In CHXR, one method to overcome increasing membrane rigidity may be through greater amounts of vesicles produced in this strain, by the deletion on *mlaA* that increases phospholipid accumulation in the OM (144). Lastly, the membrane morphology of the COLR strain, which is resistant to 300 μg/mL COL, is the most unique, and to our knowledge has never been described before. Interestingly, regardless of the shape, all of the vesicles from the COLR strain appear to be fully enclosed in a membrane, discounting the idea that COLR vesicles are the result of generalized membrane lysis (Figure 4.8). The production of tube-shaped structures by bacteria has been reported before for *Francisella novicida* and *S. enterica*, and although the mechanism behind their production was not elucidated, their nanotubes were visualized to interconnect bacteria in biofilms (216, 217). As COL-resistant mechanisms in *E. coli* are known to alter and converge on LPS biosynthesis and modifying enzymes (48), the COL-adapted strain would be expected to have profound membrane perturbations that ultimately lead to the losses in LPS production and/or significant LPS modifications to observed after COL exposure (27, 183). The elongated tubular vesicles observed for COLR strains herein

may suggest that membrane fusion and cell division malfunctions may play added roles in the COL mechanism of action but it is not clear if they are cause or effect of the LPS alterations.

Together, the phenotypes and contents of the CA-adapted OMVs demonstate that there are significant differences in mechanisms of action/tolerance to each CAs that were evident from their respective vesicles. Future studies should investigate the morphology of these strains under various CA exposure conditions to elucidate the mechanisms of OMV formation in the presence of these antimicrobials.

5.3 What are the consequences of increased OMV production for AMR?

The increasing prevalence of MDR Gram-negative pathogens is a serious threat to global health due to severely limited treatment options, especially in species such as *E. coli*, a top blood and urinary tract bacterial pathogen (4, 5). Hence, it is vital to understand the mechanisms of resistance utilized by this bacteria so that we can develop new therapeutics and ways to combat resistance. This thesis sought to understand how OMV production was influenced by a set of lab-generated, CA-adapted, tolerant strains using the non-pathogenic model *E. coli* K-12. Although this species lacks clinically relevant AMR genes, mobile genetic elements or plasmids carrying AMR genes or virulence factors establishing it as a pathogen, *E. coli* K-12 was a perfect model to test how intrinsic AMR emerges in bacterial species, as many pathogens are believed to have commensal origins (218, 219). The utility of *E. coli* BW25113 and its associated Keio and ASKA plasmid libraries is immense for exploring intrinsic AMR by gradual CA adaptation, as we know the underlying genetic and proteomic characteristics of the originating strain and possess tools to study the genes altered in these processes (9–12). Given this information, we were able to explore mechanisms of CA tolerance and learn more about AMR and OMV biogenesis based on the changes we saw in vesicle production in this project. Specifically, we were able to demonstrate significantly increased production of OMVs from CA-adapted strains, and prove that their OMV morphological characteristics and proteomic constituents were greatly altered compared to the WT *E. coli* strain (Chapter 4; Figures 4.7-4.10).

Recent studies conducted on OMVs have shown that they may play a role in AMR in bacteria, although their precise mechanisms are not clear. As discussed in Section 1.5.2, current theories suggest OMVs participate in AMR in two possible ways; by acting as decoys that directly bind antimicrobials in the cell's environment, or by acting as an antimicrobial removal system to shed membrane-bound antimicrobials by increasing OMV production (59, 82, 86, 212). OMVs have also been shown to carry AMR genes/ biomarkers, such as β-lactamases (59, 220, 221) that can be shared and transmitted between cells by membrane fusion when vesicles are absorbed by cells for internalization of their materials (88–90) (Section 1.5.2.1). Our proteomic analysis (Chapter 4; Figure 4.9, Figure 4.10) determined that OMVs released from CA-adapted strains were enriched with more proteins from the cell than the un-adapted WT strain, and included a variety of stress response proteins and established AMR proteins that contribute to CA tolerance. For instance, the presence of EptC in COLR-OMVs suggested that this protein is in high abundance due to the exposure to COL, and that resistance to this antimicrobial likely involves modification of lipid A with pEtN groups, a known COL resistance mechanism (48, 192). However, when these COLR-OMVs were supplemented into WT *E. coli* cultures (Figure 4.11; Table 4.3), we did not see any OMV protective effects, instead, OMV antagonism was observed. This may support the vesicle-to-cell fusion theory and suggest that the COLR-OMVs fused with the OM of recipient bacteria (WT). OMV fusion may introduce its modified lipid cargo into the membrane as well as the release of OMV luminal proteins into the recipient bacterium, making the cells more fragile and possibly more susceptible to COL. We did observe OMV protective effects during CA-OMV supplementation for several other conditions, including supplementation of WT-OMVs and CHXR-OMVs into WT *E. coli* cultures (Table 4.3), supporting the OMV decoy and antimicrobial removal theories. OMVs from the bacterium *P. gingivalis* have been shown *in vitro* to bind CHX and provide protection against CHX treatment, further supporting this idea (222). Altogether, our results demonstrated that OMVs from our CA-adapted strains were able to modulate antimicrobial susceptibility against CAs, and recommend that future studies should explore the roles of CA-adapted OMVs in protecting or potentially harming bacterial cells in-more depth.

Finally, we suggest that if OMV production can help bacteria to survive stressors such as the host immune system and antimicrobials (ie. the OMV decoy theory), then designing therapies to interfere with vesiculation could increase bacterial antimicrobial susceptibility or reduce bacterial virulence. In the case of our CA-adapted strains, we found that exposure to COLR-OMVs reduced the growth rate of WT cells, and increased their susceptibility against the antibiotic COL. Further research could look at exploiting COLR and other CA-adapted strain OMVs for their potential effects to decrease bacterial growth and increase susceptibility against antimicrobials.

5.4 What are the implications of OMV production for bacteria-host cell interactions/ infections?

Our results show that CA-adaptation impacts both OMV production and OMV molecular composition dramatically, likely reflecting the precise mechanism of action of each CA. As these studies were conducted *in vitro* only and involved a non-pathogenic *E. coli* K-12 lab strain, it is difficult to predict the implications of our findings to human host infection and treatment involving these CAs. Previous OMV studies have demonstrated that vesicle production occurs *in vivo* during bacterial infection, and *E. coli* OMVs are detectable in host tissues and body fluids such as blood and urine (72, 223). In addition, OMVs have been shown to modulate the host immune response by inducing immune cell activation and cytokine secretion, and by delivering cytotoxic factors that induce apoptosis and tissue damage (224, 225). Given that the CA-adapted *E. coli* K-12 strains tested in this thesis were derived from a non-pathogenic laboratory strain, it is unlikely that they possess the virulence factors necessary to pose the same risk in a host infection scenario. Unlike MDR *E. coli* that is commonly isolated from hospitalized patients, our *E. coli* strains lack important virulence determinants (toxins, adhesins, antibiotic resistance genes, O-antigen) that are key in immune activation. However, LPS and its modifications have been shown to alter innate immune responses in Enterobacteria (226, 227) and given that these strains have significant alterations in their lipid content, we expect that CA-adapted *E. coli* OMVs will likely trigger inflammation and other innate immune reponses. Previous studies have shown that OMVs derived from non pathogenic strains of *E. coli* actively

engage in both the innate and adaptive immune systems through surface displayed and soluble pathogen-associated molecular patterns (228, 229). A recent collaboration with Dr. Thomas Murooka's lab and the Bay lab have tested COLR *E. coli* for its ability to activate dendritic cell innate immune reponses, and preliminary data from this study shows COLR *E. coli* significantly enhances dendritic cell cytokine and inflammatory responses as compared to WT (data not shown; unpublished results; manuscript in preparation). Therefore, CA adapted *E. coli* K-12 OMVs may similarily increase immune activation and inflammation. Future studies in the Bay lab seek to explore the consequences of LPS alterations in CA-adapted and CA-tolerant *E. coli*.

5.5 What is the therapeutic potential of OMVs?

OMVs are naturally and constitutively secreted from bacterial cells at various stages of their growth, under diverse environmental conditions, and in response to internal cellular triggers (97, 129, 230). Their particle sizes, strong immunogenicity, targeted delivery, and stability in solution makes OMVs an attractive target and model for therapeutic development, including vaccine and drug delivery systems (96, 150, 231, 232). Unlike liposomes or other artifically manufactured liponanoparticles, OMVs are more complex in structure and derived directly from bacterial cells. As a result, OMVs can be inexpensive to produce as compared to artifical liposomes/ nanoparticles, they are non-toxic and are more stable in solution (as we demonstrate in Chapter 4; Figure 4.2), and their surface antigens promote targeting to specific host and bacterial cells, potentially allowing them to deliver therapeutic cargo. Bioengineering studies have proposed using 'designer' OMVs that are modified using molecular biology tools to contain specific constituents and have specific membrane compositions (96, 232). The CA-OMVs studied herein may be instructive towards these bioengineering efforts as we have produced protective and antagonistic functioning vesicles to *E. coli* (Table 4.3).

Given their immunogenicity, self-adjuvation, and uptake by immune cells, OMVs have also been utilized as vaccine platforms against pathogenic bacteria (139, 233–235). The efficacy of bacterial OMV vaccines has been tested with a number species, including *Burkholderia mallei* (236), *A. baumannii* (237),

N. meningitidis (140, 238), and *E. coli* (229, 234, 239). OMVs are ideal for vaccines against bacterial infections because they possess antigens that stimulate the immune system such as LPS, lipoproteins, and OM porin proteins, but they are unable to self-replicate or cause infections. They can also be modified by the addition of exogenous peptides or surface-associated glycotopes to induce the immune system to produce protective antibodies. By fully characterizing OMVs from non-pathogenic strains such as *E. coli* K-12 as in this thesis, we will be able to build upon this information to understand the effect of host cell modifications on OMV production and composition, and design safer and more effective OMV vaccine and drug delivery systems.

5.6 Limitations of this study

There were a number of important limitations due to the design and time available to complete these studies. The first was the inability to isolate vesicles from CA-adapted *E. coli* strains under more varied growth conditions. Given the timeframe of a MSc project, the COVID-19 pandemic restricting lab access last year, and technical resources available, all of the CA-OMV findings presented in Chapter 4 of this thesis was from CA-adapated *E. coli* cells grown in the presence of antimicrobial selection (ie. at concentrations selective for WT MICs). As a result, we do not know whether the effects that we see in the CA-adapted strains, their phenotypic, morphological, and proteomic differences were due solely to antimicrobial exposure or due to the genetic changes present in the CA-adapted strains. Future studies should look into assessing these CA-adapted strains without antimicrobial selection, as this may be a confounding factor for determining how CAs influence OMV biogenesis in un-adapted WT *E. coli*.

Secondly, at the start of this project, we determined that greater yields of OMVs were harvested from *E. coli* cultures grown to stationary phase rather than to mid-log phase, as reported in other OMV studies (135). It is important to note that by stationary phase, contamination with membrane components and cytosolic proteins due to cell lysis is a concern for OMV yield and purity. As well, other factors such as nutrient availability/ depletion, secondary metabolite waste build-up, pH and temperature are known to affect OMV morphology and compositions (124, 135, 240). Although we were consistent with how we

grew bacterial cultures and conducted OMVs isolations by UF or UC, minute differences in growth conditions (i.e. pH, humidity, oxygen availability) can affect cell growth rates, lag times, cell yields, and consequently OMV properties and yields.

Finally, our antimicrobial susceptibility tests and growth curves did not show consistent results for OMV-mediated protection against the CAs used in this study. For both MICs and growth curves, we used low concentrations of OMVs (0.4 – 2.0 μg/mL) to see whether or not OMV supplementation altered *E. coli* MIC values, similar to the work done by Kulkarni *et al.* 2015 (86). While we did find an effect for several conditions, the MIC values for these conditions were all within two-fold of the WT MIC except in one condition (WT OMVs supplemented to WT cells against COL; Table 4.3). Considering other studies have used much higher concentrations of OMVs to assess protective capabilities, the concentration ranges used in this study may have been too low for AST determination (59, 82, 212). It should be noted however, that the amounts we used in OMV supplementation assays do not reflect the true maximum biological amounts of OMVs secreted from cells in culture (241), as they were concentrated from 1L cultures before being diluted into *E. coli* cultures for AST (Chapter 2; Section 2.4). Hence, the OMVs supplemented are in significant excess of naturally secreted maximum amounts (10-1000 times). Another risk in using concentrated OMV supplementation to *E. coli* cultures, is that it increases the possibility for carryover of other materials from OMV isolation preparations, including flagella, protein aggregates, and potentially some CA particles that may confound results. The OMVs added to rich growth medium may also become a carbon and nutrient source themselves, skewing *E. coli* growth and potentially biasing MIC values determined by losses of growth in the assay. As well, given the extremely low concentration of WT-OMVs obtained from 1L cultures, it would be incredibly time- and resource-consuming to obtain high enough yields of OMVs in order to conduct assays with higher OMV concentrations.

5.7 Thesis conclusions

In Chapter 1 of this thesis we proposed that CA-tolerant Enterobacteriacae would have altered OMV production and composition. We hypothesized that the CA-tolerant strains would produce greater

amounts of OMVs compared to susceptible strains, with protein and lipid changes indicative of membrane modfiications, and that OMVs isolated from these strains would provide additional protection against antimicrobial exposure. To address these hypotheses we posed the following questions which we answer below.

1. What OMV isolation method is most effective for obtaining high yield heterogenous OMV populations with minimal impurities?

    In Chapter 3, we assessed two of the most common methods for OMV isolation, UC and UF. We found that although both methods were comparable in terms of vesicle morphology and purity, the UF method resulted in a higher yield of smaller and averaged-sized vesicles and UC increased the recovery of larger sized vesicles (Figure 2.4).

2. Does a single-gene deletion mutant affecting cell membrane integrity increase OMV production compared to a wild-type control strain?

    In Chapter 3, we determined that the single gene-deletion mutant *E. coli* K-12 Δ*tolA* produced significantly more OMVs compared to the wild-type control using NTA. Depending on the OMV isolation method used, these values differed slightly, but UC methods showed that the Δ*tolA* strain produced 2.2 ± 0.45-fold more OMVs than WT, and UF methods showed that the Δ*tolA* strain produced 4.1 ± 0.41-fold more OMVs than WT (Figure 2.2).

3. Do CA-adapted strains of *E. coli* produce more OMVs compared to a susceptible wild-type control strain?

    Chapter 4 demonstrated that CA-adapted strains with increased tolerance to CET, CHX, and COL all produced significantly more OMVs compared to the wild-type control using NTA and DLS (Figure 4.3, Figure 4.4).

4. Are there differences in lipid and protein contents between OMVs isolated from CA-adapted strains and a wild-type control?

In Chapter 4, we noted significant differences in total OMV protein and phosphate detection from our CA-adapted strains, with greater phosphate to protein ratios in all strains except WT (Figure 4.5). Additionally, we analyzed the proteomic content of the CA-adapted OMVs, and found a number of proteins whose functions were associated with stress response and CA tolerance. Unexpectedly, we noted that there was a large number of IM and cytoplasmic proteins present in our proteomic data set, suggesting that there may have been some membrane disruption or damage that occurred during cell growth prior to OMV isolation.

5. Are OMVs isolated from CA-adapted strains able to increase or decrease susceptibility against CAs when they are supplemented into cultures of wild-type or CA-adapted strains of *E. coli*?

In Chapter 4, CA-adapted and WT-OMVs were tested for their ability to decrease susceptibility to various *E. coli* strains against the CAs CET, CHX, and COL. Growth curves and OMV supplementation antimicrobial susceptibility testing assays suggested that CA MICs can be modulated by the addition of OMVs. We found that CHXR-OMVs and CETR-OMVs may have mild 2-fold MIC value protective effects on *E. coli* cell growth, whereas COLR-OMVs had some antagonistic effects by reducing WT *E. coli* MICs by 2 fold (Table 4.3).

Altogether, our results lend insights into the production and composition of OMVs using a wild-type *E. coli* laboratory strain, a mutant with impaired membrane integrity, and several CA-adapted strains. During the research performed in this thesis, I developed and troubleshot a number of methodologies for OMV isolation and analysis, paving the way for future studies in the field of OMVs. The results presented here are novel, and characterize OMV phenotypes from mutant and CA-adapted *E. coli* strains, highlighting the need for further research on OMV morphologies and compositions.

5.8 Future directions

While the findings presented in this thesis provide a distinct contribution to knowledge in the field of OMV research, our results generate many new questions regarding OMV morphology and the effects of

CA exposure on OMV production and composition. Given the findings of the COLR-OMVs on cell growth/fitness and antimicrobial susceptibility in Chapter 4, future work should look at assessing the mechanisms of OMV protection by visualizing the dynamics of OMV-cell interactions. In addition, the in-depth characterization of OMVs should be expanded to pathogenic bacteria, to determine whether the same trends in OMV production and composition in our CA-adapted strains are seen in pathogens. To fully address whether OMVs are relevant to study in the context of pathogenesis and host infection, human and animal model immunological studies both *in vitro* and *in vivo* should be conducted to ascertain whether increased production of OMVs or the presence of specific markers on OMVs elicits a strong immune response.

Chapter 6. References

1. Reimer SL, Beniac DR, Hiebert SL, Booth TF, Chong PM, Westmacott GR, Zhanel GG, Bay DC. 2021. Comparative analysis of outer membrane vesicle isolation methods with an *Escherichia coli tolA* mutant reveals a hypervesiculating phenotype with outer-inner membrane vesicle content. Front Microbiol 12:383.
2. Kaper JB, Nataro JP, Mobley HLT. 2004. Pathogenic *Escherichia coli*. Nat Rev Microbiol 2:123–140.
3. Rojas-Lopez M, Monterio R, Pizza M, Desvaux M, Rosini R. 2018. Intestinal pathogenic *Escherichia coli*: Insights for vaccine development. Front Microbiol 9:440.
4. Zhanel GG, Adam HJ, Baxter MR, Fuller J, Nichol KA, Denisuik AJ, Golden AR, Hink R, Lagacé-Wiens PRS, Walkty A, Mulvey MR, Schweizer F, Bay D, Hoban DJ, Karlowsky JA. 2019. 42936 pathogens from Canadian hospitals: 10 years of results (2007-16) from the CANWARD surveillance study. J Antimicrob Chemother 74:iv5–iv21.
5. Denisuik AJ, Garbutt LA, Golden AR, Adam HJ, Baxter M, Nichol KA, Lagacé-Wiens P, Walkty AJ, Karlowsky JA, Hoban DJ, Mulvey MR, Zhanel GG. 2019. Antimicrobial-resistant pathogens in Canadian ICUs: Results of the CANWARD 2007 to 2016 study. J Antimicrob Chemother 74:645–653.
6. Idalia V-MN, Bernardo F. 2017. *Escherichia coli* as a model organism and its application in biotechnology, p. 253–274. *In Escherichia coli*: Recent Advances on Physiology, Pathogenesis and Biotechnological Applications.
7. Gibson B, Wilson DJ, Feil E, Eyre-Walker A. 2018. The distribution of bacterial doubling times in the wild. Proc R Soc B Biol Sci 285:20180789.
8. Cronan JE. 2014. *Escherichia coli* as an Experimental Organism eLS. John Wiley & Sons, Ltd.
9. Baba T, Ara T, Hasegawa M, Takai Y, Okumura Y, Baba M, Datsenko KA, Tomita M, Wanner BL, Mori H. 2006. Construction of *Escherichia coli* K-12 in-frame, single-gene knockout mutants: The Keio collection. Mol Syst Biol 2:2006–2008.

10. Kitagawa M, Ara T, Arifuzzaman M, Ioka-Nakamichi T, Inamoto E, Toyonaga H, Mori H. 2005. Complete set of ORF clones of *Escherichia coli* ASKA library (A complete set of E. coli K-12 ORF archive): Unique resources for biological research. DNA Res 12:291–299.

11. Blattner FR, Plunkett G, Bloch CA, Perna NT, Burland V, Riley M, Collado-Vides J, Glasner JD, Rode CK, Mayhew GF, Gregor J, Davis NW, Kirkpatrick HA, Goeden MA, Rose DJ, Mau B, Shao Y. 1997. The complete genome sequence of *Escherichia coli* K-12. Science (80-) 277:1453–1462.

12. Vijayendran C, Polen T, Wendisch VF, Friehs K, Niehaus K, Flaschel E. 2007. The plasticity of global proteome and genome expression analyzed in closely related W3110 and MG1655 strains of a well-studied model organism, *Escherichia coli*-K12. J Biotechnol 128:747–761.

13. Soufi B, Krug K, Harst A, Macek B. 2015. Characterization of the *E. coli* proteome and its modifications during growth and ethanol stres. Front Microbiol 6:103.

14. Ghatak S, King ZA, Sastry A, Palsson BO. 2019. The y-ome defines the 35% of *Escherichia coli* genes that lack experimental evidence of function. Nucleic Acids Res 47:2446–2454.

15. Molloy MP, Herbert BR, Slade MB, Rabilloud T, Nouwens AS, Williams KL, Gooley AA. 2000. Proteomic analysis of the *Escherichia coli* outer membrane. Eur J Biochem 267:2871–2881.

16. Xu C, Lin X, Ren H, Zhang Y, Wang S, Peng X. 2006. Analysis of outer membrane proteome of *Escherichia coli* related to resistance to ampicillin and tetracycline. Proteomics 6:462–473.

17. Kapoor G, Saigal S, Elongavan A. 2017. Action and resistance mechanisms of antibiotics: A guide for clinicians. J Anaesthesiol Clin Pharmacol 33:300–305.

18. Gilbert P, Moore LE. 2005. Cationic antiseptics : diversity of action under a common epithet. J Appl Microbiol 99:703–715.

19. Gilbert P, McBain AJ. 2003. Potential impact of increased use of biocides in consumer products on prevalence of antibiotic resistance. Clin Microbiol Rev 16:189–208.

20. Gnanadhas DP, Marathe SA, Chakravortty D. 2013. Biocides – resistance, cross-resistance mechanisms and assessment. Expert Opin Investig Drugs 22:191–206.

21. Roden K. 2010. Preservatives in personal care products. Off Journale Aust Soc Microbiol Inc 31:195–197.

22. Russell AD. 2002. Antibiotic and biocide resistance in bacteria : comments and conclusions. J Appl Microbiol Symp Suppl 92:171–173.

23. Poole K. 2002. Mechanisms of bacterial biocide and antibiotic resistance. J Appl Microbiol Symp Suppl 92:55S-64S.

24. Poirel L, Jayol A, Nordmann P. 2017. Polymyxins: antibacterial activity, susceptibility testing, and resistance mechanisms encoded by plasmids or chromosomes. Clin Microbiol Rev 30:557–596.

25. Nation R, Li J. 2009. Colistin in the 21st century. Curr Opin Infect Dis 22:535–543.

26. Bialvaei AZ, Kafil HS. 2015. Colistin, mechanisms and prevalence of resistance. Curr Med Res Opin 31:707–721.

27. O'Driscoll NH, Cushnie TPT, Matthews KH, Lamb AJ. 2018. Colistin causes profound morphological alteration but minimal cytoplasmic membrane perforation in populations of *Escherichia coli* and *Pseudomonas aeruginosa*. Arch Microbiol 200:793–802.

28. Deris ZZ, Akter J, Sivanesan S, Roberts KD, Philip E, Nation RL, Li J, Velkov T, Kerian K. 2014. A secondary mode of action of polymyxins against Gram-negative bacteria involves the inhibition of NADH-quinone oxidoreductase activity. J Antibiot (Tokyo) 67:147–151.

29. Hegstad K, Langsrud S, Lunestad BT, Scheie AA, Sunde M, Yazdankhah SP. 2010. Does the wide use of quaternary ammonium compounds enhance the selection and spread of antimicrobial resistance and thus threaten our health? Microb Drug Resist 16:91–104.

30. Buffet-Bataillon S, Tattevin P, Bonnaure-Mallet M, Jolivet-Gougeon A. 2012. Emergence of resistance to antibacterial agents : the role of quaternary ammonium compounds - a critical review. Int J Antimicrob Agents 39:381–389.

31. Hora PI, Pati SG, McNamara PJ, Arnold WA. 2020. Increased use of quaternary ammonium compounds during the SARS-CoV-2 pandemic and beyond: consideration of environmental implications. Environ Sci Technol Lett 7:622–631.

32. Mcdonnell G, Russell AD. 1999. Antiseptics and disinfectants: Activity, action, and resistance. Clin Microbiol Rev 12:147–179.

33. Deo AA, Kulkarni AS, Meshram SU. 2010. Monocationic surfactant induced ultra structural changes in antibiotic resistant *Escherichia coli.* Indian J Med Res 131:825–828.

34. Kampf G. 2016. Acquired resistance to chlorhexidine - is it time to establish an ‘ antiseptic stewardship ’ initiative ? J Hosp Infect 94:213–227.

35. Houari A, Martino P Di. 2007. Effect of chlorhexidine and benzalkonium chloride on bacterial biofilm formation. Lett Appl Microbiol 45:652–656.

36. Cheung H, Wong MM, Cheung S, Liang LY, Lam Y, Chiu S. 2012. Differential actions of chlorhexidine on the cell wall of *Bacillus subtilis* and *Escherichia coli*. PLoS One 7:1–11.

37. Cerf O, Carpentier B, Sanders P. 2010. Tests for determining in-use concentrations of antibiotics and disinfectants are based on entirely different concepts: “Resistance” has different meanings. Int J Food Microbiol 136:247–254.

38. Gadea R, Glibota N, Pérez Pulido R, Gálvez A, Ortega E. 2017. Adaptation to biocides cetrimide and chlorhexidine in bacteria from organic foods: Association with tolerance to other antimicrobials and physical stresses NC. J Agric Food Chem 65:1758–1770.

39. Wand ME, Bock LJ, Bonney LC, Sutton JM. 2016. Mechanisms of increased resistance to chlorhexidine and cross-resistance to colistin following Eeposure of *Klebsiella pneumoniae* clinical isolates to chlorhexidine 61:1–12.

40. Andrade FF, Silva D, Rodrigues A, Pina-Vaz C. 2020. Colistin update on its mechanism of action and resistance, present and future challenges. Microorganisms 8:1–12.

41. Aghapour Z, Gholizadeh P, Ganbarov K, Bialvaei AZ, Mahmood SS, Tanomand A, Yousefi M, Asgharzadeh M, Yousefi B, Kafil HS. 2019. Molecular mechanisms related to colistin resistance in Enterobacteriaceae. Infect Drug Resist 12:965–975.

42. Ortega Morente E, Fernandez-Fuentes MA, Grande Burgos MJ, Abriouel H, Perez Pulido R, Galvez A. 2013. Biocide tolerance in bacteria. Int J Food Microbiol 162:13–25.

43. Fernández L, Hancock REW. 2012. Adaptive and mutational resistance: Role of porins and efflux pumps in drug resistance. Clin Microbiol Rev 25:661–681.

44. Poole K. 2005. Efflux-mediated antimicrobial resistance. J Antimicrob Chemother 56:20–51.

45. Silhavy TJ, Kahne D, Walker S. 2010. The Bacterial Cell Envelope. Cold Spring Harb Perspect Biol 2:1–16.

46. Jeannot K, Bolard A, Plésiat P. 2017. Resistance to polymyxins in Gram-negative organisms. Int J Antimicrob Agents 49:526–535.

47. Moosavian M, Emam N, Pletzer D, Savari M. 2020. Rough-type and loss of the LPS due to *lpx* genes deletions are associated with colistin resistance in multidrug-resistant clinical *Escherichia coli* isolates not harbouring mcr genes. PLoS One 15:e0233518.

48. Olaitan A, Morand S, Rolain J. 2016. Emergence of colistin-resistant bacteria in humans without colistin usage: a new worry and cause for vigilance. Int J Antimicrob Agents 47:1–3.

49. Quesada A, Porrero M, Tellez S, Palomo G, Garcia M, Dominguez L. 2015. Polymorphism of genes encoding PmrAB in colistin-resistant strains of *Escherichia coli* and *Salmonella enterica* isolated from poultry and swine. J Antimicrob Chemotherherapy 70:71–74.

50. Du H, Chen L, Tang Y. 2016. Emergence of the mcr-1 colistin resistance gene in carbapenem-resistant Enterobacteriaceae. Lancet Infect Dis 16:287–288.

51. Bore E, Hébraud M, Chafsey I, Chambon C, Skjæret C, Moen B, Møretrø T, Langsrud Ø, Rudi K, Langsrud S. 2007. Adapted tolerance to benzalkonium chloride in *Escherichia coli* K-12 studied by transcriptome and proteome analyses. Microbiology 153:935–946.

52. Slipski CJ, Zhanel GG, Bay DC. 2018. Biocide selective TolC-independent efflux pumps in Enterobacteriaceae. J Membr Biol 251:15–33.

53. Soumet C, Méheust D, Pissavin C, Le Grandois P, Frémaux B, Le Roux A, Denis M, Maris P. 2016. Reduced susceptibilities to biocides and resistance to antibiotics in food-associated bacteria following exposure to quaternary ammonium compounds. J Appl Microbiol 121:1275–1281.

54. Zhang Y, Zhao Y, Xu C, Zhang X, Li J, Dong G, Cao J, Zhou T. 2019. Chlorhexidine exposure of

clinical *Klebsiella pneumoniae s*trains leads to acquired resistance to this disinfectant and to colistin. Int J Antimicrob Agents 53:864–867.

55. Naparstek L, Carmeli Y, Chmelnitsky I, Banin E, Navon-Venezia S. 2012. Reduced susceptibility to chlorhexidine among extremely-drug-resistant strains of *Klebsiella pneumoniae*. J Hosp Infect 81:15–19.

56. Bas S, Kramer M, Stopar D. 2017. Biofilm surface density determines biocide effectiveness. Front Microbiol 8:2443.

57. Sun Y, Hu X, Guo D, Shi C, Zhang C, Peng X, Yang H, Xia X. 2019. Disinfectant resistance profiles and biofilm formation capacity of *Escherichia coli* isolated from retail chicken. Microb Drug Resist 25:703–711.

58. Tipton KA, Chin CY, Farokhyfar M, Weiss DS, Rathera PN. 2018. Role of capsule in resistance to disinfectants, host antimicrobials, and desiccation in *Acinetobacter baumannii*. Antimicrob Agents Chemother 62:e01188-18.

59. Kim SW, Park S Bin, Im SP, Lee JS, Jung JW, Gong TW, Lazarte JMS, Kim J, Seo JS, Kim JH, Song JW, Jung HS, Kim GJ, Lee YJ, Lim SK, Jung TS. 2018. Outer membrane vesicles from β-lactam-resistant *Escherichia coli* enable the survival of β-lactam-susceptible *E. coli* in the presence of β-lactam antibiotics. Sci Rep 8:1–13.

60. Ruiz N, Kahne D, Silhavy TJ. 2009. Transport of lipopolysaccharide across the cell envelope: The long road of discovery. Nat Rev Microbiol 7:677–683.

61. Raetz CRH, Dowhan W. 1990. Biosynthesis and function of phospholipids in *Escherichia coli*. J Biol Chem 265:1235–1238.

62. Sohlenkamp C, Geiger O. 2015. Bacterial membrane lipids: Diversity in structures and pathways. FEMS Microbiol Rev 40:133–159.

63. Bogdanov M, Pyrshev K, Yesylevskyy S, Ryabichko S, Boiko V, Ivanchenko P, Kiyamova R, Guan Z, Ramseyer C, Dowhan W. 2020. Phospholipid distribution in the cytoplasmic membrane of Gram-negative bacteria is highly asymmetric, dynamic, and cell shape-dependent. Sci Adv

6:eaaz6333.

64. Miller SI, Salama NR. 2018. The gram-negative bacterial periplasm: Size matters. PLoS Biol 16:e2004935.

65. Powers MJ, Trent MS. 2019. Intermembrane transport: Glycerophospholipid homeostasis of the Gram-negative cell envelope. PNAS 116:17147–17155.

66. Polissi A, Sperandeo P. 2014. The lipopolysaccharide export pathway in *Escherichia coli:* Structure, organization and regulated assembly of the Lpt machinery. Mar Drugs 12:1023–1042.

67. Raetz CRH, Reynolds CM, Trent MS, Bishop RE. 2007. Lipid a modification systems in Gram-negative bacteria. Annu Rev Biochem 76:295–329.

68. Stead CM, Beasley A, Cotter RJ, Trent MS. 2008. Deciphering the unusual acylation pattern of *Helicobacter pylori* lipid A. J Bacteriol 190:7012–7021.

69. Simpson BW, Trent MS. 2019. Pushing the envelope: LPS modifications and their consequences. Nat Rev Microbiol 17:403–416.

70. Bonnington KE, Kuehn MJ. 2016. Outer membrane vesicle production facilitates LPS remodeling and transitions. MBio 7:1–15.

71. Gill S, Catchpole R, Forterre P. 2019. Extracellular membrane vesicles in the three domains of life and beyond. FEMS Microbiol Rev 43:273–303.

72. Yáñez-Mó M, Siljander PRM, Andreu Z, et al. 2015. Biological properties of extracellular vesicles and their physiological functions. J Extracell Vesicles 4:27066.

73. Zaborowski MP, Balaj L, Breakefield XO, Lai CP. 2015. Extracellular vesicles: Composition, biological relevance, and methods of study. Bioscience 65:783–797.

74. Kuehn MJ, Kesty NC. 2005. Bacterial outer membrane vesicles and the host-pathogen interaction. Genes Dev 19:2645–2655.

75. Toyofuku M, Nomura N, Eberl L. 2019. Types and origins of bacterial membrane vesicles. Nat Rev Microbiol 17:13–24.

76. Nagakubo T, Nomura N, Toyofuku M. 2020. Cracking open bacterial membrane vesicles. Front

Microbiol 10:3026.

77. MacDonald IA, Kuehn MJ. 2012. Offense and defense: Microbial membrane vesicles play both ways. Res Microbiol 163:607–618.

78. Kadurugamuwa JL, Beveridge TJ. 1999. Membrane vesicles derived from *Pseudornonas aeruginosa* and *Shigella flexneri* can be integrated into the surfaces of other Gram-negative bacteria. Microbiology 145:2051–2060.

79. Mashburn-Warren LM, Whiteley M. 2006. Special delivery: Vesicle trafficking in prokaryotes. Mol Microbiol 61:839–846.

80. Kulp A, Kuehn MJ. 2012. Biological functions and biogenesis of secreted bacterial outer membrane vesicles. Annu Rev Microbiol 63:163–184.

81. Kulp AJ, Sun B, Ai T, Manning AJ, Orench-Rivera N, Schmid AK, Kuehn MJ. 2015. Genome-wide assessment of outer membrane vesicle production in *Escherichia coli*. PLoS One 10:1–16.

82. Manning AJ, Kuehn MJ. 2011. Contribution of bacterial outer membrane vesicles to innate bacterial defense. BMC Microbiol 11:1–14.

83. Deatherage BL, Cookson BT. 2012. Membrane vesicle release in bacteria, eukaryotes, and archaea: A conserved yet underappreciated aspect of microbial life. Infect Immun 80:1948–1957.

84. Deatherage BL, Lara JC, Bergsbaken T, Barrett SLR, Lara S, Cookson BT. 2009. Biogenesis of bacterial membrane vesicles. Mol Microbiol 72:1395–1407.

85. McBroom AJ, Johnson AP, Vemulapalli S, Kuehn MJ. 2006. Outer membrane vesicle production by *Escherichia coli* is independent of membrane instability. J Bacteriol 188:5385–5392.

86. Kulkarni HM, Nagaraj R, Jagannadham M V. 2015. Protective role of *E. coli* outer membrane vesicles against antibiotics. Microbiol Res 181:1–7.

87. Post DMB, Zhang D, Eastvold JS, Teghanemt A, Gibson BW, Weiss JP. 2005. Biochemical and functional characterization of membrane blebs purified from *Neisseria meningitidis* serogroup B. J Biol Chem 280:38383–38394.

88. Kadurugamuwa J, Beveridge TJ. 1996. Bacteriolytic effect of membrane vesicles from

Pseudomonas aeruginosa on other bacteria including pathogens : conceptually new antibiotics. J Bacteriol 178:2767–2774.

89. Yaron S, Kolling GL, Simon LEE, Matthews KR. 2000. Vesicle-mediated transfer of virulence genes from *Escherichia coli* O157:H7 to other enteric bacteria. Appl Environ Microbiol 66:4414–4420.

90. Ciofu O, Beveridge TJ, Kadurugamuwa J, Walther-Rasmussen J, Høiby N. 2000. Chromosomal β-lactamase is packaged into membrane vesicles and secreted from *Pseudomonas aeruginosa*. J Antimicrob Chemother 45:9–13.

91. Alaniz RC, Deatherage BL, Lara JC, Cookson BT, Alaniz RC, Deatherage BL, Lara JC, Cookson BT. 2007. Membrane vesicles are immunogenic facsimiles of *Salmonella typhimurium* that potently activate dendritic cells, prime B and T cell responses, and stimulate protective immunity in vivo. J Immunol 179:7692–7701.

92. Bauman SJ, Kuehn MJ. 2006. Purification of outer membrane vesicles from *Pseudomonas aeruginosa* and their activation of an IL-8 response. Microbes Infect 8:2400–2408.

93. Lin J, Zhang W, Cheng J, Yang X, Zhu K, Wang Y, Wei G, Qian P, Luo Z, Shen X. 2017. A *Pseudomonas* T6SS effector recruits PQS-containing outer membrane vesicles for iron acquisition. Nat Commun 8:1–12.

94. Prados-Rosales R, Weinrick BC, Jacobs WR, Casadevall A, Rodriguez GM. 2014. Role for *Mycobacterium tuberculosis* membrane vesicles in iron acquisition. J Bacteriol 196:1250–1256.

95. Kulkarni HM, Jagannadham M V. 2014. Biogenesis and multifaceted roles of outer membrane vesicles from Gram-negative bacteria. Microbiology 160:2109–2121.

96. Jagannadham M V, Chattopadhyay MK. 2018. Therapeutic and biotechnological importance of bacterial vesicles and their inhibitors. J Clin Microbiol Antimicrob 1:1–2.

97. Schwechheimer C, Kuehn MJ. 2015. Outer-membrane vesicles from Gram-negative bacteria: biogenesis and functions. Nat Publ Gr 13:605–619.

98. MacDonald IA, Kuehn MJ. 2013. Stress-induced outer membrane vesicle production by

Pseudomonas aeruginosa. J Bacteriol 195:2971–2981.

99. Schwechheimer C, Kuehn MJ. 2013. Synthetic effect between envelope stress and lack of outer membrane vesicle production in *Escherichia coli*. J Bacteriol 195:4161–4173.

100. Elhenawy W, Bording-Jorgensen M, Valguarnera E, Haurat MF, Wine E, Feldman MF. 2016. LPS remodeling triggers formation of outer membrane vesicles in *Salmonella*. MBio 7:1–12.

101. Jagannadham M V, Chattopadhyay MK. 2015. Role of outer membrane vesicles of bacteria. Resonance 8:711–725.

102. Volgers C, Savelkoul PHM, Stassen FRM. 2018. Gram-negative bacterial membrane vesicle release in response to the host-environment: different threats, same trick? Crit Rev Microbiol 44:258–273.

103. Bernadac A, Gavioli M, Lazzaroni JC, Raina S, Lloubès R. 1998. *Escherichia coli tol-pal* mutants form outer membrane vesicles. J Bacteriol 180:4872–4878.

104. McBroom AJ, Kuehn MJ. 2007. Release of outer membrane vesicles by Gram-negative bacteria is a novel envelope stress response. Mol Microbiol 63:545–558.

105. Schwechheimer C, Rodriguez DL, Kuehn MJ. 2015. NlpI-mediated modulation of outer membrane vesicle production through peptidoglycan dynamics in *Escherichia coli*. Microbiologyopen 4:375–389.

106. Cascales E, Bernadac A, Gavioli M, Lazzaroni J-C, Lloubes R. 2002. Pal lipoprotein of *Escherichia coli* plays a major role in outer membrane integrity. J Bacteriol 184:754–759.

107. Pérez-Cruz C, Cañas MA, Giménez R, Badia J, Mercade E, Baldomà L, Aguilera L. 2016. Membrane vesicles released by a hypervesiculating *Escherichia coli* Nissle 1917 tolR mutant are highly heterogeneous and show reduced capacity for epithelial cell interaction and entry. PLoS One 11:1–20.

108. Turner L, Praszkier J, Hutton ML, Steer D, Ramm G, Kaparakis-Liaskos M, Ferrero RL. 2015. Increased outer membrane vesicle formation in a *Helicobacter pylori tolB* mutant. Helicobacter 20:269–283.

109. Sonntag I, Schwarz H, Hirota Y. 1978. Cell envelope and shape of *Escherichia coli* : multiple mutants missing the outer membrane lipoprotein and other major outer membrane proteins. J Bacteriol 136:280–285.

110. Moon DC, Choi CH, Lee JH, Choi C-W, Kim H-Y, Park JS, Kim S Il, Lee JC. 2012. *Acinetobacter baumannii* outer membrane protein a modulates the biogenesis of outer membrane vesicles. J Microbiol 50:155–160.

111. Wessel AK, Liew J, Kwon T, Marcotte EM, Whiteley M. 2013. Role of *Pseudomonas aeruginosa* peptidoglycan-associated outer membrane proteins in vesicle formation. J Bacteriol 195:213–219.

112. Tashiro Y, Sakai R, Toyofuku M, Sawada I, Nakajima-Kambe T, Uchiyama H, Nomura N. 2009. Outer membrane machinery and alginate synthesis regulators control membrane vesicle production in *Pseudomonas aeruginosa*. J Bacteriol 191:7509–7519.

113. Roier S, Zingl FG, Cakar F, Durakovic S, Kohl P, Eichmann TO, Klug L, Gadermaier B, Weinzerl K, Prassl R, Lass A, Daum G, Reidl J, Feldman MF, Schild S. 2016. A novel mechanism for the biogenesis of outer membrane vesicles in Gram-negative bacteria. Nat Commun 7:1–13.

114. Davies C, Taylor AJ, Elmi A, Winter J, Liaw J, Grabowska AD, Gundogdu O, Wren BW, Kelly DJ, Dorrell N. 2019. Sodium taurocholate stimulates *Campylobacter jejuni* outer membrane vesicle production via down-regulation of the Maintenance of Lipid Asymmetry Pathway. Front Cell Infect Microbiol 9:1–12.

115. Clarke AJ. 2018. The “hole” story of predatory outer-membrane vesicles. Can J Microbiol 64:589–599.

116. Hong J, Dauros-Singorenko P, Whitcombe A, Payne L, Blenkiron C, Phillips A, Swift S. 2019. Analysis of the *Escherichia coli* extracellular vesicle proteome identifies markers of purity and culture conditions. J Extracell Vesicles 8:1.

117. Lappann M, Otto A, Becher D, Vogel U. 2013. Comparative proteome analysis of spontaneous outer membrane vesicles and purified outer membranes of *Neisseria meningitidis*. J Bacteriol 195:4425–4435.

118. Elhenawy W, Debelyy MO, Feldman MF. 2014. Preferential packing of acidic glycosidases and proteases into *Bacteroides* outer membrane vesicles. MBio 5:1–12.

119. Couto N, Schooling SR, Dutcher JR, Barber J. 2015. Proteome profiles of outer membrane vesicles and extracellular matrix of *Pseudomonas aeruginosa* biofilms. J Proteome Res 14:4207–4222.

120. Lee EY, Joo YB, Gun WP, Choi DS, Ji SK, Kim HJ, Park KS, Lee JO, Kim YK, Kwon KH, Kim KP, Yong SG. 2007. Global proteomic profiling of native outer membrane vesicles derived from *Escherichia coli.* Proteomics 7:3143–3153.

121. Aguilera L, Toloza L, Giménez R, Odena A, Oliveira E, Aguilar J, Badia J, Baldomà L. 2014. Proteomic analysis of outer membrane vesicles from the probiotic strain *Escherichia coli* Nissle 1917. Proteomics 14:222–229.

122. Kim SW, Park S Bin, Im SP, Lee JS, Jung JW, Won T, Lazarte JMS, Kim J, Seo J, Kim J, Jung HS, Kim GJ, Lee YJ, Lim S, Jung TS. 2018. Outer membrane vesicles from β -lactam-resistant *Escherichia coli* enable the survival of β -lactam- susceptible *E . coli* in the presence of β -lactam antibiotics. Sci Rep 8:1–13.

123. Tashiro Y, Inagaki A, Shimizu M, Ichikawa S, Takaya N, Nakajima-Kambe T, Uchiyama H, Nomura N. 2011. Characterization of phospholipids in membrane vesicles derived from *Pseudomonas aeruginosa.* Biosci Biotechnol Biochem 75:605–607.

124. Tashiro Y, Ichikawa S, Nakajima-Kambe T, Uchiyama H, Nomura N. 2010. Pseudomonas quinolone signal affects membrane vesicle production in not only Gram-negative but also Gram-positive bacteria. Microbes Environ 25:120–125.

125. Bager RJ, Persson G, Nesta B, Soriani M, Serino L, Jeppsson M, Nielsen TK, Bojesen AM. 2013. Outer membrane vesicles reflect environmental cues in *Gallibacterium anatis*. Vet Microbiol 167:565–572.

126. Keenan JI, Allardyce RA. 2000. Iron influences the expression of *Helicobacter pylori* outer membrane vesicle-associated virulence factors. Eur J Gastroenterol Hepatol 12:1267–1273.

127. Toyofuku M, Zhou S, Sawada I, Takaya N, Uchiyama H, Nomura N. 2014. Membrane vesicle formation is associated with pyocin production under denitrifying conditions in *Pseudomonas aeruginosa* PAO1. Environ Microbiol 16:2927–2938.

128. Devos S, Van Oudenhove L, Stremersch S, Van Putte W, De Rycke R, Van Driessche G, Vitse J, Raemdonck K, Devreese B. 2015. The effect of imipenem and diffusible signaling factors on the secretion of outer membrane vesicles and associated Ax21 proteins in *Stenotrophomonas maltophilia*. Front Microbiol 6:1–9.

129. Orench-Rivera N, Kuehn MJ. 2016. Environmentally-controlled bacterial vesicle-mediated export. Cell Microbiol 18:1525–1536.

130. Elmi A, Watson E, Sandu P, Gundogdu O, Mills DC, Inglis NF, Manson E, Imrie L. 2012. *Campylobacter jejuni* outer membrane vesicles play an important role in bacterial interactions with human intestinal epithelial cells. Infect Immun 80:4089–4098.

131. Chattopadhyay MK, Jagannadham M V. 2015. Vesicles-mediated resistance to antibiotics in bacteria. Front Microbiol 6:1–3.

132. Kesty NC, Kuehn MJ. 2004. Incorporation of heterologous outer membrane and periplasmic proteins into *Escherichia coli* outer membrane vesicles. J Biol Chem 279:2069–2076.

133. Horstman AL, Kuehn MJ. 2000. Enterotoxigenic *Escherichia coli* secretes active heat-labile enterotoxin via outer membrane vesicles. J Biol Chem 275:12489–12496.

134. Thoma J, Manioglu S, Kalbermatter D, Bosshart PD, Fotiadis D, Müller DJ. 2018. Protein-enriched outer membrane vesicles as a native platform for outer membrane protein studies. Commun Biol 1:23.

135. Klimentová J, Stulík J. 2015. Methods of isolation and purification of outer membrane vesicles from gram-negative bacteria. Microbiol Res 170:1–9.

136. Gasperini G, Biagini M, Arato V, Gianfaldoni C, Vadi A, Norais N, Bensi G, Delany I, Pizza M, Aricò B, Leuzzi R. 2018. Outer membrane vesicles (OMV)-based and proteomics-driven antigen selection identifies novel factors contributing to *Bordetella pertussis* adhesion to epithelial cells.

Mol Cell Proteomics 17:205–215.

137. Qing G, Gong N, Chen X, Chen J, Zhang H, Wang Y, Wang R, Zhang S, Zhang Z, Zhao X, Luo Y, Liang X-J. 2019. Natural and engineered bacterial outer membrane vesicles. Biophys Reports 5:184–198.

138. Balhuizen MD, Veldhuizen EJA, Haagsman HP. 2021. Outer membrane vesicle induction and isolation for vaccine development. Front Microbiol 12:629090.

139. van der Pol L, Stork M, van der Ley P. 2015. Outer membrane vesicles as platform vaccine technology. Biotechnol J 10:1689–1706.

140. van de Waterbeemd B, Zomer G, Kaaijk P, Ruiterkamp N, Wijffels RH, van den Dobbelsteen GPJM, van der Pol LA. 2013. Improved production process for native outer membrane vesicle vaccine against *Neisseria meningitidis*. PLoS One 8:e65157.

141. Yuana Y, Levels J, Grootemaat A, Sturk A, Nieuwland R. 2014. Co-isolation of extracellular vesicles and high-density lipoproteins using density gradient ultracentrifugation. J Extracell Vesicles 3:23262.

142. Bore E, Hébraud M, Chafsey I, Chambon C, Skjæret C, Moen B, Møretrø T, Langsrud Ø, Rudi K, Langsrud S. 2007. Adapted tolerance to benzalkonium chloride in *Escherichia coli* K-12 studied by transcriptome and proteome analyses. Microbiology 153:935–946.

143. Cartwright N. 2019. Examination of cationic antimicrobial tolerance in *Escherichia coli* to identify phenotypic and genotypic adaptations. University of Manitoba.

144. Gregorchuk BSJ, Reimer SL, Green KAC, Cartwright NH, Beniac DR, Hiebert SL, Booth TF, Chong PM, Westmacott GR, Zhanel GG, Bay DC. 2021. Phenotypic and multi-omics characterization of *Escherichia coli* K-12 adapted to chlorhexidine identifies the role of MlaA and other cell envelope alterations regulated by stress inducible pathways in CHX resistance. Front Mol Biosci 8:659058.

145. Cold Spring Harbor Protocols. 2006. LB (Luria-Bertani) liquid medium. Cold Spring Harb Protoc.

146. Yaron S, Kolling GL, Simon L, Matthews KR. 2000. Vesicle-mediated transfer of virulence genes

from *Escherichia coli* O157:H7 to other enteric bacteria. Appl Environ Microbiol 66:4414–4420.

147. Ladner CL, Yang J, Turner RJ, Edwards RA. 2004. Visible fluorescent detection of proteins in polyacrylamide gels without staining. Anal Biochem 326:13–20.

148. Davarinejad H. 2015. Quantifications of Western Blots with ImageJ, p. Accessed 20 October 2020. *In* http://www.yorku.ca.uml.idm.oclc.org/yisheng/Internal/Protocols/ImageJ.pdf.

149. Alves NJ, Turner KB, Medintz IL, Walper SA. 2016. Protecting enzymatic function through directed packaging into bacterial outer membrane vesicles. Sci Rep 6:1–10.

150. Bitto NJ, Kaparakis-Liaskos M. 2017. The therapeutic benefit of bacterial membrane vesicles. Int J Mol Sci 18:1–15.

151. Arigita C, Jiskoot W, Westdijk J, Van Ingen C, Hennink WE, Crommelin DJA, Kersten GFA. 2004. Stability of mono- and trivalent meningococcal outer membrane vesicle vaccines. Vaccine 22:629–642.

152. Abràmoff MD, Magalhães PJ, Ram SJ. 2007. Image Processing with ImageJ. Biophotonics Int 11:36–42.

153. Wiśniewski JR, Zougman A, Nagaraj N, Mann M. 2009. Universal sample preparation method for proteome analysis. Nat Methods 6:359–362.

154. Yu NY, Wagner JR, Laird MR, Melli G, Rey S, Lo R, Dao P, Sahinalp SC, Ester M, Foster LJ, Brinkman FSL. 2010. PSORTb 3.0: improved protein subcellular localization prediction with refined localization subcategories and predictive capabilities for all prokaryotes 26:1608–1615.

155. Doncheva NT, Morris JH, Gorodkin J, Jensen LJ. 2019. Cytoscape StringApp: Network Analysis and Visualization of Proteomics Data. J Proteome Res 18:623–632.

156. Bindea G, Mlecnik B, Hackl H, Charoentong P, Tosolini M, Kirilovsky A, Fridman WH, Pagès F, Trajanoski Z, Galon J. 2009. ClueGO: A Cytoscape plug-in to decipher functionally grouped gene ontology and pathway annotation networks. Bioinformatics 25:1091–1093.

157. Gerritzen MJH, Martens DE, Wijffels RH, Stork M. 2017. High throughput nanoparticle tracking analysis for monitoring outer membrane vesicle production. J Extracell Vesicles 6:1333883.

158. Filipe V, Hawe A, Jiskoot W. 2010. Critical evaluation of nanoparticle tracking analysis (NTA) by NanoSight for the measurement of nanoparticles and protein aggregates. Pharm Res 27:796–810.

159. Gardiner C, Ferreira YJ, Dragovic RA, Redman CWG, Sargent IL. 2013. Extracellular vesicle sizing and enumeration by nanoparticle tracking analysis. J Extracell Vesicles 2:19671.

160. Takaki K, Tahara YO, Nakamichi N, Hasegawa Y, Shintani M, Ohkuma M, Miyata M, Futamata H, Tashiro Y. 2020. Multilamellar and multivesicular outer membrane vesicles produced by a *Buttiauxella agrestis tolB* mutant. Appl Environ Microbiol 86:1131–1151.

161. McBroom AJ, Johnson AP, Vemulapalli S, Kuehn MJ. 2006. Outer membrane vesicle production by *Escherichia coli* is independent of membrane instability. J Bacteriol 188:5385–5392.

162. Bielaszewska M, Rüter C, Bauwens A, Greune L, Jarosch KA, Steil D, Zhang W, He X, Lloubes R, Fruth A, Kim KS, Schmidt MA, Dobrindt U, Mellmann A, Karch H. 2017. Host cell interactions of outer membrane vesicle-associated virulence factors of enterohemorrhagic *Escherichia coli* O157: Intracellular delivery, trafficking and mechanisms of cell injury. PLoS Pathog 13:e1006159.

163. Koning RI, de Breij A, Oostergetel GT, Nibbering PH, Koster AJ, Dijkshoorn L. 2013. Cryo-electron tomography analysis of membrane vesicles from *Acinetobacter baumannii* ATCC19606T. Res Microbiol 164:397–405.

164. Berlanda Scorza F, Doro F, Rodríguez-Ortega MJ, Stella M, Liberatori S, Taddei AR, Serino L, Moriel DG, Nesta B, Fontana MR, Spagnuolo A, Pizza M, Norais N, Grandi G. 2008. Proteomics characterization of outer membrane vesicles from the extraintestinal pathogenic *Escherichia coli* Δ*tolR* IHE3034 mutant. Mol Cell Proteomics 7:473–485.

165. Hong J, Dauros-Singorenko P, Whitcombe A, Payne L, Blenkiron C, Phillips A, Swift S. 2019. Analysis of the *Escherichia coli* extracellular vesicle proteome identifies markers of purity and culture conditions. J Extracell Vesicles 8:1632099.

166. Cvjetkovic A, Lötvall J, Lässer C. 2014. The influence of rotor type and centrifugation time on the yield and purity of extracellular vesicles. J Extracell Vesicles 3:23111.

167. Dragovic RA, Gardiner C, Brooks AS, Tannetta DS, Ferguson DJP, Hole P, Carr B, Redman CWG, Harris AL, Dobson PJ, Harrison P, Sargent IL. 2011. Sizing and phenotyping of cellular vesicles using Nanoparticle Tracking Analysis. Nanomedicine Nanotechnology, Biol Med 7:780–788.

168. Alexander RP, Chiou N-T, Ansel KM. 2016. Improved exosome isolation by sucrose gradient fractionation of ultracentrifuged crude exosome pellets. Protoc Exch.

169. Witwer KW, Buzás EI, Bemis LT, Bora A, Lässer C, Lötvall J, Nolte-'t Hoen EN, Piper MG, Sivaraman S, Skog J, Théry C, Wauben MH, Hochberg F. 2013. Standardization of sample collection, isolation and analysis methods in extracellular vesicle research. J Extracell Vesicles 2:20360.

170. Théry C, Amigorena S, Raposo G, Clayton A. 2006. Isolation and characterization of exosomes from cell culture supernatants and biological fluids. Curr Protoc Cell Biol 30:3.22.1-3.22.29.

171. Issman L, Brenner B, Talmon Y, Aharon A. 2013. Cryogenic transmission electron microscopy nanostructural study of shed microparticles. PLoS One 8:e83680.

172. Linares R, Tan S, Gounou C, Arraud N, Brisson AR. 2015. High-speed centrifugation induces aggregation of extracellular vesicles. J Extracell Vesicles 4:29509.

173. Fiocca R, Necchi V, Sommi P, Ricci V, Telford J, Cover TL, Solcia E. 1999. Release of Helicobacter pylori vacuolating cytotoxin by both a specific secretion pathway and budding of outer membrane vesicles. Uptake of released toxin and vesicles by gastric epithelium. J Pathol 188:220–226.

174. Pérez-Cruz C, Delgado L, López-Iglesias C, Mercade E. 2015. Outer-inner membrane vesicles naturally secreted by gram-negative pathogenic bacteria. PLoS One 10:e0116896.

175. Yakhnina AA, Bernhardt TG. 2020. The Tol-Pal system is required for peptidoglycan-cleaving enzymes to complete bacterial cell division. Proc Natl Acad Sci U S A 117:6777–6783.

176. Godlewska R, Wiśniewska K, Pietras Z, Jagusztyn-Krynicka EK. 2009. Peptidoglycan-associated lipoprotein (Pal) of Gram-negative bacteria: Function, structure, role in pathogenesis and potential

application in immunoprophylaxis: Minireview. FEMS Microbiol Lett 298:1–11.

177. Hews CL, Cho T, Rowley G, Raivio TL. 2019. Maintaining integrity under stress: Envelope stress response regulation of pathogenesis in Gram-negative bacteria. Front Cell Infect Microbiol 9:313.

178. Snyder WB, Davis LJB, Danese PN, Cosma CL, Silhavy TJ. 1995. Overproduction of *nlpE*, a new outer membrane lipoprotein, suppresses the toxicity of periplasmic *lacZ* by activation of the Cpx signal transduction pathway. J Bacteriol 177:4216–4223.

179. Danese PN, Snyder WB, Cosma CL, Davis LJB, Silhavy TJ. 1995. The Cpx two-component signal transduction pathway of *Escherichia coli* regulates transcription of the gene specifying the stress-inducible periplasmic protease, DegP. Genes Dev 9:387–398.

180. Danese PN, Silhavy TJ. 1998. CpxP, a stress-combative member of the Cpx regulon. J Bacteriol 180:831–839.

181. Raivio TL, Leblanc SKD, Price NL. 2013. The *Escherichia coli* Cpx envelope stress response regulates genes of diverse function that impact antibiotic resistance and membrane integrity. J Bacteriol 195:2755–2767.

182. Devos S, Van Putte W, Vitse J, Van Driessche G, Stremersch S, Van Den Broek W, Raemdonck K, Braeckmans K, Stahlberg H, Kudryashev M, Savvides SN, Devreese B. 2017. Membrane vesicle secretion and prophage induction in multidrug-resistant *Stenotrophomonas maltophilia* in response to ciprofloxacin stress. Environ Microbiol 19:3930–3937.

183. Sabnis A, Hagart KLH, Klöckner A, Becce M, Evans LE, Furniss RCD, Mavridou DAI, Murphy R, Stevens MM, Davies JC, Larrouy-Maumus GJ, Clarke TB, Edwards AM. 2021. Colistin kills bacteria by targeting lipopolysaccharide in the cytoplasmic membrane. Elife 10:e65836.

184. Green K, Gregorchuk B, Reimer S, Cartwright N, Beniac D, Hiebert S, Booth T, Slipski C, Chong P, Westmacott G, Zhanel G, Bay D. 2020. Phenotypic and multi-omics characterization of *Escherichia coli* K-12 adapted to quaternary ammonium compounds identifies lipid A and cell envelope alterations regulated by mar-sox-rob and stress inducible pathways. bioRxiv 2020.07.13.201814.

185. Sarra A, Celluzzi A, Bruno SP, Ricci C, Sennato S, Ortore MG, Casciardi S, Del Chierico F, Postorino P, Bordi F, Masotti A. 2020. Biophysical characterization of membrane phase transition profiles for the discrimination of outer membrane vesicles (OMVs) from *Escherichia coli* grown at different temperatures. Front Microbiol 11:290.

186. Kim A, Ng WB, Bernt W, Cho NJ. 2019. Validation of Size Estimation of Nanoparticle Tracking Analysis on Polydisperse Macromolecule Assembly. Sci Rep 9:1–14.

187. Knox KW, Vesk M, Work E. 1966. Relation between excreted lipopolysaccharide complexes and surface structures of a lysine-limited culture of *Escherichia coli*. J Bacteriol 92:1206–1217.

188. Erickson DL, Lew CS, Kartchner B, Porter NT, McDaniel SW, Jones NM, Mason S, Wu E, Wilson E. 2016. Lipopolysaccharide biosynthesis genes of *Yersinia pseudotuberculosis* promote resistance to antimicrobial chemokines. PLoS One 11:e0157092.

189. Jiang SS, Lin TY, Wang WB, Liu MC, Hsueh PR, Liaw SJ. 2010. Characterization of UDP-glucose dehydrogenase and UDP-glucose pyrophosphorylase mutants of proteus mirabilis: Defectiveness in polymyxin B resistance, swarming, and virulence. Antimicrob Agents Chemother 54:2000–2009.

190. Paradis-Bleau C, Markovski M, Uehara T, Lupoli TJ, Walker S, Kahne DE, Bernhardt TG. 2010. Lipoprotein cofactors located in the outer membrane activate bacterial cell wall polymerases. Cell 143:1110–1120.

191. Bishop RE, Penfold SS, Frost LS, Höltje JV, Weiner JH. 1995. Stationary phase expression of a novel *Escherichia coli* outer membrane lipoprotein and its relationship with mammalian apolipoprotein D: Implications for the origin of lipocalins. J Biol Chem 270:23097–23103.

192. Huang J, Zhu Y, Han ML, Li M, Song J, Velkov T, Li C, Li J. 2018. Comparative analysis of phosphoethanolamine transferases involved in polymyxin resistance across 10 clinically relevant Gram-negative bacteria. Int J Antimicrob Agents 51:586–593.

193. Olaitan AO, Morand S, Rolain JM. 2014. Mechanisms of polymyxin resistance: Acquired and intrinsic resistance in bacteria. Front Microbiol 5:643.

194. Klein G, Müller-Loennies S, Lindner B, Kobylak N, Brade H, Raina S. 2013. Molecular and structural basis of inner core lipopolysaccharide alterations in *Escherichia coli*: Incorporation of glucuronic acid and phosphoethanolamine in the heptose region. J Biol Chem 288:8111–8127.

195. May KL, Grabowicz M. 2018. The bacterial outer membrane is an evolving antibiotic barrier. Proc Natl Acad Sci U S A 115:8852–8854.

196. Powers MJ, Trent MS. 2018. Phospholipid retention in the absence of asymmetry strengthens the outer membrane permeability barrier to last-resort antibiotics. Proc Natl Acad Sci U S A 115:E8518–E8527.

197. Kapach G, Nuri R, Schmidt C, Danin A, Ferrera S, Savidor A, Gerlach RG, Shai Y. 2020. Loss of the periplasmic chaperone Skp and mutations in the efflux pump AcrAB-TolC play a role in acquired resistance to antimicrobial peptides in *Salmonella typhimurium*. Front Microbiol 11:189.

198. Tezel U, Pavlostathis SG. 2011. Role of quaternary ammonium compounds on antimicrobial resistance in the environment, p. 349–388. *In* Keen, PL, Montforts, MHMM (eds.), Antimicrobial Resistance in the Environment, 1st ed.

199. Block C, Furman M. 2002. Association between intensity of chlorhexidine use and micro-organisms of reduced susceptibility in a hospital environment. J Hosp Infect 51:201–206.

200. Wand ME, Bock LJ, Bonney LC, Sutton JM. 2017. Mechanisms of increased resistance to chlorhexidine and cross-resistance to colistin following exposure of *Klebsiella pneumoniae* clinical isolates to chlorhexidine. Antimicrob Agents Chemother 61:1–12.

201. Wand ME, Bock LJ, Mark Sutton J. 2017. Retention of virulence following colistin adaptation in *Klebsiella pneumoniae* is strain-dependent rather than associated with specific mutations. J Med Microbiol 66:959–964.

202. Viau R, Adams M, Rojas LJ, Bonomo RA, Villegas MV. 2015. *basS* mutations linked to colistin resistance (Colr) among *Enterobacter cloacae*. Open Forum Infect Dis 2:1179.

203. Chubiz LM, Rao C V. 2011. Role of the mar-sox-rob regulon in regulating outer membrane porin expression. J Bacteriol 193:2252–2260.

204. Mu X, Wang N, Li X, Shi K, Zhou Z, Yu Y, Hua X. 2016. The effect of colistin resistance-associated mutations on the fitness of *Acinetobacter baumannii*. Front Microbiol 7:1715.

205. Andersson DI. 2006. The biological cost of mutational antibiotic resistance: any practical conclusions? Curr Opin Microbiol 9:461–465.

206. MacLean RC, Vogwill T. 2015. Limits to compensatory adaptation and the persistence of antibiotic resistance in pathogenic bacteria. Evol Med Public Heal 2015:4–12.

207. Malinverni JC, Silhavy TJ. 2009. An ABC transport system that maintains lipid asymmetry in the Gram-negative outer membrane. Proc Natl Acad Sci U S A 106:8009–8014.

208. Beveridge TJ. 1999. Structures of gram-negative cell walls and their derived membrane vesicles. J Bacteriol 181:4725–4733.

209. Kadurugamuwa JL, Beveridge TJ. 1995. Virulence factors are released from *Pseudomonas aeruginosa* in association with membrane vesicles during normal growth and exposure to gentamicin: a novel mechanism of enzyme secretion. J Bacteriol 177:3998–4008.

210. Pérez-Cruz C, Carrión O, Delgado L, Martinez G, López-Iglesias C, Mercade E. 2013. New type of outer membrane vesicle produced by the gram-negative bacterium *Shewanella vesiculosa* M7T: Implications for DNA content. Appl Environ Microbiol 79:1874–1881.

211. Gregorchuk BSJ, Reimer SL, Beniac DR, Hiebert SL, Booth TF, Wuzinski M, Funk BE, Milner KA, Cartwright NH, Doucet AN, Mulvey MR, Khajehpour M, Zhanel GG, Bay DC. 2020. Antiseptic quaternary ammonium compound tolerance by gram-negative bacteria can be rapidly detected using an impermeant fluorescent dye-based assay. Sci Rep 10:1–16.

212. Murray BO, Dawson RA, Alsharaf LM, Winter JA. 2020. Protective effects of Helicobacter pylori membrane vesicles against stress and antimicrobial agents. Microbiology 166:751–758.

213. Yokoyama F, Kawamoto J, Imai T, Kurihara T. 2017. Characterization of extracellular membrane vesicles of an Antarctic bacterium, *Shewanella livingstonensis* Ac10, and their enhanced production by alteration of phospholipid composition. Extremophiles 21:723–731.

214. Hugo WB, Longworth AR. 1965. Cytological aspects of the mode of action of chlorhexidine

diacetate. J Pharm Pharmacol 17:28–32.

215. Hugo WB, Longworth AR. 1966. The effect of chlorhexidine on the electrophoretic mobility, cytoplasmic constituents, dehydrogenase activity and cell walls of *Escherichia coli* and Staphylococcus aureus. J Pharm Pharmacol 18:569–578.

216. McCaig WD, Koller A, Thanassi DG. 2013. Production of outer membrane vesicles and outer membrane tubes by *Francisella novicida*. J Bacteriol 195:1120–1132.

217. Galkina SI, Romanova JM, Bragina EE, Tiganova IG, Stadnichuk VI, Alekseeva N V., Polyakov VY, Klein T. 2011. Membrane tubules attach *Salmonella typhimurium* to eukaryotic cells and bacteria. FEMS Immunol Med Microbiol 61:114–124.

218. Proença JT, Barral DC, Gordo I. 2017. Commensal-to-pathogen transition: One-single transposon insertion results in two pathoadaptive traits in *Escherichia coli*-macrophage interaction. Sci Rep 7:1–12.

219. Miskinyte M, Sousa A, Ramiro RS, de Sousa JAM, Kotlinowski J, Caramalho I, Magalhães S, Soares MP, Gordo I. 2013. The genetic basis of *Escherichia coli* pathoadaptation to macrophages. PLoS Pathog 9:1–15.

220. Schaar V, Nordström T, Mörgelin M, Riesbeck K. 2011. *Moraxella catarrhalis* outer membrane vesicles carry β-lactamase and promote survival of *Streptococcus pneumoniae* and *Haemophilus influenzae* by inactivating amoxicillin. Antimicrob Agents Chemother 55:3845–3853.

221. Kim SW, Lee JS, Park S Bin, Lee AR, Jung JW, Chun JH, Lazarte JMS, Kim J, Seo J-S, Kim J-H, Song J-W, Ha MW, Thompson KD, Lee C-R, Jung M, Jung TS. 2020. The importance of porins and β-Lactamase in outer membrane vesicles on the hydrolysis of β-lactam antibiotics. Int J Mol Sci 21:2822.

222. Grenier D, Bertrand J, Mayrand D. 1995. *Porphyromonas gingivalis* outer membrane vesicles promote bacterial resistance to chlorhexidine. Oral Microbiol Immunol 10:319–320.

223. Jang SC, Kim SR, Yoon YJ, Park KS, Kim JH, Lee J, Kim OY, Choi EJ, Kim DK, Choi DS, Kim YK, Park J, Di Vizio D, Gho YS. 2015. In vivo kinetic biodistribution of nano-sized outer

membrane vesicles derived from bacteria. Small 11:456–461.

224. O'Donoghue EJ, Krachler AM. 2016. Mechanisms of outer membrane vesicle entry into host cells. Cell Microbiol 18:1508–1517.

225. Cecil JD, Sirisaengtaksin N, O'Brien-Simpson NM, Krachler AM. 2019. Outer membrane vesicle-host cell interactions, p. 201–214. *In* Protein Secretion in Bacteria. American Society for Microbiology.

226. Pastelin-Palacios R, Gil-Cruz C, Pérez-Shibayama CI, Moreno-Eutimio MA, Cervantes-Barragán L, Arriaga-Pizano L, Ludewig B, Cunningham AF, García-Zepeda EA, Becker I, Alpuche-Aranda C, Bonifaz L, Gunn JS, Isibasi A, López-Macías C. 2011. Subversion of innate and adaptive immune activation induced by structurally modified lipopolysaccharide from *Salmonella typhimurium*. Immunology 133:469–481.

227. Matsuura M. 2013. Structural modifications of bacterial lipopolysaccharide that facilitate gram-negative bacteria evasion of host innate immunity. Front Immunol 4:109.

228. Wang S, Huang W, Li K, Yao Y, Yang X, Bai H, Sun W, Liu C, Ma Y. 2017. Engineered outer membrane vesicle is potent to elicit HPV16E7-specific cellular immunity in a mouse model of TC-1 graft tumor. Int J Nanomedicine 12:6813–6825.

229. Rosenthal JA, Huang C, Doody AM, Leung T, Mineta K, Feng DD, Wayne EC, Nishimura N, Leifer C, DeLisa MP, Mendez S, Putnam D. 2014. Mechanistic insight into the Th1-biased immune response to recombinant subunit vaccines delivered by probiotic bacteria-derived outer membrane vesicles. PLoS One 9:e112802.

230. Hoekstra D, Llem Van Der Laan JW], De Leij L, Wit-Holt B. 1976. Release of outer membrane fragments from normally growing *Escherichia coli*. Biochim Biophys Acta 455:889–899.

231. Uddin MJ, Dawan J, Jeon G, Yu T, He X, Ahn J. 2020. The role of bacterial membrane vesicles in the dissemination of antibiotic resistance and as promising carriers for therapeutic agent delivery. Microorganisms 8:670.

232. Alves NJ, Turner KB, Medintz IL, Walper SA. 2015. Emerging therapeutic delivery capabilities

and challenges utilizing enzyme/protein packaged bacterial vesicles. Ther Deliv 6:873–887.

233. Gerritzen MJH, Martens DE, Wijffels RH, van der Pol L, Stork M. 2017. Bioengineering bacterial outer membrane vesicles as vaccine platform. Biotechnol Adv 35:565–574.

234. Kim SH, Kim KS, Lee SR, Kim E, Kim MS, Lee EY, Gho YS, Kim JW, Bishop RE, Chang KT. 2009. Structural modifications of outer membrane vesicles to refine them as vaccine delivery vehicles. Biochim Biophys Acta - Biomembr 1788:2150–2159.

235. Cai W, Kesavan DK, Wan J, Abdelaziz MH, Su Z, Xu H. 2018. Bacterial outer membrane vesicles, a potential vaccine candidate in interactions with host cells based. Diagn Pathol 13:1–12.

236. Norris MH, Khan MSR, Chirakul S, Schweizer HP, Tuanyok A. 2018. Outer membrane vesicle vaccines from biosafe surrogates prevent acute lethal glanders in mice. Vaccines 6:1–20.

237. Pulido MR, García-Quintanilla M, Pachón J, McConnell MJ. 2020. A lipopolysaccharide-free outer membrane vesicle vaccine protects against *Acinetobacter baumannii* infection. Vaccine 38:719–724.

238. Gerritzen MJH, Salverda MLM, Martens DE, Wijffels RH, Stork M. 2019. Spontaneously released *Neisseria meningitidis* outer membrane vesicles as vaccine platform: production and purification. Vaccine 37:6978–6986.

239. Zanella I, König E, Tomasi M, Gagliardi A, Frattini L, Fantappiè L, Irene C, Zerbini F, Caproni E, Isaac SJ, Grigolato M, Corbellari R, Valensin S, Ferlenghi I, Giusti F, Bini L, Ashhab Y, Grandi A, Grandi G. 2021. Proteome-minimized outer membrane vesicles from *Escherichia coli* as a generalized vaccine platform. J Extracell Vesicles 10:e12066.

240. Jan AT. 2017. Outer membrane vesicles (OMVs) of Gram-negative bacteria: A perspective update. Front Microbiol 8:1–11.

241. Gankema H, Wensink J, Guinee PAM, Jansen WH, Witholt B. 1980. Some characteristics of the outer membrane material released by growing enterotoxigenic *Escherichia coli*. Infect Immun 29:704–713.

Appendix

This appendix contains the information associated with the WT vs. CA-adapted OMV proteomic analysis (Chapter 4).

Table A.1 All proteins identified in Chapter 4 proteomic analysis. Proteins are sorted based on their subcellular localization as determined by pSORTb.

Protein Name	Identified Proteins	Accession Number	Entrez Gene ID	Molecular Weight	Normalized Total Spectra			
					WT	CETR	CHXR	COLR
			CY					
aceA	Isocitrate lyase	P0A9G6	948517	48 kDa	13.077	9.893	0	1.7344
aceB	Malate synthase A	P08997	948512	60 kDa	0	50.701	0	0
aceE	Pyruvate dehydrogenase E1 component	P0AFG8	944834	100 kDa	0	14.839	4.408	16.477
aceF	Dihydrolipoyllysine-residue acetyltransferase component of pyruvate dehydrogenase complex	P06959	944794	66 kDa	0	189.2	520.14	209
acnA	Aconitate hydratase A	P25516	946724	98 kDa	0	3.7099	0	0
acnB	Aconitate hydratase B	P36683	944864	94 kDa	0	3.7099	0	4.336
adhE	Aldehyde-alcohol dehydrogenase	P0A9Q7	945837	96 kDa	0	3.7099	8.816	27.751
alaS	Alanine--tRNA ligase	P00957	947175	96 kDa	0	9.893	0	5.2032
argS	Arginine--tRNA ligase	P11875	946452	65 kDa	0	53.175	0	0
aspC	Aspartate aminotransferase	P00509	945553	44 kDa	0	0	0	0
aspS	Aspartate--tRNA ligase	P21889	946385	66 kDa	0	9.893	0	0
atpA	ATP synthase subunit alpha	P0ABB0	948242	55 kDa	0	37.099	13.224	65.908
bfr	Bacterioferritin	P0ABD3	947839	18 kDa	0	2.4732	0	5.2032
cnoX	Chaperedoxin	P77395	947119	32 kDa	0	2.4732	0	0
crp	cAMP-activated global transcriptional regulator CRP	P0ACJ8	947867	24 kDa	0	0	0	7.8048
cysK	Cysteine synthase A	P0ABK5	946877	34 kDa	13.077	8.6563	0	0
deoD	Purine nucleoside phosphorylase DeoD-type	P0ABP8	945654	26 kDa	0	28.442	0	4.336
dnaK	Chaperone protein DnaK	P0A6Y8	944750	69 kDa	0	17.313	0	4.336
dps	DNA protection during starvation protein	P0ABT2	945101	19 kDa	0	1.2366	13.224	11.274
eno	Enolase	P0A6P9	945032	46 kDa	0	2.4732	0	4.336
fabB	3-oxoacyl-[acyl-carrier-protein] synthase 1	P0A953	946799	43 kDa	0	11.13	0	0
fabZ	3-hydroxyacyl-[acyl-carrier-protein] dehydratase FabZ	P0A6Q6	944888	17 kDa	0	0	0	1.7344
fadB	Fatty acid oxidation complex subunit alpha	P21177	948336	80 kDa	0	0	0	0

ftnA	Bacterial non-heme ferritin	P0A998	946410	19 kDa	65.383	7.4197	17.632	1.7344
fusA	Elongation factor G	P0A6M8	947847	78 kDa	0	3.7099	0	0.8672
gadB	Glutamate decarboxylase beta	P69910	946058	53 kDa	0	0	0	0
gapA	Glyceraldehyde-3-phosphate dehydrogenase A	P0A9B2	947679	36 kDa	91.536	68.014	0	2.6016
gatY	D-tagatose-1,6-bisphosphate aldolase subunit GatY	P0C8J6	946636	31 kDa	0	165.71	8.816	15.61
glmM	Phosphoglucosamine mutase	P31120	947692	48 kDa	13.077	0	0	3.4688
glmS	Glutamine--fructose-6-phosphate aminotransferase [isomerizing]	P17169	948241	67 kDa	0	1.2366	0	0
glnA	Glutamine synthetase	P0A9C5	948370	52 kDa	0	0	8.816	0.8672
glpK	Glycerol kinase	P0A6F3	948423	56 kDa	39.23	6.1831	0	0
glyA	Serine hydroxymethyltransferase	P0A825	947022	45 kDa	0	6.1831	0	0.8672
gnd	6-phosphogluconate dehydrogenase, decarboxylating	P00350	946554	51 kDa	0	3.7099	0	11.274
groL	60 kDa chaperonin	P0A6F5	948665	57 kDa	235.38	829.77	537.78	528.99
hemB	Delta-aminolevulinic acid dehydratase	P0ACB2	945017	36 kDa	0	12.366	0	2.6016
hflC	Modulator of FtsH protease HflC	P0ABC3	948697	38 kDa	0	0	0	3.4688
hldD	ADP-L-glycero-D-manno-heptose-6-epimerase	P67910	948134	35 kDa	0	0	0	1.7344
icd	Isocitrate dehydrogenase [NADP]	P08200	945702	46 kDa	0	6.1831	0	0
kbp	Potassium binding protein Kbp	P0ADE6	947144	16 kDa	0	4.9465	0	13.875
kdsA	2-dehydro-3-deoxyphosphooctonate aldolase	P0A715	945785	31 kDa	0	107.59	0	3.4688
lpdA	Dihydrolipoyl dehydrogenase	P0A9P0	944854	51 kDa	0	3.7099	0	10.406
lysU	Lysine--tRNA ligase, heat inducible	P0A8N5	948645	58 kDa	0	2.4732	0	1.7344
maeB	NADP-dependent malic enzyme	P76558	946947	82 kDa	0	1.2366	0	0
malP	Maltodextrin phosphorylase	P00490	947922	91 kDa	0	0	0	0.8672
mtnN	5'-methylthioadenosine/S-adenosylhomocysteine nucleosidase	P0AF12	948542	24 kDa	0	4.9465	0	0
ompR	Transcriptional regulatory protein OmpR	P0AA16	947913	27 kDa	0	0	0	0.8672
pdxJ	Pyridoxine 5'-phosphate synthase	P0A794	947039	26 kDa	0	25.969	0	0.8672
pflB	Formate acetyltransferase 1	P09373	945514	85 kDa	52.306	4.9465	0	8.672
pgk	Phosphoglycerate kinase	P0A799	947414	41 kDa	0	1.2366	0	0
pnp	Polyribonucleotide nucleotidyltransferase	P05055	947672	77 kDa	0	23.496	0	4.336
ppc	Phosphoenolpyruvate carboxylase	P00864	948457	99 kDa	0	0	0	0
ppsA	Phosphoenolpyruvate synthase	P23538	946209	87 kDa	0	3.7099	0	1.7344
pta	Phosphate acetyltransferase	P0A9M8	946778	77 kDa	0	0	0	1.7344
ptsI	Phosphoenolpyruvate-protein phosphotransferase	P08839	946879	64 kDa	26.153	3.7099	0	5.2032
purA	Adenylosuccinate synthetase	P0A7D4	948695	47 kDa	0	92.746	4.408	4.336

pykF	Pyruvate kinase I	P0AD61	946179	51 kDa	0	2.4732	0	0
pyrG	CTP synthase	P0A7E5	946116	60 kDa	0	4.9465	0	16.477
rne	Ribonuclease E	P21513	945641	118 kDa	0	0	0	1.7344
rplB	50S ribosomal protein L2	P60422	947820	30 kDa	13.077	3.7099	0	2.6016
rplF	50S ribosomal protein L6	P0AG55	947803	19 kDa	0	0	0	2.6016
rplL	50S ribosomal protein L7/L12	P0A7K2	948489	12 kDa	156.92	9.893	8.816	13.008
rplQ	50S ribosomal protein L17	P0AG44	947784	14 kDa	0	0	8.816	0
rplT	50S ribosomal protein L20	P0A7L3	945152	13 kDa	0	0	26.448	22.547
rpoA	DNA-directed RNA polymerase subunit alpha	P0A7Z4	947794	37 kDa	0	0	0	9.5392
rpoB	DNA-directed RNA polymerase subunit beta	P0A8V2	948488	151 kDa	0	3.7099	0	6.0704
rpoC	DNA-directed RNA polymerase subunit beta'	P0A8T7	948487	155 kDa	0	0	8.816	3.4688
rpoD	RNA polymerase sigma factor RpoD	P00579	947567	70 kDa	0	0	0	1.7344
rpsA	30S ribosomal protein S1	P0AG67	945536	61 kDa	0	1.2366	0	21.68
rpsB	30S ribosomal protein S2	P0A7V0	947874	27 kDa	0	1.2366	8.816	13.875
rpsC	30S ribosomal protein S3	P0A7V3	947814	26 kDa	0	0	0	2.6016
rpsE	30S ribosomal protein S5	P0A7W1	947795	18 kDa	0	0	13.224	5.2032
rpsG	30S ribosomal protein S7	P02359	947846	20 kDa	0	0	0	1.7344
rpsH	30S ribosomal protein S8	P0A7W7	947802	14 kDa	0	1.2366	4.408	11.274
rpsI	30S ribosomal protein S9	P0A7X3	949000	15 kDa	0	0	0	1.7344
rpsR	30S ribosomal protein S18	P0A7T7	948721	9 kDa	0	0	0	1.7344
sucB	Dihydrolipoyllysine-residue succinyltransferase component of 2-oxoglutarate dehydrogenase complex	P0AFG6	945307	44 kDa	0	2.4732	0	18.211
sucC	Succinate--CoA ligase [ADP-forming] subunit beta	P0A836	945312	41 kDa	0	3.7099	0	3.4688
talA	Transaldolase A	P0A867	947006	36 kDa	0	8.6563	0	0.8672
talB	Transaldolase B	P0A870	944748	35 kDa	0	25.969	0	8.672
tnaA	Tryptophanase	P0A853	948221	53 kDa	379.22	154.58	0	6.9376
tufA	Elongation factor Tu 1	P0CE47	947838	43 kDa	78.46	46.992	4.408	45.095
ubiK	Ubiquinone biosynthesis accessory factor UbiK	Q46868	947524	11 kDa	0	0	0	0.8672
ugd	UDP-glucose 6-dehydrogenase	P76373	946571	44 kDa	0	0	0	12.141
wrbA	NAD(P)H dehydrogenase (quinone)	P0A8G6	947263	21 kDa	0	50.701	0	0.8672
ydgH	Protein YdgH	P76177	945117	34 kDa	0	75.434	13.224	45.095
yghA	Uncharacterized oxidoreductase YghA	P0AG84	947478	31 kDa	0	28.442	0	0
zwf	Glucose-6-phosphate 1-dehydrogenase	P0AC53	946370	56 kDa	13.077	3.7099	0	0
			EXTRACELLULAR					
fliC	Flagellin	P04949	949101	51 kDa	26.153	14.839	8.816	275.77
			IM					
acrA	Multidrug efflux pump subunit AcrA	P0AE06	945112	42 kDa	0	6.1831	0	41.626

atpF	ATP synthase subunit b	P0ABA0	948247	17 kDa	13.077	3.7099	4.408	9.5392
borD	Prophage lipoprotein Bor homolog	P77330	948980	10 kDa	0	1.2366	4.408	1.7344
cydA	Cytochrome bd-I ubiquinol oxidase subunit 1	P0ABJ9	945341	58 kDa	0	0	0	0.8672
cydC	ATP-binding/permease protein CydC	P23886	945504	63 kDa	0	0	0	3.4688
damX	Cell division protein DamX	P11557	947930	46 kDa	0	0	0	10.406
dld	Quinone-dependent D-lactate dehydrogenase	P06149	946653	65 kDa	0	0	0	0
elaB	Protein ElaB	P0AEH5	946751	11 kDa	0	1.2366	0	2.6016
eptC	Phosphoethanolamine transferase EptC	P0CB39	948458	67 kDa	0	0	0	54.634
ftsN	Cell division protein FtsN	P29131	948428	36 kDa	0	0	4.408	11.274
ftsZ	Cell division protein FtsZ	P0A9A6	944786	40 kDa	0	0	0	19.946
hemX	Protein HemX	P09127	948446	43 kDa	0	2.4732	0	11.274
hflK	Modulator of FtsH protease HflK	P0ABC7	948698	46 kDa	0	1.2366	0	21.68
lpoA	Penicillin-binding protein activator LpoA	P45464	947663	73 kDa	0	4.9465	0	8.672
maeA	NAD-dependent malic enzyme	P26616	946031	63 kDa	0	3.7099	0	1.7344
mltB	Membrane-bound lytic murein transglycosylase B	P41052	947184	40 kDa	0	0	0	1.7344
nuoG	NADH-quinone oxidoreductase subunit G	P33602	946762	100 kDa	0	0	4.408	0
osmE	Osmotically-inducible putative lipoprotein OsmE	P0ADB1	945305	12 kDa	52.306	17.313	22.04	15.61
ppiD	Peptidyl-prolyl cis-trans isomerase D	P0ADY1	946056	68 kDa	0	2.4732	0	6.9376
prc	Tail-specific protease	P23865	946096	77 kDa	0	0	0	0
pstB	Phosphate import ATP-binding protein PstB	P0AAH0	948240	29 kDa	0	0	0	9.5392
sdhA	Succinate dehydrogenase flavoprotein subunit	P0AC41	945402	64 kDa	0	0	0	0.8672
sdhB	Succinate dehydrogenase iron-sulfur subunit	P07014	945300	27 kDa	0	1.2366	0	0
secA	Protein translocase subunit SecA	P10408	944821	102 kDa	0	0	0	8.672
secD	Protein translocase subunit SecD	P0AG90	949133	67 kDa	0	0	0	13.008
yajG	Uncharacterized lipoprotein YajG	P0ADA5	945521	21 kDa	26.153	7.4197	26.448	6.0704
ybjP	Uncharacterized lipoprotein YbjP	P75818	945491	19 kDa	0	1.2366	0	6.0704
ydcL	Uncharacterized lipoprotein YdcL	P64451	948203	24 kDa	0	0	0	0
ydgA	Protein YdgA	P77804	946172	55 kDa	0	13.603	0	23.415
yedD	Uncharacterized lipoprotein YedD	P31063	949082	15 kDa	0	6.1831	0	17.344
ygdI	Uncharacterized lipoprotein YgdI	P65292	947276	8 kDa	52.306	4.9465	17.632	7.8048
yifL	Uncharacterized lipoprotein YifL	P0ADN6	1450304	7 kDa	26.153	106.35	4.408	36.423
yqjD	Uncharacterized protein YqjD	P64581	947614	11 kDa	0	1.2366	4.408	189.92
			OUTER MEMBRANE					
bamA	Outer membrane protein assembly factor BamA	P0A940	944870	91 kDa	0	12.366	8.816	41.626
bamB	Outer membrane protein assembly factor BamB	P77774	946982	42 kDa	13.077	4.9465	0	12.141
bamC	Outer membrane protein assembly factor BamC	P0A903	946954	37 kDa	0	3.7099	4.408	32.087

bamD	Outer membrane protein assembly factor BamD	P0AC02	947086	28 kDa	0	192.91	105.79	202.06
blc	Outer membrane lipoprotein Blc	P0A901	948670	20 kDa	0	0	0	0.8672
btuB	Vitamin B12 transporter BtuB	P06129	948468	68 kDa	0	42.045	26.448	14.742
fadL	Long-chain fatty acid transport protein	P10384	946820	49 kDa	0	1.2366	13.224	1.7344
fepA	Ferrienterobactin receptor	P05825	945193	82 kDa	0	1.2366	8.816	8.672
fhuA	Ferrichrome outer membrane transporter/phage receptor	P06971	944856	82 kDa	0	51.938	0	19.946
flu	Antigen 43	P39180	946540	107 kDa	0	2.4732	4.408	1.7344
lamB	Maltoporin	P02943	948548	50 kDa	0	1.2366	48.488	13.875
loiP	Metalloprotease LoiP	P25894	945173	27 kDa	0	8.6563	4.408	19.946
lpoB	Penicillin-binding protein activator LpoB	P0AB38	948536	23 kDa	0	3.7099	0	39.024
lpp	Major outer membrane prolipoprotein Lpp	P69776	946175	8 kDa	104.61	12.366	44.08	19.078
lptD	LPS-assembly protein LptD	P31554	945011	90 kDa	0	3.7099	0	0.8672
lptE	LPS-assembly lipoprotein LptE	P0ADC1	946257	21 kDa	0	12.366	0	36.423
mipA	MltA-interacting protein	P0A908	946301	28 kDa	78.46	19.786	8.816	11.274
mliC	Membrane-bound lysozyme inhibitor of C-type lysozyme	P28224	946811	13 kDa	0	87.8	0	23.415
mltA	Membrane-bound lytic murein transglycosylase A	P0A935	944964	40 kDa	0	1.2366	4.408	2.6016
nfrA	Bacteriophage adsorption protein A	P31600	944741	111 kDa	0	0	0	0
nlpD	Murein hydrolase activator NlpD	P0ADA3	947011	40 kDa	0	0	0	17.344
nlpE	Lipoprotein NlpE	P40710	946782	26 kDa	0	4.9465	0	0
ompA	Outer membrane protein A	P0A910	945571	37 kDa	366.14	116.24	709.69	211.6
ompC	Outer membrane porin C	P06996	946716	40 kDa	1490.7	247.32	1344.4	176.91
ompF	Outer membrane porin F	P02931	945554	39 kDa	0	0	74.936	11.274
ompT	Protease 7	P09169	945185	36 kDa	143.84	13.603	44.08	13.875
ompW	Outer membrane protein W	P0A915	945128	23 kDa	143.84	29.679	8.816	11.274
ompX	Outer membrane protein X	P0A917	944967	19 kDa	0	7.4197	17.632	21.68
pal	Peptidoglycan-associated lipoprotein	P0A912	945004	19 kDa	104.61	16.076	48.488	22.547
rcsF	Outer membrane lipoprotein RcsF	P69411	949113	14 kDa	13.077	7.4197	13.224	6.9376
rlpA	Endolytic peptidoglycan transglycosylase RlpA	P10100	945241	38 kDa	13.077	9.893	22.04	10.406
slp	Outer membrane protein Slp	P37194	948022	21 kDa	0	1.2366	4.408	19.078
slyB	Outer membrane lipoprotein SlyB	P0A905	946801	16 kDa	117.69	23.496	96.976	71.111
tolC	Outer membrane protein TolC	P02930	947521	54 kDa	39.23	132.32	26.448	107.53
tsx	Nucleoside-specific channel-forming protein Tsx	P0A927	946242	34 kDa	0	1.2366	0	0.8672
ybhC	Putative acyl-CoA thioester hydrolase YbhC	P46130	945381	46 kDa	0	4.9465	8.816	22.547
yiaD	Probable lipoprotein YiaD	P37665	948075	22 kDa	0	1.2366	0	6.9376
yncD	Probable TonB-dependent receptor YncD	P76115	946015	77 kDa	0	6.1831	0	0
ynfB	UPF0482 protein YnfB	P76170	946119	13 kDa	13.077	1.2366	8.816	5.2032

		PP						
agp	Glucose-1-phosphatase	P19926	945773	46 kDa	0	38.335	0	46.829
amiC	N-acetylmuramoyl-L-alanine amidase AmiC	P63883	947293	46 kDa	0	0	0	0
ansB	L-asparaginase 2	P00805	947454	37 kDa	0	1.2366	30.856	16.477
artI	Putative ABC transporter arginine-binding protein 2	P30859	948988	27 kDa	0	29.679	0	47.696
cpdB	2',3'-cyclic-nucleotide 2'-phosphodiesterase/3'-nucleotidase	P08331	948729	71 kDa	0	0	0	0.8672
cpoB	Cell division coordinator CpoB	P45955	947227	28 kDa	0	7.4197	8.816	8.672
cysP	Thiosulfate-binding protein	P16700	946883	38 kDa	0	1.2366	0	4.336
degP	Periplasmic serine endoprotease DegP	P0C0V0	947139	49 kDa	0	4.9465	0	49.431
degQ	Periplasmic pH-dependent serine endoprotease DegQ	P39099	947812	47 kDa	0	0	0	0
dppA	Periplasmic dipeptide transport protein	P23847	948062	60 kDa	0	4.9465	0	92.791
dsbA	Thiol:disulfide interchange protein DsbA	P0AEG4	948353	23 kDa	0	2.4732	0	2.6016
dsbC	Thiol:disulfide interchange protein DsbC	P0AEG6	947363	26 kDa	0	0	0	0
eco	Ecotin	P23827	946700	18 kDa	0	4.9465	0	20.813
fkpA	FKBP-type peptidyl-prolyl cis-trans isomerase FkpA	P45523	947850	29 kDa	0	2.4732	0	8.672
fliY	L-cystine-binding protein FliY	P0AEM9	948833	29 kDa	0	183.02	0	104.06
glnH	Glutamine-binding periplasmic protein	P0AEQ3	944872	27 kDa	0	6.1831	0	3.4688
hdeB	Acid stress chaperone HdeB	P0AET2	948026	12 kDa	0	115.01	48.488	52.032
livJ	Leu/Ile/Val-binding protein	P0AD96	947971	39 kDa	0	0	0	5.2032
lolA	Outer-membrane lipoprotein carrier protein	P61316	948989	22 kDa	0	2.4732	0	21.68
lolB	Outer-membrane lipoprotein LolB	P61320	945775	24 kDa	0	1.2366	0	5.2032
malE	Maltose/maltodextrin-binding periplasmic protein	P0AEX9	948538	43 kDa	0	2.4732	4.408	27.751
mdoD	Glucans biosynthesis protein D	P40120	945994	63 kDa	0	0	0	1.7344
mdoG	Glucans biosynthesis protein G	P33136	945005	58 kDa	0	9.893	0	13.875
mglB	D-galactose-binding periplasmic protein	P0AEE5	949041	36 kDa	0	4.9465	0	13.008
modA	Molybdate-binding protein ModA	P37329	945364	27 kDa	0	0	0	0.8672
oppA	Periplasmic oligopeptide-binding protein	P23843	945830	61 kDa	0	4.9465	0	10.406
osmY	Osmotically-inducible protein Y	P0AFH8	948895	21 kDa	39.23	13.603	8.816	16.477
potD	Spermidine/putrescine-binding periplasmic protein	P0AFK9	945682	39 kDa	0	4.9465	0	21.68
pstS	Phosphate-binding protein PstS	P0AG82	948237	37 kDa	0	53.175	0	26.016
rbsB	Ribose import binding protein RbsB	P02925	948261	31 kDa	26.153	1.2366	0	8.672
skp	Chaperone protein Skp	P0AEU7	944861	18 kDa	0	7.4197	0	7.8048
slt	Soluble lytic murein transglycosylase	P0AGC3	948908	73 kDa	0	1.2366	0	9.5392
spy	Periplasmic chaperone Spy	P77754	946253	18 kDa	0	0	0	33.821
surA	Chaperone SurA	P0ABZ6	944812	47 kDa	0	86.563	4.408	113.6

tolB	Tol-Pal system protein TolB	P0A855	945429	46 kDa	52.306	13.603	39.672	27.751
ugpB	sn-glycerol-3-phosphate-binding periplasmic protein UgpB	P0AG80	947962	48 kDa	0	3.7099	0	0.8672
ushA	Protein UshA	P07024	947331	61 kDa	130.77	29.679	79.344	20.813
ybaY	Uncharacterized lipoprotein YbaY	P77717	945070	19 kDa	0	2.4732	0	5.2032
ybiS	Probable L,D-transpeptidase YbiS	P0AAX8	945441	33 kDa	0	0	0	0.8672
yfhG	Uncharacterized protein YfhG	P0AD44	947010	27 kDa	0	0	0	6.0704
yggE	Uncharacterized protein YggE	P0ADS6	947398	27 kDa	0	1.2366	0	0.8672
ygiW	Protein YgiW	P0ADU5	946051	14 kDa	13.077	9.893	30.856	9.5392
yncE	Uncharacterized protein YncE	P76116	946006	39 kDa	0	19.786	0	25.149
ynjE	Thiosulfate sulfurtransferase YnjE	P78067	946505	48 kDa	0	0	0	9.5392
yraP	Uncharacterized protein YraP	P64596	947659	20 kDa	13.077	49.465	0	45.962
ytfQ	ABC transporter periplasmic-binding protein YtfQ	P39325	948746	34 kDa	0	0	0	0
			UNKNOWN					
hslJ	Heat shock protein HslJ	P52644	946525	15 kDa	0	0	0	0.8672
yggN	Uncharacterized protein YggN	P0ADS9	947453	26 kDa	0	6.1831	0	11.274